**STATE OF OREGON**

**DEPARTMENT OF GEOLOGY AND MINERAL INDUSTRIES**

**Suite 965, 800 NE Oregon St., #28**
**Portland, Oregon 97232**

**OPEN-FILE REPORT O-95-67**

# EXPLANATION OF MAPPING METHODS AND USE OF THE TSUNAMI HAZARD MAPS OF THE OREGON COAST

Prepared by
George R. Priest
Oregon Department of Geology and Mineral Industries

December, 1995

## NOTICE

The Oregon Department of Geology and Mineral Industries is publishing this paper because the information furthers the mission of the Department. To facilitate timely distribution of the information this report has not been edited to our usual standards.

# TABLE OF CONTENTS

Page


INTRODUCTION..... 1
MAPPING METHOD..... 4
RESULTS OF THE NUMERICAL SIMULATIONS..... 13
VALIDATION FROM PREHISTORIC TSUNAMI RUN-UP ESTIMATES..... 14
VALIDATION FROM OBSERVATIONS OF THE 1964 TSUNAMI..... 17
PRECISION AND ACCURACY OF THE INUNDATION LINES..... 18
CONCLUSION..... 19
USE OF THE MAPS..... 19
RELATED HAZARDS..... 19
WHAT TO DO IN THE EVENT OF AN EARTHQUAKE..... 20
ACKNOWLEDGMENTS..... 20
REFERENCES CITED..... 20
APPENDIX A: TECHNICAL DISCUSSION OF FAULT SLIP AND DIP USED FOR THE MODELS..... 23
Fault Length..... 23
Amount and direction of fault slip..... 23
Fault dip..... 24
Methods and uncertainties in simulating earthquake deformation..... 24
Effect of source uncertainties on predicted tsunami run-up..... 27
Implications of recent research for revision of the inundation maps..... 32
Summary and recommendations..... 35
APPENDIX B: MAXIMUM TSUNAMI RUN-UP ELEVATIONS AT THE OPEN COAST IN OREGON..... 36


## FIGURES


FIGURE 1. Regional map of the Cascadia subduction zone..... 2
FIGURE 2. Explanation of tsunami run-up and other terms..... 2
FIGURE 3. Index of published tsunami inundation maps used to implement ORS 455.446 and 455.447. ..... 3
FIGURES 4a, 4b, and 4c. Maps of sea floor deformation from Models 1, 2, and 3..... 5
FIGURE 5. Cross section showing coseismic deformation of fault ruptures for Models 1, 2, and 3..... 6
FIGURE 6. Coseismic deformation: models versus wetland soils data..... 7
FIGURE 7. Numerical grid used for modeling..... 9
FIGURE 8. Numerical grid used for the finite element simulation of the Columbia estuary..... 10
FIGURE 9. Variation of run-up with distance from the open coast at Siletz Bay and the Columbia River..... 12
FIGURE 10. Maximum run-up elevation versus latitude for Models 1, 2, and 3..... 13
FIGURE 11 Offshore bathymetry and location of areas with highest tsunami run-up..... 15

FIGURE A1. Interseismic vertical deformation rates above the Cascadia subduction zone fault in Oregon..... 25
FIGURE A2. Map of transects modeled for vertical deformation by Hyndman and Wang (1993) ..... 25
FIGURE A3. Coseismic vertical deformation predicted by Models 1, 2, 3, and Hyndman and Wang (1993)..... 26
FIGURE A4. Maximum run-up of Model 2 with and without the "spike" of uplift..... 28
FIGURE A5. Map of coseismic deformation from data of Hyndman and Wang (1993) accumulation..... 29
FIGURE A6. Maximum run-up of Models 2, 3, and the HW model versus latitude..... 30
FIGURE A7. Time histories for Models 2, 3, and the HW model, northern Oregon..... 31
FIGURE A8. Time histories for Models 2, 3, and the HW model, southern Oregon..... 31
FIGURE A9. Comparison of zero isobase from buried wetland soil data and the Hyndman and Wang (1995)..... 33
FIGURE A10. Coseismic deformation from buried wetland soil data versus models..... 34

## TABLES

TABLE 1. Length, width, dip, rake, depth, and slip values for the models..... 4
TABLE 2. Geographic location parameters for the modeled fault ruptures. ..... 4
TABLE 3. Earthquake magnitude, maximum uplift, and maximum subsidence for each model..... 6
TABLE B1. Decimal equivalents of minutes and seconds of latitude bounding 7.5' quadrangles..... 36

# EXPLANATION OF MAPPING METHODS AND USE OF THE TSUNAMI HAZARD MAPS OF THE OREGON COAST

## INTRODUCTION

This report explains, in abbreviated form, the methods used and results of a tsunami hazard mapping project focused on the Oregon coast. Maps at a scale of 1:24,000 (1 inch = 2,000 ft) depict the expected inundation for tsunamis produced by a $M_w$ 8.8-8.9 undersea earthquake. The maps were produced to help implement Senate Bill 379 (SB 379), which was passed by the 1995 regular session of the Oregon Legislature. SB 379, implemented as Oregon Revised Statutes (ORS) 455.446 and 455.447, limits construction of new essential facilities and special occupancy structures in tsunami flooding zones. The focus of the maps is therefore on implementation of this public safety bill and not on land use or emergency planning.

Tsunamis are caused by any large-scale disturbance of the sea floor. In nature these disturbances are generally caused by faulting, landslides, or volcanic eruptions. This project addresses only the most common cause, the simultaneous uplift and subsidence of the sea floor accompanying undersea earthquakes on large fault zones termed "subduction zones" (Figure 1). The shape of the deformed sea floor after an earthquake is transmitted to the overlying sea surface, forming the initial tsunami wave. Waves so generated can arrive at nearby coastlines in minutes, causing extensive damage and loss of life. These subduction zone earthquakes also typically cause landslides which can greatly amplify the tsunami run-up should they occur under the sea or slide from land into water (see Figure 2 for explanation of run-up and other technical terms). This latter hazard is not directly addressed here but could be an important consideration when adding factors of safety for evacuation planning.

Scientific findings of the last several years have shown that the Oregon coast is vulnerable to great (M 8-9) earthquakes that can occur on the offshore Cascadia subduction zone fault system (Figure 1; see Madin, 1992, Atwater and others, 1995, and Nelson and others, 1995, for summaries). The estimated chance in the next 50 years of a great subduction zone earthquake is between 10 and 20 percent, assuming that the recurrence is on the order of 400 ± 200 years and that the last one occurred about 300 years ago (calculations on data of Peterson and others, 1991b, and Darienzo and Peterson, 1995; see Appendix A for discussion of additional evidence of a 400 year recurrence).

Prediction of sea floor deformation from these great subduction zone earthquakes is fraught with uncertainty, so potential tsunami hazard was examined through three possible scenarios for earthquake deformation. Numerical simulations of tsunami run-up (Appendix B) from these three scenarios were checked against estimates of prehistoric tsunami run-up, where such data are available. The numerically simulated run-up elevations for scenarios with the highest and lowest tsunami run-up were used to infer inundation on 1:24,000-scale topographic base maps (see the library-access Open-File Report O-95-68). DOGAMI map GMS-99 (1:12,000 scale) and Open-File Report O-95-6 (1:4,800 scale map) illustrate these inundation boundaries in more detail for the Lincoln City-Siletz Bay area. Appendix C illustrates the time histories (sequence and relative height of tsunami waves) at coastal population centers for these two models. Inundation from the highest run-up, which was also most consistent with the prehistoric tsunami data, was adopted to implement ORS 455.446 and 455.447 and was illustrated on widely available published maps (see Figure 3 for index).

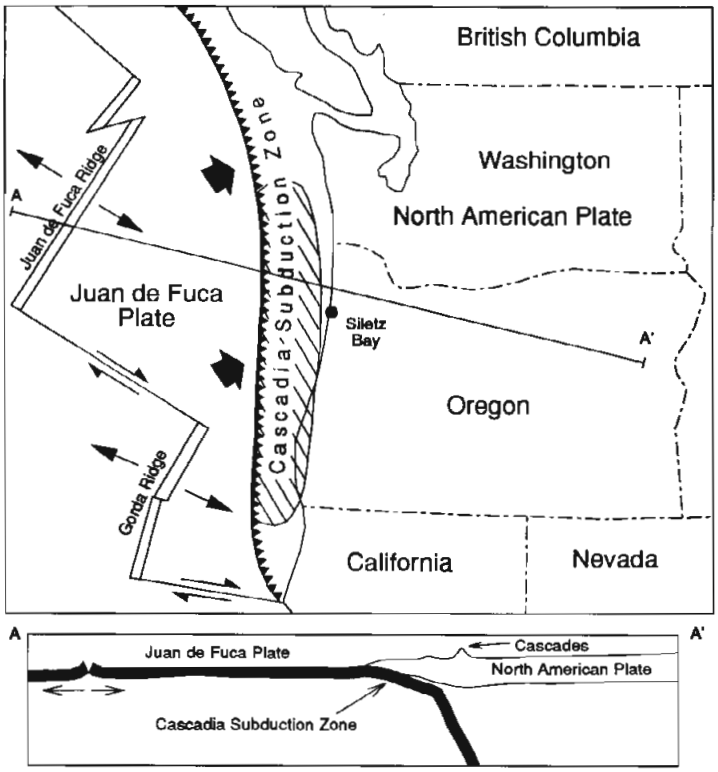


*Figure 1. The length of the crosshatched area is the approximate length of the postulated fault rupture for a magnitude 8.8 earthquake on the Cascadia subduction zone.*

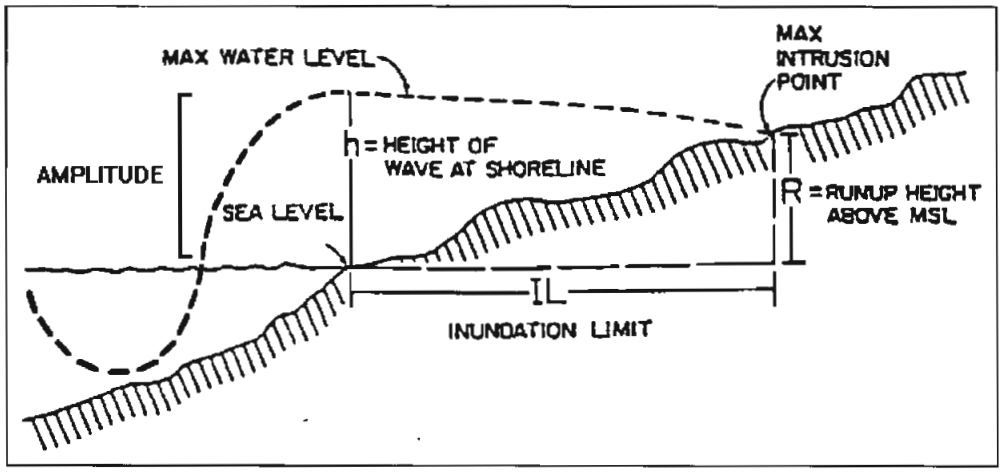


*Figure 2. Explanation of the terms tsunami inundation, run-up elevation, wave height, and wave amplitude.*

(Note: this map does not show changes made by the Oregon Department of Geology and Mineral Industries in 1997)

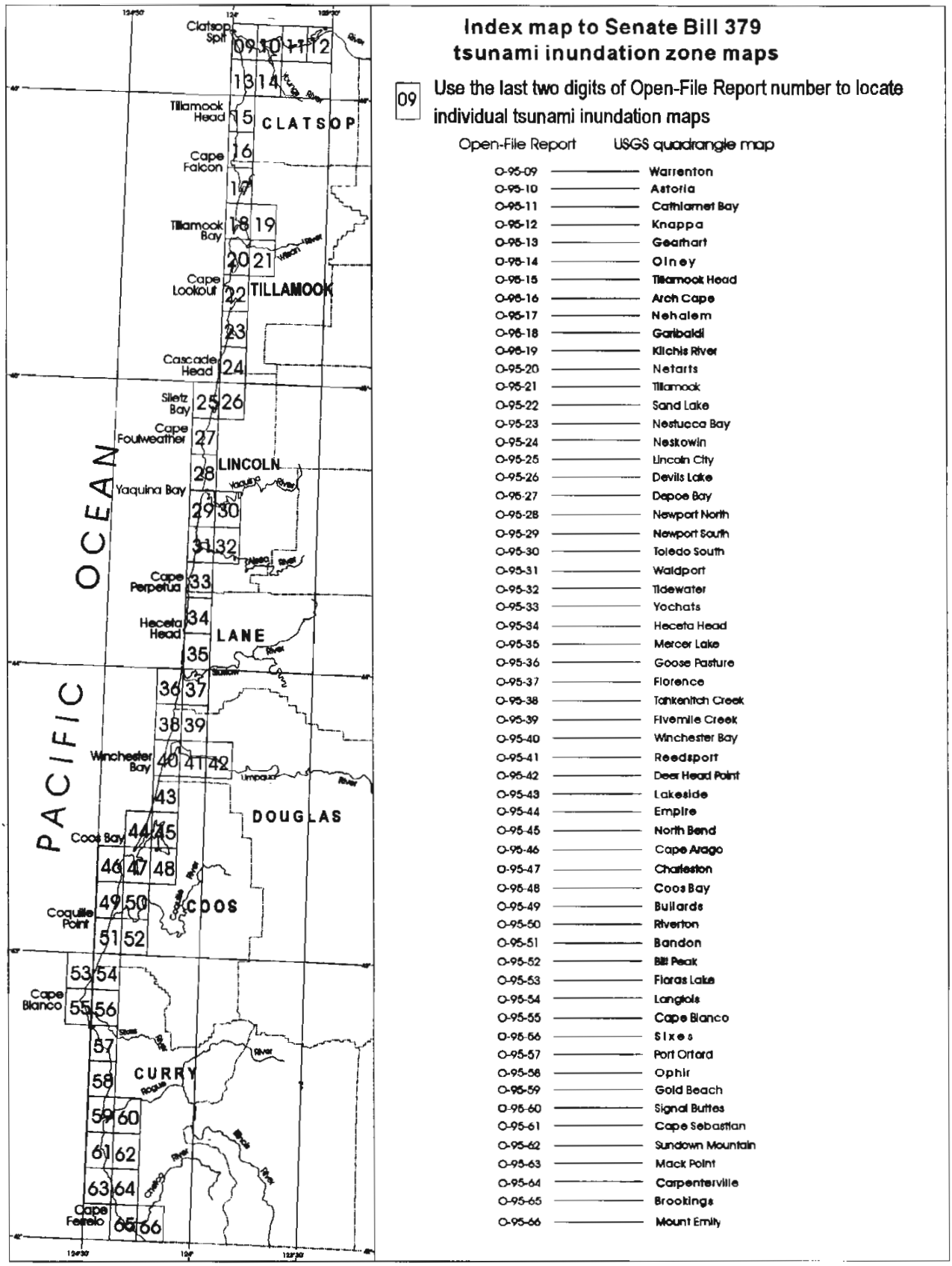


*Figure 3. Index to tsunami hazard maps published by the Oregon Department of Geology and Mineral Industries to implement ORS 455.446 and 455.447*

MAPPING METHOD

The inundation maps were produced by modeling the deformation from an earthquake, numerically simulating the resulting tsunamis waves, and mapping the maximum inland flooding limit. The first two steps were done by computer methods. The third step was accomplished chiefly by inference using professional judgment and available topographic data.

Modeling the Earthquake Deformation

Introduction Using the fault plane model of Okada (1985), three simulations of the bottom deformation by subduction zone faulting were constructed and used to generate numerical simulations of the tsunami waves. The input parameters are summarized in Tables 1 and 2. The results are given in Table 3.

*Table 1. Input parameters for simulations of ground deformation caused by a great subduction zone earthquake on the Cascadia subduction zone. See Appendix A for details.* ***Dip*** *is the inclination of the fault in degrees.* ***Rake*** *is the trend of the fault slip measured in the plane of the fault as an angle from horizontal.* ***Depth*** *is the vertical distance to the toe of the rupture.* ***Slip*** *is the distance the two fault blocks move relative to one another.*

| Model | Length (mi.) | Width (mi) | Dip (°) | Rake (°) | Depth (mi) | Slip (ft) |
|---|---|---|---|---|---|---|
| **1** | 404 | 49.7 | 13.0 | 90 | 12.4 | 28.5 |
| **2** | 404 | 41.3 | 12.1 | 90 | 9.3 | 37.7 |
| **3** | 404 | 71.2 | 12.1 | 90 | 15.6 | 34.4 |

*Table 2. Location of the two rectangular fault ruptures utilized for simulation of a single rupture stretching from Oregon to Washington.* ***Strike*** *is the trend of the fault in degrees clockwise from north.*

| Model | Segment | Strike (°) | Lat. (°) SE corner | Long. (°) of SE corner |
|---|---|---|---|---|
| **1** | N segment | 347.46 | 46.1631N | 124.3753W |
| **1** | S segment | 358.00 | 41.5000N | 124.1200W |
| **2** | N segment | 347.46 | 46.1631N | 124.4699W |
| **2** | S segment | 358.00 | 41.5000N | 124.4707W |
| **3** | N segment | 347.46 | 46.2245N | 123.8187W |
| **3** | S segment | 0.13 | 41.5000N | 123.8796W |

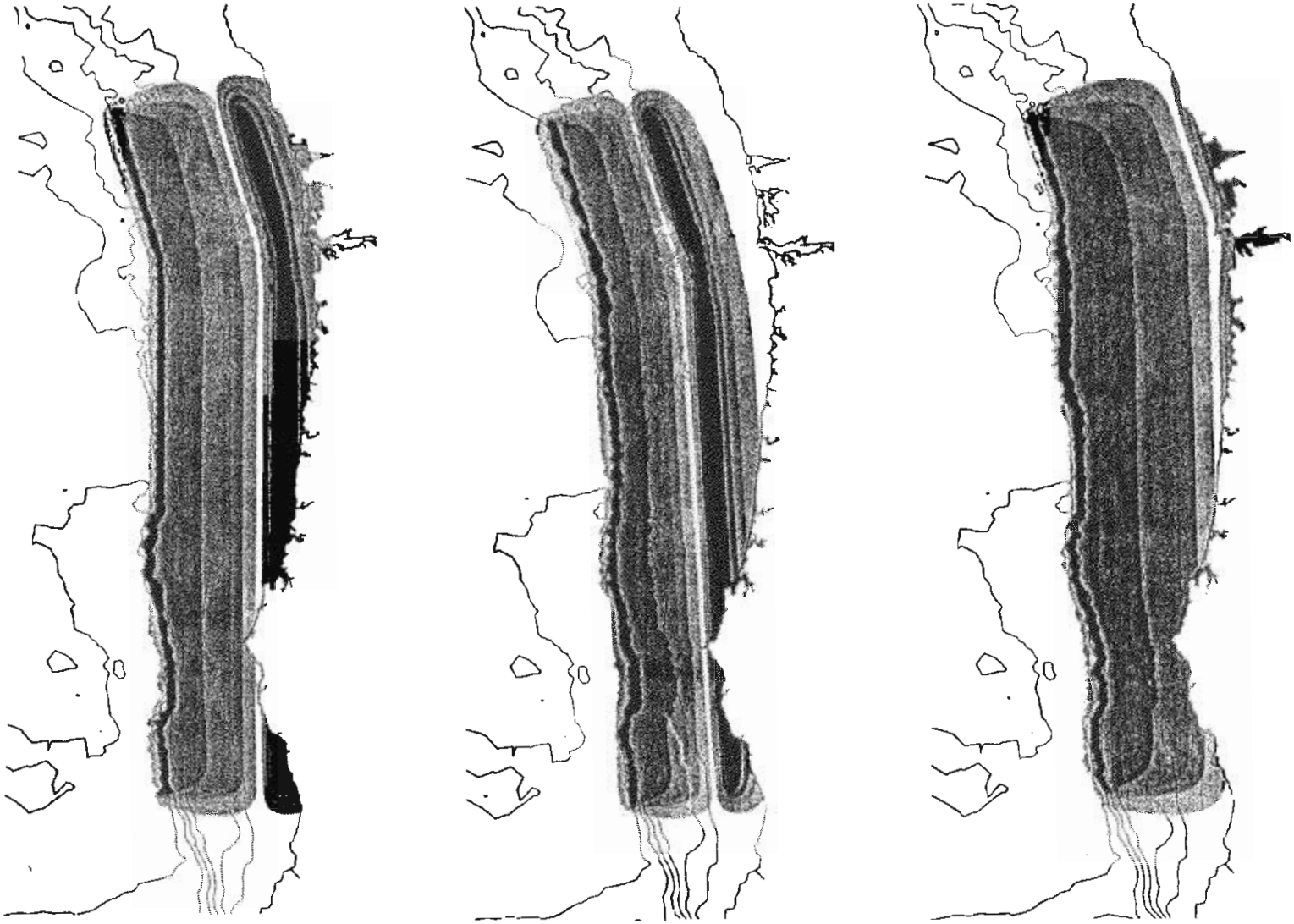

**4a (Model 1)** **4b (Model 2)** **4c (Model 3)**

*Figure 4. Figures show isolines of predicted uplift and subsidence from a subduction zone earthquake. Darker colors are higher values of deformation. Uplift occurs in the left (west) rectangular area, subsidence on the right (east). The two areas are separated by a zone of no deformation shown in white. Black irregular lines are bathymetric contours at intervals of 1600 feet (500 m) starting at the coastline on the right and getting deeper toward the left. Note how the trough of subsidence is closest to shore (0 foot contour) in Figure 4c ((Model 3), and furthest from shore in Figure 4b (Model 2).*

*Table 3. Bottom deformation and earthquake magnitude produced by the simulation. Mw refers to the moment magnitude of the resulting earthquake calculated from the formula of Hanks and Kanamori (1979).*

| Model | Mw | Max. uplift (ft) | Max. subsid. (ft) |
|---|---|---|---|
| **1** | 8.8 | 12.2 | 6.0 |
| **2** | 8.8 | 16.6 | 8.2 |
| **3** | 8.9 | 15.2 | 7.1 |

The simulations differ chiefly with respect to the width and location of the locked part of the theoretical fault rupture. The width and location are the most uncertain and, from the standpoint of tsunami and earthquake hazard, the most important factors. It is this locked portion of the fault that builds up strain, rupturing catastrophically during a great earthquake. The following is a brief summary of each simulation; Figures 4a, 4b, and 4c illustrate the simulated crustal uplift and subsidence of each model. Figure 5 illustrates the differences in vertical deformation above the fault ruptures for each referenced to a generalized cross section of the fault zone from Hyndman and Wang (1993). See Appendix A for a detailed technical discussion of fault dislocation models and their accuracy.

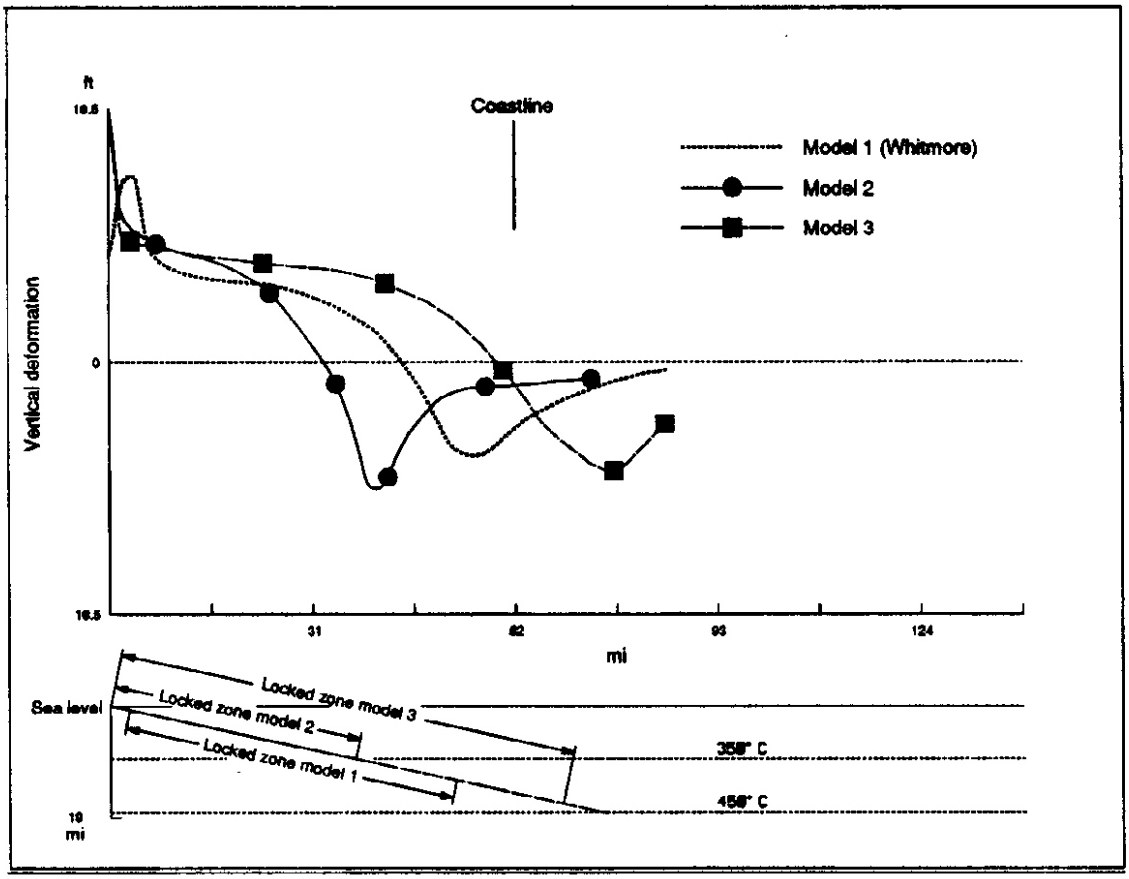


*Figure 5. Upper diagram plots deformation of the earth's surface by earthquakes from rupture of three different locked widths of the subduction zone. Lower diagram shows a simplified vertical cross section of the Cascadia subduction zone fault with zones of complete (solid line) and partial (dashed line) locking. Degree of locking is primarily dependent on rock temperature. Above 450 °C rock deforms plastically rather than by stick-slip motion.*

Model : Whitmore (1993) published a prediction of theoretical tsunami height for the Oregon coast that has been used by local communities for tsunami hazard planning, so his fault model was investigated as a reference. He estimated that the locked zone on the Cascadia subduction zone extends to 12.4 miles depth, starting about 12-22 miles east of the surface trace of the subduction zone. The surface trace is at the foot of the continental slope at about 10,000 foot depth. He also assumed that the inclination of the subduction zone fault is about 13°. The width of his locked zone is therefore 49.7 miles.

Model 2: Using the preferred crustal temperature model of Hyndman and Wang (1993, Figure 9b, p. 2051) and fault dip of 12.1° inferred from seismic data of Trehu and others (1994, Figure 5a, p. 241; see Appendix A), the locked zone in Oregon extends to 9.3 miles depth, the depth where the fault reaches a rock temperature of 350 °C. Hyndman and Wang (1993) argue that, at greater depths (higher temperatures), the fault is only partially locked and not locked at all once the rocks become totally plastic at 450 °C. They also propose that the locked zone starts about 3 miles from the surface trace of the subduction zone. This leads to a fairly narrow locked zone only 41.3 miles wide at the latitude of the seismic data of Trehu and others (1994). Okada's (1985) numerical modeling technique does not explicitly simulate partial locking of the fault, so only the fully locked portion was modeled (see Appendix A for technical discussion). The resulting sea floor deformation produces a narrow zone of uplift and subsidence located further out to sea than Model 1. The zone of undersea subsidence is therefore much more extensive than in Model 1.

Model 3 This simulation uses the same fault inclination as Model 2, but provides a fairly good fit to the ground subsidence estimated from prehistoric coseismic subsidence in Oregon estuaries of the northern and central coast, where most of the prehistoric database was gathered (Figure 6; unpublished 1995 compilation by Curt D. Peterson, 1995; zero deformation line taken from Peterson and Briggs, 1992 and from Briggs, 1994). In this case the locked zone must extend to 15.6 miles depth in order to bring the main trough of subsidence on land where it is observed. The simulation, as in Model 2, starts the locked zone about 3 miles from the deformation front, so the rupture must be 71.2 miles wide, nearly twice as wide as Model 2. This simulation of the earthquake rupture produces mostly uplift off the coast and much less undersea subsidence than either Model 1 or 2.

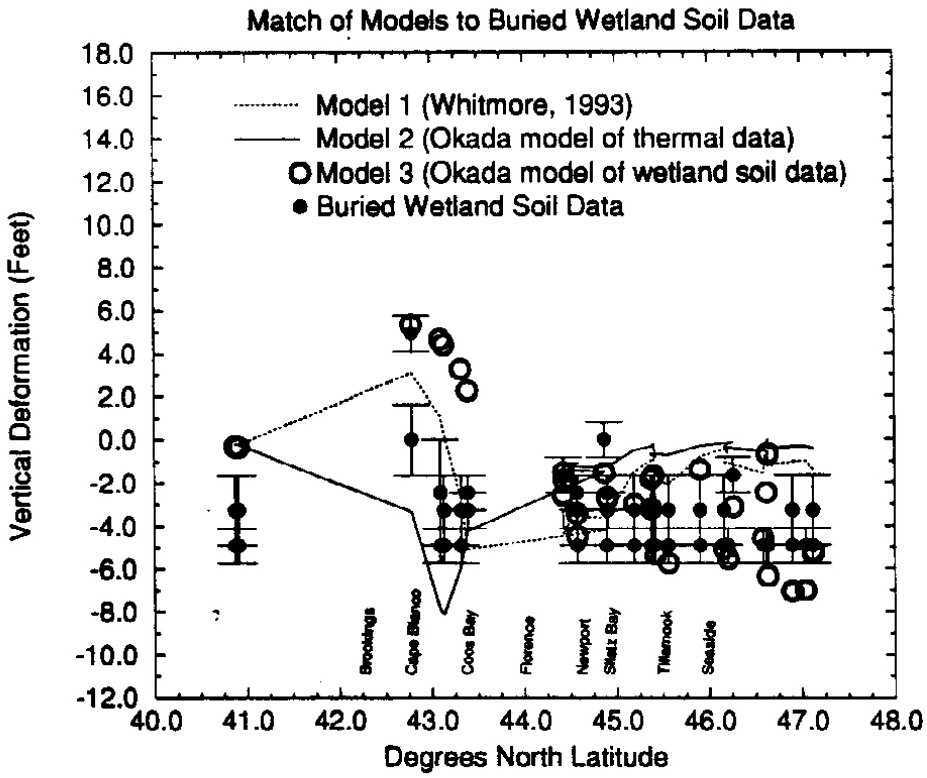


*Figure 6. Correlation of vertical coseismic deformation estimated from models versus buried wetland soil data.*

Discussion The fault ruptures assumed for Model 2 and Model 3 use the most accurate available dip for the subduction zone in Oregon (Trehu and others, 1994) and the most recent available geological and geophysical data. The Model 2 locked zone is based on an interpretation of crustal heat flow data (Hyndman and Wang, 1993), whereas Model 3 fits estimates of prehistoric subsidence (Peterson and Briggs, 1992; Briggs, 1994; unpublished 1995 compilation of Curt D. Peterson). Both models are presented, because numerous trials with the numerical fault modeling technique of Okada (1985) revealed that the thermal and the subsidence data could not easily be reconciled with this technique. The thermal data demands that the fully locked part of the fault zone be narrow and be located well offshore of northern Oregon, which, when modeled with Okada's (1985) technique, causes the subsidence to be offshore. The prehistoric subsidence in northern Oregon was mostly onshore, which, when using Okada's method, demands a fully locked zone nearly twice as wide as that of the thermal data. The incompatibility in the two models could be caused by (1) inaccuracies in the thermal data, (2) the underlying assumption that regional suduction zone faulting causes the prehistoric subsidence, or (3) inaccurate simulation of subduction zone faulting by the Okada (1985) technique. As discussed in Appendix A and below, the third factor is probably the main reason for the disparity.

Simulating the Tsunami Waves

Tsunami waves were simulated from the three fault models using the numerical technique of Luettich and Westerink (1995a; b) modified as in Myers and Baptista (1995) to account for sea floor deformation and transmissive boundaries (Myers and others, in preparation; Baptista, Myers and Priest, in preparation ). The tide was assumed to be at mean higher high water, which is about 4 feet above mean sea level. Final run-up elevation along the shoreline at the limit of the numerical simulation was estimated by adding the coseismic subsidence to the maximum run-up elevation reached in each simulation. Initial draft inundation maps (Open-File Report O-95-68) were produced using the run-up elevations from Models 2 and 3. These two simulations illustrate the uncertainties in the process, since Model 2 generally produces the highest and Model 3 the lowest run-up in most areas. The final maps (Open-File Reports O-95-9 through O-95-66; Figure 3) used for implementation of ORS 455.446 and 455.447 are based on inundation inferred from the Model 2 simulation.

Because the time and resources were not available to do detailed numerical modeling of tsunami inundation, the numerical grid (Figure 7) was not refined enough to accurately model any of the bays or estuaries, with one partial exception. The Columbia River estuary is large enough for even a relatively coarse numerical grid (Figure 8) to simulate the decrease in wave height within the estuary; however, dry land inundation was poorly simulated, owing to the small size of dry land barriers and coarseness of the grid. The inability of the numerical simulation to "see" barriers such as small sand spits, jetties, sea walls, and dikes because of the coarse numerical grid was a major source of error, except for one area. The large jetties that guard the mouth of the Columbia River and the Highway 101 embankment on the west side of Youngs Bay were accurately modeled with refined grids (Figure 8).

Mapping Tsunami Inundation

Inundation was mapped by first adding coseismic subsidence to the simulated run-up elevations and then inferring the location of the inundation limit on 1:24,000-scale topographic maps. The coseismic subsidence was estimated from study of wetland soils buried during prehistoric subsidence events. Curt D. Peterson of Portland State University provided an unpublished compilation of subsidence estimates based on his field data in Oregon. At the open coast an additional run-up of 0-1 feet was added from Florence to Waldport, 1-2 feet from Waldport to Newport, 2-3 feet from Newport to Siletz Bay, and 3-4 feet from Siletz Bay to the mouth of the Columbia River. These adjustments made only minor differences in the mapped inundation. Subsidence inferred from the prehistoric geologic record also changes eastward in large estuaries like the Columbia River, reaching a maximum and then decreasing further inland. Maximum prehistoric subsidence of about 6-7 feet occurred in the vicinity of Blind Slough immediately east of Astoria (unpublished 1995 data of Curt D. Peterson).

Owing to generally low values of prehistoric subsidence (<3 feet) recorded in estuaries on the south coast (Peterson and Briggs, 1992; Briggs, 1994), complications from local geologic structures, and uncertainties in the regional fault model there, neither uplift nor subsidence was assumed. As illustrated by Model 3 (Figure 4c) and the work of Hyndman and Wang (1993), a modest amount (<5 feet) of coseismic uplift may affect some parts of the open coast south of Florence, so assuming zero deformation generally errs on the conservative side (higher run-up).

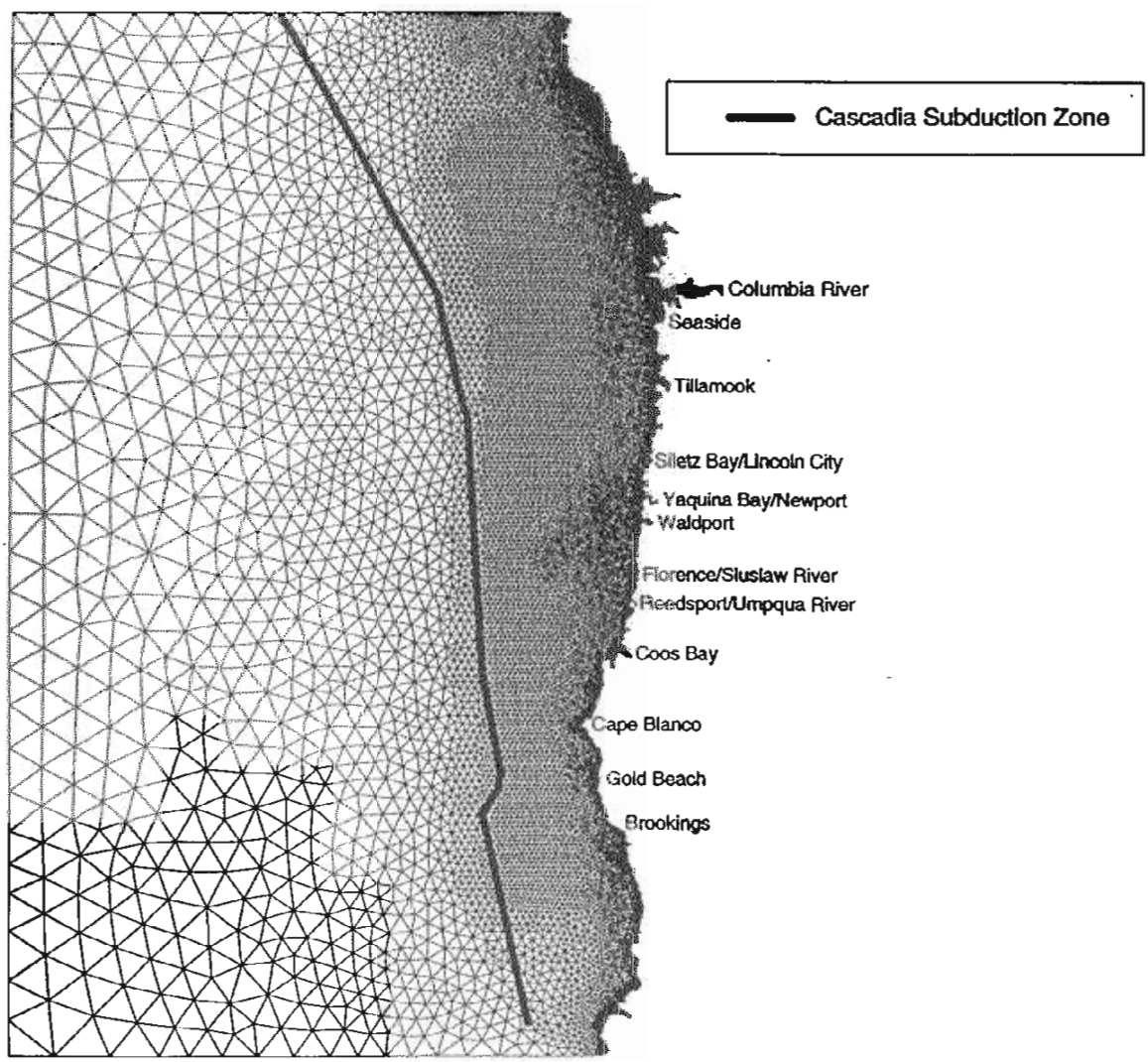


***Figure 7. Numerical grid utilized for modeling.***

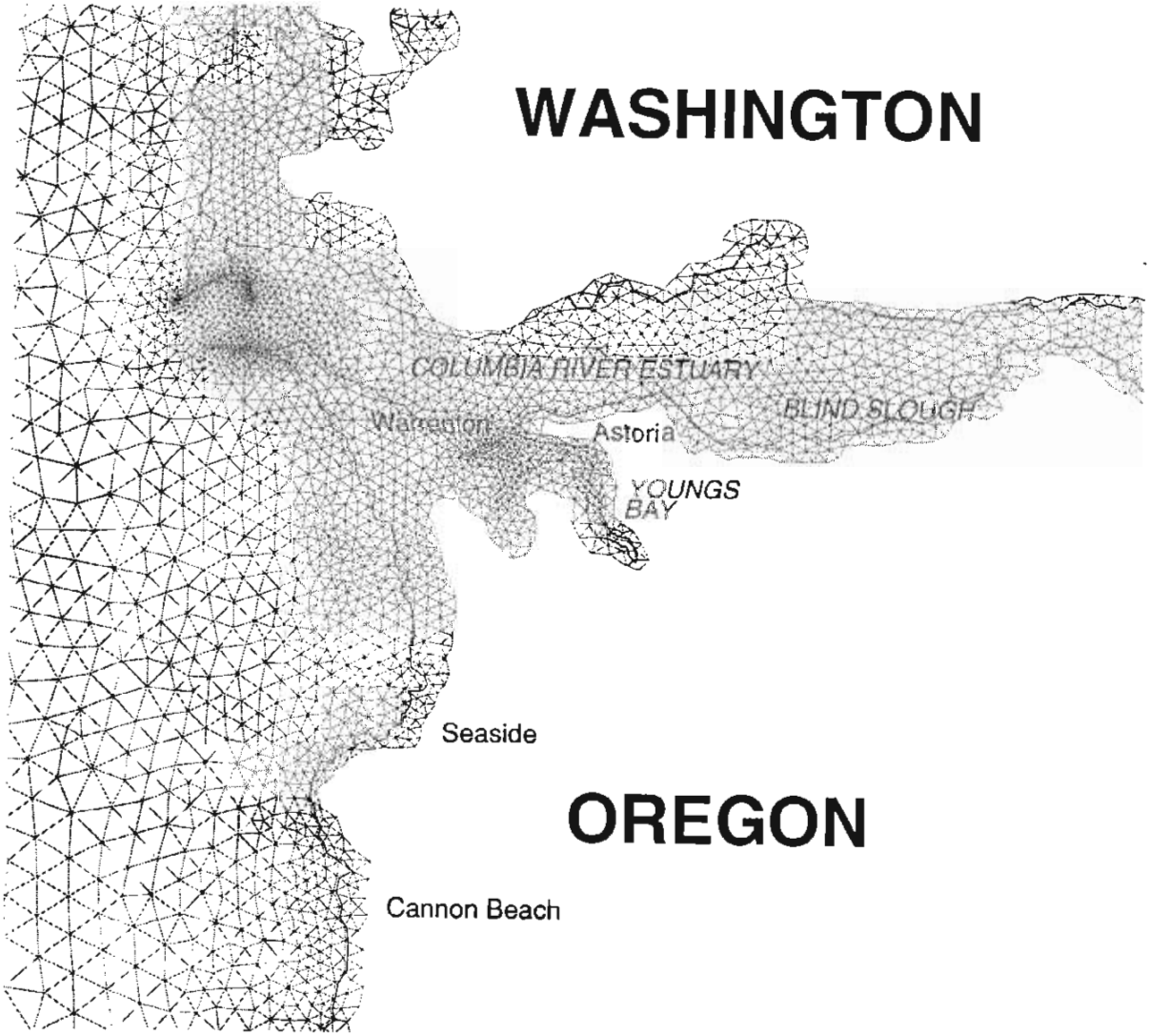


*Figure 8. Numerical grid utilized for the Columbia River estuary. The closely spaced grids are at the Columbia River jetties and the Highway 101 bridge embankment at the entrance to Youngs Bay.*

This may not be the case for some areas, however, if the basic earthquake model is in error (see Appendix A for discussion).

The inundation limit drawn on the maps was ultimately inferred by professional judgment based on (1) the model run-up corrected for coseismic subsidence, (2) topographic elevation contours on the 1:24,000-scale USGS quadrangles, and (3) any detailed topographic data that could be obtained within the time constraints of the project. Professional judgment was based on studies of inundation at Siletz Bay (Priest and others, in preparation) and the Columbia estuary (Figure 8), tempered by field observations of inundation caused by the 1992 Nicaraguan and 1993 Sea of Japan tsunamis (Baptista and others 1993a, b; Baptista and others, 1995a). The limits are thus subject to considerable error and should be supplemented by future, more detailed studies such as that done for Siletz Bay (Priest and others, 1995). These studies are particularly essential for the major estuaries and bays where the inland distance of inundation is greatest and uncertainty is equally great.

Professional judgment was guided by the following procedures:

1. Run-up elevation was inferred from the maximum elevation reached by any wave during 8 hours of simulated tsunami wave activity following the earthquake.

2. No tsunami run-up was assumed to be lower than (a) the run-up predicted for distant tsunamis striking the area at an average recurrence of 500 years (see data of Houston and Garcia, 1978), and (b) any historic run-up from distant tsunamis. The highest well documented historic run-up is from distant tsunamis that struck the Oregon coast from the 1964 Alaskan earthquake (see data of Schatz and others, 1964).

3. Open coastal run-up was assumed to decrease inland in barrier-protected bays and estuaries similar to numerical simulations of run-up at Siletz Bay and the Columbia River (Figure 9). Both estuaries reach the ocean through barrier-protected channels, but the Columbia channel is quite deep, opening into a large estuary, whereas the Siletz estuary is a narrow shallow channel opening into a small shallow bay. The two represent extremes that cover much of the variation in coastal Oregon. Figure 9 shows that in both estuaries run-up is about 30-50 percent lower than open coastal values within the first mile inland of the coastline. Detailed examination of the simulations reveals considerable variation, represented in Figure 9 by error bars. For example, run-up is locally higher if the tsunami partially or completely overtops the barrier, strikes a shoreline directly behind the entrance to an estuary, or enters a constriction in the estuary. The error was generally added to the average run-up value to obtain the final run-up elevation.

4. It was assumed that in barrier-protected bays, the tsunami 1 mile inland of open water would be reduced to a limited surge that would mainly affect areas immediately adjacent to the banks of tidal channels or rivers (Thomas J. Sokolowski, written communication from the Alaska Tsunami Warning Center, 1995). In all small estuaries (smaller than the Columbia River) the run-up more than 14 mi. (22 km) inland was assumed to be confined to existing high water river banks, based on the maximum upstream occurrence of possible overbank deposits from prehistoric tsunamis (unpublished 1995 data of Curt D. Peterson). Run-up was generally not extended inland a significant distance past the tidally influenced portion of any river.

5. Dry-land inundation distance across relatively flat ground was inferred by extrapolating the run-up elevation at the shoreline inland until a barrier was encountered or until a lateral distance was reached that conforms approximately to the following equation: inundation (miles) = run-up (feet)/14. This equation was derived empirically from general observations of dry land and wetland inundation simulated at Siletz Bay and the Columbia River, assuming the largest inundation distances from that data.

6. Shoreline dunes less than two elevation contours higher than the inferred run-up elevation were shown as inundated, if discontinuous. In this case the inundation boundary was drawn landward in a position where more continuous highlands occurred. This seemed prudent, since dunes right at the shoreline could easily be overtopped, if the model elevation were in error by a few feet. Likewise, the ephemeral nature of shoreline dunes and the age of the base maps (1973-1986) cast doubt on the reliability of their mapped location and elevation.

[1] Senate Bill 379 rules (ORS 455.446 and 455.447) provide for an exceptions process and appeals to accommodate future refinement of the inundation maps.

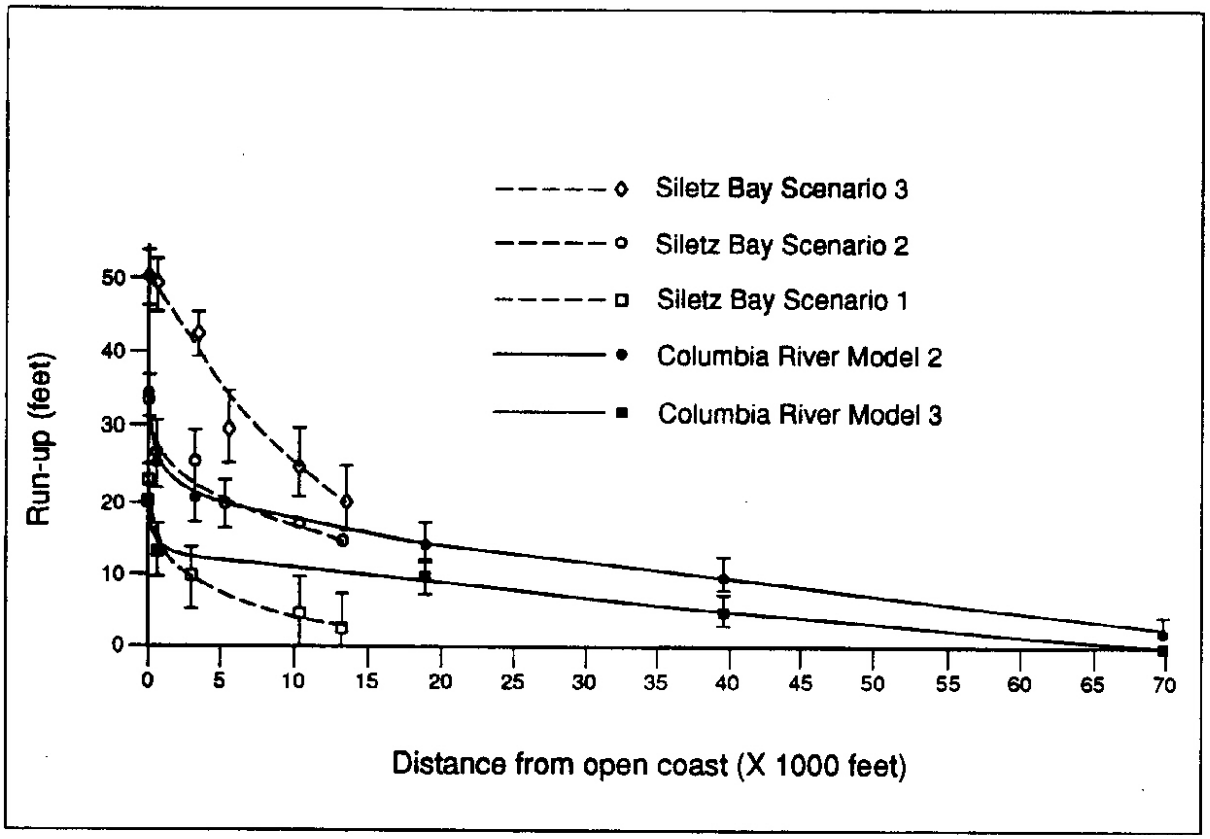


*Figure 9. Variation in numerically simulated run-up elevation in Siletz Bay and the Columbia River at several distances eastward from the open coast. Compiled from numerical simulations at Siletz Bay by Baptista and others (1995) and at the Columbia River by E. P. Myers III and A. M. Baptista of the Oregon Graduate Institute of Science & Technology.*

7. In cases where there were few elevation data, the inundation line was placed where it would provide maximum safety. For example, where the inferred inundation line was between elevation contours, the elevation of the line was estimated by assuming that the slope was about as steep or slightly steeper than surrounding topography. In some cases bench marks provided clues to elevation in areas without detailed contours. In other cases mapped railroad grades, highway grades, and levees that rise above the general land level provided convenient boundaries at the extreme limits of inundation. Areas indicated as wetlands or marsh were generally shown as inundated, particularly where subject to coseismic subsidence.

8. In some areas like Blind Slough on the Columbia River, the numerical models predict little tsunami run-up, but the data from soils buried after prehistoric earthquakes suggest significant subsidence. The flooding that would occur from subsidence in these areas was mapped as the minimum inundation.

9. Areas underlain by deposits inferred to be from historic or prehistoric tsunamis were included in the inundation boundaries. Since tsunamis can inundate without leaving behind a sediment deposit, presence of deposits was considered a good indication of minimum inundation. Maps of deposits and inferred tsunami surge distances up estuaries were referenced from Darienzo and others (1993), Gallaway and others (1992), Peterson and others (1991a), Peterson and others (1993), Peterson and others (1995), and Paul Visher (written communication, 1995).

RESULTS OF THE NUMERICAL SIMULATIONS

Maximum run-up predicted from the simulations is summarized in Figure 10. Appendix B shows detailed graphs for each quadrangle map of the maximum open coastal run-up for Models 2 and 3. Time histories of the arrival of waves for Models 2 and 3 at selected localities (chiefly population centers) are illustrated in Appendix C.

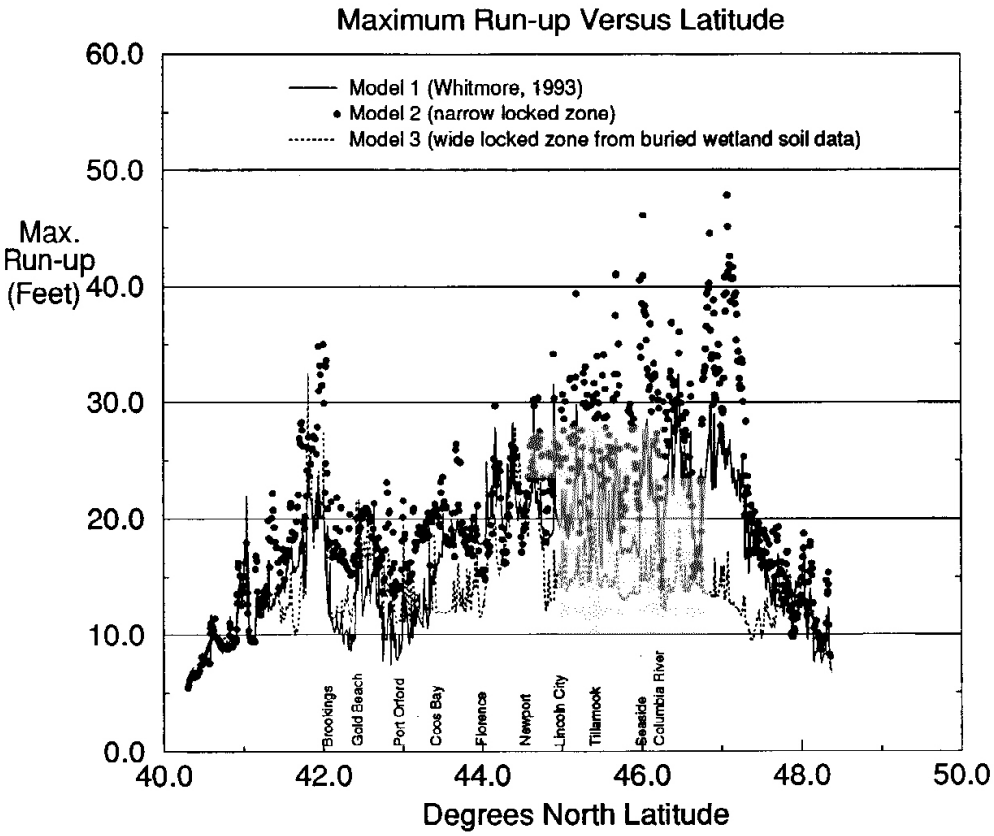


*Figure 10. Maximum run-up elevation at each latitude for Models 1, 2, and 3.*

Figure 11 illustrates parts of the coast that received the highest run-up from all three of the models. In each case it is apparent that offshore banks and canyons cause many of these variations, the canyons funneling wave energy, the banks refracting it in complex ways. Of particular importance is Heceta Bank (Figure 11) which creates an "island" effect, causing the waves to refract around the bank, constructively interfering at Newport and Waldport where run-up is anomalously high (Figure 10).

The location of the sea floor deformation, especially the subsidence, was the key difference between the models with respect to tsunami hazard. As illustrated in Figures 4a, 4b, and 4c, the location of undersea subsidence predicted by each model is increasingly different northward from Coos Bay. The coseismic subsidence of Model 2 is always furthest out to sea and consistently produced the highest run-ups (Figure 10). Model 1 produced intermediate values, and Model 3 the lowest. Model 2 predicted run-ups on the north-central coast mostly clustering around 30-35 feet. North of Tillamook, Model 2 produced open coastal run-ups mostly in the 30- to 40-foot range, reaching a high of 40 to 49 feet in the Seaside area. Model 1 was generally about 25-40 percent lower, and Model 3 about 40-50 percent lower.

All of the models produced little undersea subsidence and relatively small (15- to 25-foot) tsunami waves from Coos Bay and south, because the subduction zone fault is close to shore there. One exception is the Brookings area, where local conditions produced run-up elevations similar to those in northern Oregon. Even though run-up elevations of 15-25 feet are relatively modest, the highest model run-up values in any given locality are still generally a few feet higher than the run-up predicted for distant tsunamis that might strike every 500 years (see data of Houston and Garcia, 1978).

The simulation locally overestimates open coastal run-up by missing bay mouth barriers, owing to the coarseness of the grid. Without the barriers, these bays are modeled as valleys that funnel or focus the wave energy. Therefore, when using the run-up graphs of Appendix B, beware of any anomalous rise in run-up height at a barrier-protected embayment. The clearest example of this problem is at Siletz Bay where predicted run-up for all of the models rises dramatically at the latitude of the Bay relative to bluffs to the north and south. This is not accurate, because detailed numerical simulations (Priest and others, 1995; Baptista and others, 1995b) clearly show that Salishan Spit will dissipate the tsunami energy before it can become concentrated in the embayment. Hence, for Siletz Bay, run-up values listed in Appendix B from north and south of the embayment are probably more representative of the open coastal run-up at the spit.

Open coastal run-up elevations listed here for Models 2 and 3 (Appendix B) in the Siletz Bay-Lincoln City area are within a foot or two of the run-up elevations of Scenarios 2 and 1, respectively, from the map of Priest and others (1995). This is remarkable, since rather different techniques were used in the two studies. The only exception to this generalization is the above-mentioned anomaly at Salishan Spit. Hence, the inundation mapped by Priest and others (1995) was utilized for the equivalent maps of this study.

## VALIDATION FROM PREHISTORIC TSUNAMI RUN-UP ESTIMATES

Estimates of prehistoric tsunami run-up require extensive field studies that are, in most cases, still in progress or on hold pending receipt of adequate financial support. Tsunami run-up estimates from all three models are generally within the uncertainty of the run-up elevations estimated from the prehistoric data.

A recently completed study at Salishan Spit (Priest and others, 1995; Peterson and others, 1995) concluded that prehistoric run-up at the open coast for the tsunamis that struck 300 and 800 years ago could range anywhere from 16 to 39 feet with a most likely run-up of about 23-30 feet. Model 2 predicts about 25-30 feet in the general area where these prehistoric data were studied. Model 1 predicts about 18-20 feet, and Model 3 about 16-19 feet. Hence, all of the models are possible within the range of uncertainty in the prehistoric data.

Gallaway and others (1992) have estimated from overtopped barriers at Cannon Beach that run-up for the tsunamis that struck about 300 and 800 years ago probably exceeded the minimum barrier height of 16 feet, but the maximum run-up is not known with any certainty. Model 3 predicts 17 feet there, Model 1, 19-20 feet, and Model 2, 31-33 feet, so all of the models are possible within the errors due to tides and the simulation technique itself.

Darienzo and others (1993) concluded that much of the barrier ridge on the west bank of Neawanna Creek at Seaside may not have been overtopped by the tsunamis that struck 300 and 800 years ago. This barrier is currently about

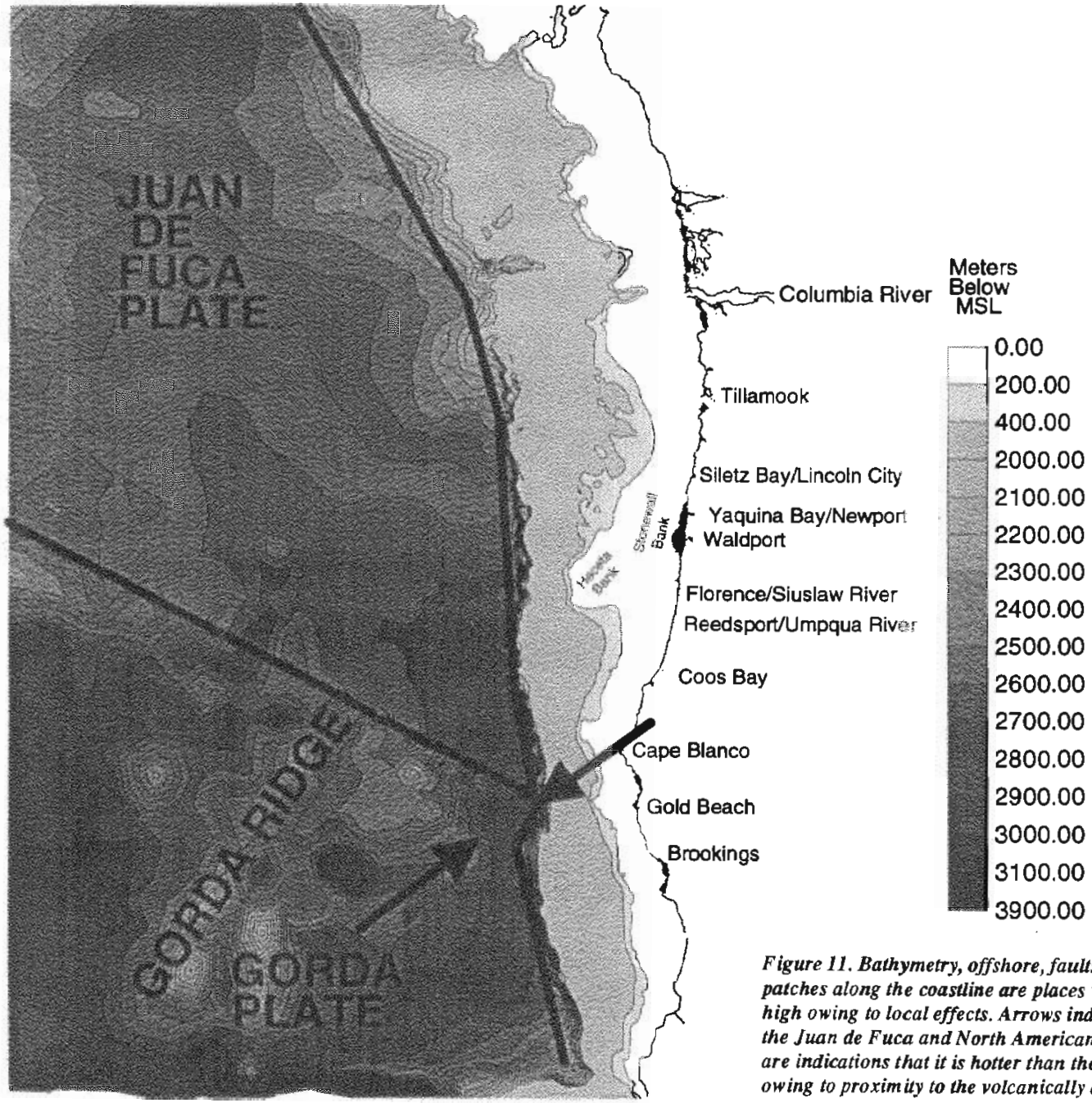


*Figure 11. Bathymetry, offshore, faults and geographic features. Dark patches along the coastline are places where tsunami run-up was particularly high owing to local effects. Arrows indicate convergence direction between the Juan de Fuca and North American plates. Highlands on the Gorda Plate are indications that it is hotter than the Juan de Fuca plate to the north, owing to proximity to the volcanically active Gorda Ridge.*

20-22 feet high, decreasing to an elevation of 15 feet at its south end, where it was breached by the prehistoric tsunamis. This 15-feet of elevation is misleading, since considerable fill has been placed there. The highest part of the barrier ridge is 2,500 feet inland of the open coast, so any ancient tsunami would have had to overtop the first barrier ridge at the shoreline and cross the Necanicum River before striking this second ridge. A tsunami would have decreased significantly in height while traveling this far. Estimating the open coastal run-up from this evidence is very difficult without detailed numerical modeling. Model 3 predicts an open coastal run-up of 18 feet where the barrier ridges were overtopped on the south, Model 1, 25 feet, and Model 2, 40 feet. None of the models can be ruled out by the evidence at Seaside.

Studies of small shoreline lakes in southern Oregon by Harvey Kelsey of Humbolt State University and Alan Nelson of the U.S. Geological Survey are still being conducted and have not yielded final results. Many of these lakes have apparent tsunami sand layers and are separated from the coast by barriers with present elevations on the order of 10-20 feet. The inferred inundation by most of the model tsunamis examined here are all very similar in southern Oregon and are high enough, within the uncertainties of the run-up estimates, to inundate all of these lakes.

VALIDATION FROM OBSERVATIONS OF THE 1964 TSUNAMI

The great Alaska earthquake of March 27, 1964 produced large tsunami waves which struck the Oregon coast several hours after the earthquake. The 1964 tsunamis approximate the run-up predicted by Houston and Garcia, (1978) for distant tsunamis that could strike on average every 500 years. One would expect that a distant tsunami would generally produce run-up significantly lower than that of a locally generated tsunami, provided that the source earthquakes were of similar magnitude. Since the earthquake simulated here and the Alaskan event approximate magnitude 9, this condition is satisfied.

The observed run-up in Oregon from the Alaskan tsunami waves, as compiled by Schatz and others (1964), was generally lower than any of the model waves examined here, except on the south coast. From Florence south to the Coquille River, the 1964 run-up was in many cases equal to or slightly larger than the modeled run-up for Model 3 but smaller or subequal to that of Model 2.

The run-up from the 1964 Alaskan wave at the Siuslaw River was 12 feet above mean high water, or about 16 feet above mean sea level. The location of this observation, as shown on the Schatz and others (1964) map, appears to be at Florence. This implies an open coastal run-up higher than 16 feet, since Florence is about 4 river miles inland of the coastline; however, the narrow estuary leading from the open coast to Florence may maintain or amplify the wave height of open coastal tsunamis. This possibility needs to be studied by detailed numerical simulations. The simulation of a 500-year distant tsunami by Houston and Garcia (1978) predicts a 16 foot run-up at the open coast, assuming a statistically average tide. Model 2 predicts open coastal run-up of 18-20 feet and Model 3, 12-18 feet, assuming tide at mean higher high water (12-16 feet and 8-14 feet, respectively, for waves arriving at a mean tidal level). Hence, Models 2 and 3 seem somewhat low in light of the simulations and actual field observations of distant tsunamis.

The maximum run-up from the 1964 Alaskan event at the mouth of the Umpqua River is on the order of 14 feet above mean high water, or about 18 feet above mean sea level. The locality of this observation is difficult to specify precisely from the map of Schatz and others (1964), but it appears to be within the estuary in the vicinity of Winchester Bay. This would imply a run-up at the open coast higher than 18 feet. Open coastal run-up for Model 3 is about 12-16 feet and for Model 2, 18-28 feet with tide at mean higher high water (8-12 feet and 14-24 feet, respectively, at a mean tidal level). Predicted open coastal run-up for the 500-year distant tsunami of Houston and Garcia (1978) is about 13 feet at a statistically average tide. The Model 3 simulation appears to underestimate the hazard.

The above observations suggest that in the Florence-Coquille River area simulations of locally generated tsunamis are not a great deal larger than the largest distant tsunamis. It also appears that the Model 3 simulation produces tsunamis that are slightly smaller than the 1964 Alaskan tsunamis. The latter observation implies that either (1) there is an error in the simulation process for Model 3, or (2) locally generated tsunamis may actually be smaller than the largest distant tsunamis in this area. As explained below and in Appendix A, the former is more likely the case.

## PRECISION AND ACCURACY OF THE INUNDATION LINES

One of the largest sources of error is uncertainty in the absolute run-up elevation at the open coast. The fault dislocation modeling technique is the reason for most of this uncertainty. As explained in detail in Appendix A, the Okada (1985) fault dislocation software inaccurately portrays certain aspects of the coseismic uplift and does not properly reproduce coseismic deformation above partially locked areas of the subduction zone fault. The discussion in Appendix A shows that coseismic (during the earthquake) sea floor deformation extrapolated directly from interseismic (between earthquakes) deformation rates of Hyndman and Wang (1993), eliminates many of the errors associated with the Okada software, but the extrapolation is only a crude approximation, particularly for the southern part of the coast. Maximum tsunami run-up predicted by a preliminary numerical simulation of the Hyndman and Wang (1993) deformation data is similar to the maximum run-up predicted by Model 2, even though the sequence and timing of simulated tsunami waves and troughs (the time history) is more similar to Model 3 (see Appendix A). Recent interpretations of the rate of rise of the Oregon coastline (Hyndman and Wang, 1995) suggest that the locked zone on the Cascadia fault may be narrower than assumed by Hyndman and Wang (1993) and much narrower than that of Models 1, 2, or 3. As illustrated by Models 2 and 3 (Figures 4b, 4c, and 10), narrowing the locked zone generally produces higher tsunamis, so this could be a source of error, particularly from Cape Blanco south (see discussion in Appendix A). Fortunately, the steep coastal terrain on the southernmost Oregon coast limits inundation, so any future revision of the maps is likely to be small.

Regarding accuracy of the lines, as explained above, the vertical uncertainty in open coastal run-up elevation is on the order of 50 percent between the numerical models. The greatest uncertainty is in the inundation distance (horizontal accuracy), since the numerical grids were not refined enough to simulate the details of the dry land topography or the shallow water bathymetry. Since professional judgment was used to infer inundation, the resulting error is difficult to quantify, but is very large at bays and estuaries and smaller at steep bluffed shorelines.

In all cases the precision of the inundation lines is limited by the scale of the maps to no better than ±40 feet horizontal and ±10 feet vertical. Horizontal precision is no more than the width of the drawn line, which is about ±0.02-0.03 inches or about ±40-60 feet on the ground. The precision of reference features such as roads, etc., on the map itself is ±0.02 inches (±40 feet on the ground). Vertical precision depended on the spacing of the elevation contours and the proximity of the contours to the inferred run-up elevation. The maximum uncertainty between contours is 100 percent of the contour interval. Contour intervals on the base maps are either 20, 25, or 40 feet. Where the inundation line fell by chance at or very close to a contour, the precision is approximately ±10 feet.

In local areas more detailed topographic data were available and were utilized. Elevation contours at intervals of 2 feet were utilized in Coos Bay, North Bend, Reedsport, Winchester Bay, Warrenton, Clatsop Spit, Gearhart, Seaside, and Cannon Beach. Contours at intervals of 5 feet were available from the D River to Gleneden Beach Wayside. Contours at intervals of 10 feet were available at Yaquina Bay and South Beach. When transferred to the 1:24,000-scale base maps of this study, much of this detail is lost, however.

In low-lying forested areas, there can be considerable error in the elevation contours. In a field check of northern Cannon Beach and several areas of southeastern Seaside, contours on the USGS quadrangle were clearly higher than the ground by 20-50 feet, owing to the air photo analyst placing them near the tops of trees. Since this error can cause the drawn inundation not to reach as far inland as it should, users should not use the published maps blindly. Instead, use field observations to make sure that forested areas not in the mapped inundation zone. Refer to run-up elevations listed in Appendix B, and, if there is a potential problem, call the Oregon Department of Geology and Mineral Industries for advice.

Finally, the tidal level and rises in sea level from storms or El Ninõs at the time of an actual tsunami could change the run-up elevation by ±3-5 feet from the mean higher high water level of +4 feet assumed in the simulation. This would also make significant changes in the horizontal position of the inundation lines.

All estuaries and bays need more detailed treatment than possible in this project. The Oregon Department of Geology and Mineral Industries will be happy to cooperate with efforts to refine any of the inundation boundaries.

## CONCLUSION

All three of the numerical simulations are possible scenarios within the uncertainty of the run-up estimated for prehistoric tsunamis, although the run-up elevations from Model 2 and time histories from Model 3 are most consistent with the available data. Based on observations of run-up on the southern Oregon coast from distant tsunamis, Model 3 may predict run-up that is too low there. In any case, Models 2 and 3 generally represent the extreme high and low scenarios for inundation using software based on the Okada (1985) fault dislocation model, but the software has a shortcoming. It cannot precisely simulate partial locking down dip and stable sliding up dip of the locked zone on the subduction zone fault (see Appendix A for discussion). When a preliminary numerical simulation was done in an attempt to eliminate these problems, while matching interseismic deformation data of Hyndman and Wang (1993), the simulated tsunamis produced maximum run-ups similar to Model 2 and time histories (sequence and timing of waves) similar to Model 3 (see Appendix A). All of the models (and the preliminary simulation) may underestimate maximum tsunami run-up, if recently published estimates of the width of the locked portion of the Cascadia subduction zone (i.e. Hyndman and Wang, 1995) are correct (Appendix A). However, this underestimate of run-up elevation may only be a problem for the coast from Cape Blanco south, and even there, only modest revision of the existing inundation maps is likely (see discussion in Appendix A).

Revision of the inundation maps is recommended once uncertainties in the width of the locked and partially locked portions of the Cascadia subduction zone are resolved and more accurate fault dislocation modeling software is available. The more accurate software will need to be fully three dimensional like the Okada (1985) model, accurately simulating partial locking, locking, and stable sliding on the subduction zone fault.

## USE OF THE MAPS

Owing to uncertainties in location of the tsunami flooding lines, the lines are not in general recommended for site-specific land use and engineering decisions. The maps are designed only for preliminary screening of sites for new essential and special occupancy structures, as required by Senate Bill 379 (ORS 455.446 and 455.447). The maps are not intended to be land use planning documents. They have been produced purely in the interest of public safety relative to essential facilities and in the context of an informed exceptions process.

Whereas the maps, when used in concert with other information, may also be useful for tsunami evacuation planning, it must be kept in mind that they were not produced for that purpose. Maps with additional factors of safety may be more appropriate for planning evacuation routes. For example, a tsunami about 10-50 percent higher than any of the model tsunamis used here is the basis for evacuation planning in the Eureka and Crescent City areas of northern California (see Scenario 3, Figure 8, of Priest and others, 1995; Toppozada and others, 1995).

## RELATED HAZARDS

In areas north of Florence and possibly on the south coast as well, coastal erosion and long term (tens of years) flooding are likely to result from the sudden subsidence that accompanies great (M 8-9) earthquakes. Beaches and foredunes on the open coast can be partially or completely removed by wave erosion over a period of years when an area subsides. Any loss of the buffering effect of beaches will make open coastal bluffs subject to severe erosion by storm waves.

Local areas south of Florence may experience up to a few feet of coseismic uplift. Docks and other facilities that need to be at the shoreline may be affected.

WHAT TO DO IN THE EVENT OF AN EARTHQUAKE

In the event of a large undersea earthquake on the coast, ***water will begin to rise in most areas immediately after the earthquake***, about 14 to 30 minutes elapsing before the first wave crest arrives (see Appendix C for guidance on tsunami arrival times). Therefore ***if you feel an earthquake with 20 seconds or more of strong ground shaking, head immediately inland or to high ground***. ***In many cases waves arriving in the second or third hour may be as high or higher than the first wave, and dangerous activity will continue for 8 to 10 hours, so do not go back to the shoreline until an official "all clear" is issued***. Strong shaking is enough to make it hard to stand up during the earthquake. These guidelines will eliminate most false alarms, but, since large tsunamis can be generated by less felt shaking, local jurisdictions may choose to use more conservative thresholds for evacuation (e.g., any felt earthquake).

ACKNOWLEDGMENTS

Eward P. Myers III and António M. Baptista of the Oregon Graduate Institute of Science & Technology provided the digital bathymetry, topography, and the fault dislocation software. They also ran the simulations of tsunami waves produced by the fault sources developed here. The project could not have been completed in its present form without their help and the resources of the Oregon Graduate Institute of Science & Technology. Curt D. Peterson graciously provided his unpublished compilation of coseismic subsidence estimates for the Oregon coast. This data set was crucial for development of Model 3, evaluation of the models, and calculation of the final tsunami run-up elevation. Paul M. Whitmore and Thomas J. Sokolowski of the Alaska Tsunami Warning Center offered advice and guidance that were essential to the project. Charles L. Mader of the Mader Consulting Company provided help in obtaining digital elevation and bathymetric data. George D. Curtis and Gus Furumoto of the University of Hawaii offered much-needed advice about general methods and realistic expectations early in the project. Hiroo Kanamori of the California Institute of Technology, Thomas S. Yelin of the U.S. Geological Survey, and Robert S. Crosson of the University of Washington gave generously of their time in discussions of possible fault slip and magnitude for subduction zone earthquakes. The project also benefited from discussions with Craig S. Weaver, U.S. Geological Survey; Kelin Wang, Geological Survey of Canada; and David D. Blackwell, Southern Methodist University, regarding earthquake source mechanisms and heat flow. Paul Visher and Alfred Aya of Cannon Beach, Oregon, provided highly detailed topographic maps of the Cannon Beach and Seaside areas, as well as guidance in mapping tsunami inundation in those areas. António Baptista, Curt Peterson, Paul Whitmore, Kelin Wang, and Tom Yelin reviewed the paper. Donald A. Hull, John D. Beaulieu, and Beverly F. Vogt of the Oregon Department of Geology and Mineral Industries also provided helpful reviews. Earlier detailed tsunami hazard studies of the Siletz Bay area greatly aided the mapping and analysis (see Priest and others, 1995, for funding sources). An unpublished topographic map of the Newport area improved the accuracy of the inundation mapped there and was produced for an ongoing tsunami hazard investigation with support from the U.S. Army Corps of Engineers and the City of Newport. Staff from local government in Clatsop County, Winchester Bay, Reedsport, Coos Bay, and North Bend provided detailed topographic maps and much needed advice.

## REFERENCES CITED

Atwater, B.F., Nelson, A.R., Clague, J.J., Carver, G.A., Yamaguchi, D.K., Bobrowsky, P.T., Bourgeois, J., Darienzo, M.E., Grant, W.C., Hemphill-Haley, E., Kelsey, H.M., Jacoby, G.C., Nishenko, S.P., Palmer, S.P., Peterson, C.D., and Reinhart, M.A., 1995, Summary of coastal geologic evidence for past great earthquakes at the Cascadia subduction zone: Earthquake Spectra, v. 11, no. 1, p. 1-18.

Baptista, A.M., Myers, E.P. III, and Priest, G.R., in preparation, Regional propagation patterns of Cascadia subduction zone tsunamis.

Baptista, A.M., Priest, G.R., and T.S. Murty, 1993a, Field survey of the 1992 Nicaragua Tsunami: Marine Geodesy, v. 16, p. 1-24.

Baptista, A.M.,. Priest, G.R, and T.S. Murty, 1993b, Field Data for the 1992 Nicaragua Tsunami: Synthesis and Interpretation: Proceedings of the IUGG/IOC International Tsunami Symposium, p. 871-880

Baptista, A.M., Priest, G.R., and Tanioka, 1995a, A post-tsunami survey of the 1993 Hokkaido tsunami [abstract]: EOS Transactions of the American Geophysical Union, v. 74, no. 43, p. 350.

Baptista, A.M., Qi, M., and Myers, E.P. III, 1995, Siletz Bay: a pilot investigation of coastal inundation by Cascadia subduction zone tsunamis, *in* Priest, G.R., ed., Explanation of mapping methods and use of the tsunami hazard map of the Siletz Bay area, Lincoln County, Oregon: Oregon Department of Geology and Mineral Industries Open-File Report O-96-5, p. 21-41.

Briggs, G.G., 1994, Coastal crossing of the elastic strain zero-isobase, Cascadia margin, south central Oregon coast: Portland, Oregon, Portland State University masters thesis, Figure 19, p. 176, 251 p.

Darienzo, M., Craig, S., Peterson, C.D., Watkins, A., Wienke, D., Wieting, and Doyle, A., 1993, Extent of tsunami sand deposits landward of the Seaside Spit, Clatsop County, Oregon: Final Report to Clatsop County Sheriff's Office, 25 p.

Darienzo, M.E., and Peterson, C.D., 1995, Magnitude and frequency of subduction-zone earthquakes along the northern Oregon coast in the past 3,000 years: Oregon Geology, v. 57, no. 1, p. 3-12.

Gallaway, P.J., Peterson, C.D., Watkins, A.M., Craig, S., and McLeod, B.L., 1992, Paleo-tsunami inundation and run-up at Cannon Beach, Oregon: Final Report submitted to Clatsop County Sheriff's Office, Clatsop, County, Oregon, 36 p.

Goldfinger, C., Kulm, L., Yeats, R., Mitchell, C., Weldon, R., II, Peterson, C., Darienzo, M., Grant, W., and Priest, G.R., 1992, Neotectonic map of the Oregon continental margin and abyssal plain: Oregon Department of Geology and Mineral Industries Open-File Report O-92-4.

Hanks, T.C., and Kanamori, H., 1979, A moment magnitude scale: Journal of Geophysical Research, v. 84, p. 2348-3250.

Houston, J.R., and Garcia, A.W., 1978, Type 16 flood insurance study: tsunami predictions for the west coast of the continental United States: P.O. Box 631, Vicksburg, Miss., U.S. Army Engineer Waterways Experiment Station, Hydraulics Laboratory, Technical Report H-78-26, 38 p.

Hyndman, R.D., and Wang, K., 1993, Thermal constraints on the zone of a major thrust earthquake failure: the Cascadia subduction zone: Journal of Geophysical research, v. 98, no. b2, p. 2039-2060.

Hyndman, R.D., and Wang, K., 1995, The rupture zone of Cascadia great earthquakes from current deformation and the thermal regime: Journal of Geophysical Research, v. 100, no. B11, p. 22,133-22,154.

Kelsey, H.M., Witter, R.C., and Polenz, M., 1993, Cascadia paleoseismic record derived from late Holocene fluvial and lake sediments, Sixes River Valley, Cape Blanco, south central Oregon.

Luettich, R.A., Jr., and Westerink, J.J., 1995a, Implementation and testing of elemental flooding and drying in the ADCIRC hydrodynamic model: Department of the Army, U.S. Army Corps of Engineers, Washington, D. C Report., Contract No. DACW39-94-5869, 16 p. plus figures.

Luettich, R.A., Jr., and Westerink, J.J., 1995b, An assessment of flooding and drying techniques for use in the AD-CIRC hydrodynamic model: Implementation and performance in one-dimensional flows: Department of the Army, U.S. Army Corps of Engineers, Washington, D.C Report., Contract No. DACW39-94-5869, 12 p. plus figures.

Madin, I., 1992, Seismic hazards on the Oregon coast, in Good, J.W and Ridlington, S.S., eds., Coastal natural hazards science, engineering, and public policy: Oregon Sea Grant, No. ORESU-B-92-001, p. 3-27.

Mitchell, C.E. Vincent, P., Weldon, R.J., II, and Richards, M.A., 1994, Present-day vertical deformation of the Cascadia margin, Pacific Northwest, U.S.A.: Journal of Geophysical Research, v. 99, p. 12,257-12,277.

Myers, E.P., and Baptista, A.M., 1995, Finite element modeling of the July 12, 1993 Hokkaido Nansei-Oki tsunami: Pure and Applied Geophysics, v. 144 , no. 3/4, p. 1070-1102 (in press).

Myers, E.P. III, Baptista, A.M., and others, in preparation, Finite element modeling of hypothetical Cascadia subduction zone tsunamis.

Nelson, A.R., Atwater, B.F., Bobrowsky, P.T., Bradley, L., Clague, J.J., Carver, G.A., Darienzo, M.N., Grant W.C., Krueger, H.W. Sparks, R., Stafford, T.W., Jr., and Stulver, M., 1995, Radiocarbon evidence for extensive plate-boundary rupture about 300 years ago at the Cascadia subduction zone: Nature, v. 378, no. 23, p. 372-374.

Okada, Y., 1985, Surface deformation due to shear and tensile faults in a half-space: Bulletin of the Seismological Society of America, v. 75, no. 4, p. 1135-1154.

Peterson, C.D., and Briggs, G.G., 1992, Response of coastal depositional systems to tectonic strain cycles in the Cascadia subduction of the U.S. Pacific Northwest [abstract]: 29th International Geological Congress, Kyoto, Japan, v. 2, p. 314, unpublished illustration handed out at the meeting.

Peterson, C.D., Darienzo, M.E., Burns, S.F., and Burris, W.K., 1993, Field trip guide to Cascadia paleoseismic evidence along the northern Oregon coast: Evidence of subduction zone seismicity in the central Cascadia margin: Oregon Department of Geology and Mineral Industries, Oregon Geology, v. 5, no. , p. 99-114.

Peterson, C.D., Darienzo, M.E., Clough, C., and Baptista, A.M., 1991a, Paleo-tsunami evidence in northern Oregon bays of the central Cascadia margin: Final technical progress report submitted to Oregon Department of Geology and Mineral Industries, 28 p.

Peterson, C.D., Darienzo, M.E., and Clough, C., 1991b, Recurrence intervals of coseismic subsidence events in northern Oregon bays of the Cascadian margin: Final technical progress report to Oregon Department of Geology and Mineral Industries, 14 p.

Peterson, C.D., Darienzo, M.E., Doyle, D.D., and Barnett, E.,1995, Evidence for coseismic subsidence and tsunami inundation during the past 3000 years at Siletz Bay, Oregon, *in*, Priest, G.R., ed., Explanation of mapping methods and use of the tsunami hazard map of the Siletz Bay area, Lincoln County, Oregon: Oregon Department of Geology and Mineral Industries Open-File Report O-96-5, p. 45-69.

Priest, G.R., Baptista, A., Qi, M., Peterson, C.D., and Darienzo, M.E., 1995, Simplified explanation of the tsunami hazard map of the Siletz Bay area, Lincoln County, Oregon *in* Priest, G.R., ed., Explanation of mapping methods and use of the tsunami hazard map of the Siletz Bay area, Lincoln County, Oregon: Oregon Department of Geology and Mineral Industries Open-File Report O-96-5, p. 1-20.

Schatz, C.E., Curl, H.C., Jr., and Burt, W.V., 1964, Tsunamis on the Oregon coast: Oregon Department of Geology and Mineral Industries, Ore Bin, v. 26, no. 12, p. 231-232.

Scholz, C. H., 1990, The mechanics of earthquakes and faulting: New York, N. Y., Cambridge University Press, p. 182.

Toppozada, T., Borchardt, G., Haydon, W., Petersen, M., Olson, R., Lagorio, H., and Anvik, T., 1995, Planning scenario in Humbolt and Del Norte Counties, California, for a great earthquake on the Cascadia subduction zone: California Division of Mines and Geology, Special Publication 115, 157 p.

Trehu, A.M., Asudeh, I., Brocher, T.M., Luetgert, J.H., Mooney, W.D., Nabelek, J.L., and Nakamura, Y., 1994, Crustal architecture of the Cascadia forearc: Science, v. 266, p. 237-243.

Weaver, C.S., and Shedlock, K. M., 1989, Potential subduction, probable intraplate, and known crustal earthquake source areas in the Cascadia subduction zone, *in* Hays, W.W., ed., Proceedings of the 3rd Annual Workshop on Earthquake Hazards in the Puget Sound, Portland area: U.S. Geological Survey Open-File Report 89-465, p. 11-26.

Whitmore, P. M., 1993, Expected tsunami amplitudes and currents along the North American coast for Cascadia subduction zone earthquakes: Natural Hazards, v. 8, p. 59-73.

## APPENDIX A

## TECHNICAL DISCUSSION OF FAULT PARAMENTERS AND RESULTING TSUNAMI SIMULATIONS

### FAULT LENGTH

Fault length was set equal to 404-miles (650-km) based on a fault segment from Weaver and Shedlock (1989). This length may, in fact, underestimate the maximum possible rupture length, if the conclusions of Atwater and others (1995) are correct. In any case this length was convenient for the simulation, since it generates tsunami waves from the closest possible source throughout the Oregon coast.

### AMOUNT AND DIRECTION OF FAULT SLIP

A fault slip as large as 43 feet (13 m) can be justified for a 404-miles (650-km) rupture based on the empirical ratio of $2 \times 10^{-5}$ determined by Scholz (1990) to be the minimum ratio of slip divided by fault length for interplate thrust faults. Assuming a Mw 8.8 earthquake, Whitmore (1993) derived a slip of 29 feet (8.7 m) using the seismic moment formula of Hanks and Kanamori (1979): Mo = (mu) (length) (width) (slip). All values were known but slip. Using this same technique and assuming a rigidity (mu) of $4 \times 10^{11}$ dyne $cm^{-2}$, a slip of 38 feet (11.5 m) is needed to generate a Mw 8.8 earthquake using the 41.3-mile (66.5 km)- wide locked zone of Model 2. The prehistoric subsidence data used in Model 3 requires a slip of about 34.4 feet (10.5 m), which allows the Okada (1985) model to generate the maximum subsidence of $6.6 \pm 0.8$ feet ($2 \pm 0.25$ m) indicated by prehistoric subsidence data from the Blind Slough area of the Columbia River (unpublished 1995 compilation by Curt D. Peterson, 1995). This slip, when combined with the rather wide rupture of Model 3, produces an earthquake of approximately Mw 8.9.

There is no data to constrain the slip direction. The rake angle, was therefore assumed to be 90° (pure dip slip motion straight up the fault plane).

FAULT DIP

According to Trehu and others (1994), the dip on the Cascadia subduction zone in Oregon at the latitude of Cape Foulweather varies from 3-5° at the continental slope to 13-16° under the Coast Range. The region of interest for use of the Okada (1985) model is the locked portion of the fault located near the coastline and under the continental shelf, extending to within 5 km of the deformation front. Using the data of Trehu and others (1994), the dip under the shelf and coastline is on the order of 11° with an average of 10.5° from the toe of the continental slope to the coast.

Okada's (1985) model assumes a horizontal surface above the fault, but the sea floor slopes at an average angle of 1.6° from the coast to the deformation front, generating a volume of water below mean sea level that the model assumes is rock. This can be corrected by scaling the dip from the sea surface directly above the trace of the fault to the coastline, where, according to Trehu and others (1994), the fault lies at 22 km depth. This operation yields a model dip of 12.1°, similar to the dip of 13° used by Whitmore (1993) and the 11.8° used by Hyndman and Wang (1993) for their Oregon simulation. This value of 12.1° was used for Models 2 and 3.

METHODS AND UNCERTAINTIES IN SIMULATING EARTHQUAKE DEFORMATION

Hyndman and Wang (1993) presented a two-dimensional fault dislocation model that predicts an overall rate of interseismic horizontal and vertical deformation that satisfies observed horizontal strain measurements and heat flow data in northern Oregon and Washington (Figures A1 and A2). Their model accounts for a locked zone approximately 43 miles (70 km) wide in northern Oregon, extending to a temperature of 350 °C, and a partially locked zone, the amount of locking decreasing linearly to zero at 450 °C over an additional 43 miles (70 km) down the dip on the fault (Figures A1 and A2). Their 1993 model did not take into account Trehu and others' (1994) data on the dip of the subduction zone. The Model 2 locked zone used here was assumed to extend to 350 °C, the depth being estimated from the Oregon temperature profile of Hyndman and Wang (1993) and the dip of the fault from Trehu and others (1994). Since the Okada (1985) fault dislocation software cannot accurately simulate partial locking of the fault, no attempt was made to extend the locked zone to higher temperatures (greater depths). As explained in the main body of the text, the width of the Model 3 locked zone was set by trial and error using the Okada (1985) technique to produce coseismic deformation matching prehistoric coastal subsidence estimated from geologic analysis of buried soils, mainly from data north of Cape Blanco. The resulting Model 3 locked zone is nearly twice as wide as that of Model 2.

An additional experiment was conducted to examine whether the disparity between Models 2 and 3 is from lack of accurate simulation of the deformation above the partially locked zone on the Cascadia subduction zone. Coseismic deformation over the locked and partially locked zones can be approximated from Hyndman and Wang's (1993) interseismic deformation rates by assuming that all deformation is recovered during the earthquake (perfect elastic recovery). The amount of deformation is then simply calculated by multiplying their rate by the time that elapses between earthquakes. The error caused by assuming perfectly elastic deformation is probably small, since inelastic deformation, as expressed in uplifted marine terraces along the coast, is about an order of magnitude smaller than interseismic deformation. For example, on the central Oregon Coast the marine terrace inferred to be about 80,000 years old is either close to sea level or only a few tens of feet about sea level. Hence, the inelastic vertical strain rate is at most about 0.05 inches/yr (0.2 mm/yr), much smaller than the interseismic rates of Figure A1. Some aseismic slip (creep) can, in some cases, release strain on deeper portions of a subduction zone fault a few days or tens of years after earthquakes (Hyndman and Wang, 1995), introducing an additional source of error. Another error is caused by not correcting the model for new data from Trehu and others' (1994) study, but this makes only a small

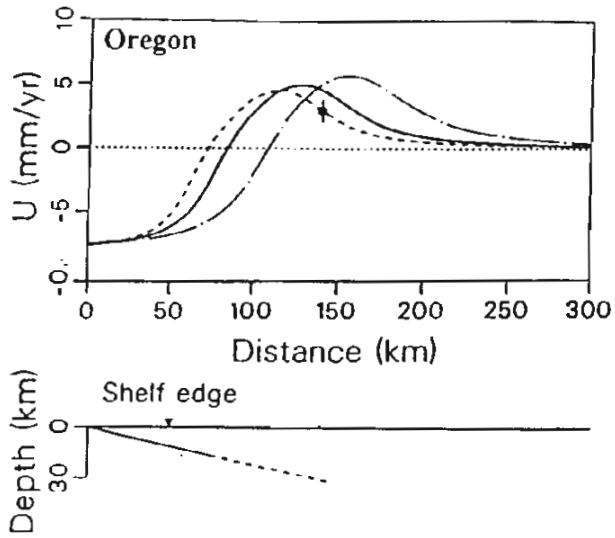


*Figure A1. The upper figure shows the vertical rate of deformation (U) versus distance along the Oregon transect mapped in Figure A2. The lower figure shows a vertical cross section of the model subduction zone fault with zones of full (solid line) and partial (dashed line) locking. Taken from Hyndman and Wang (1993).*

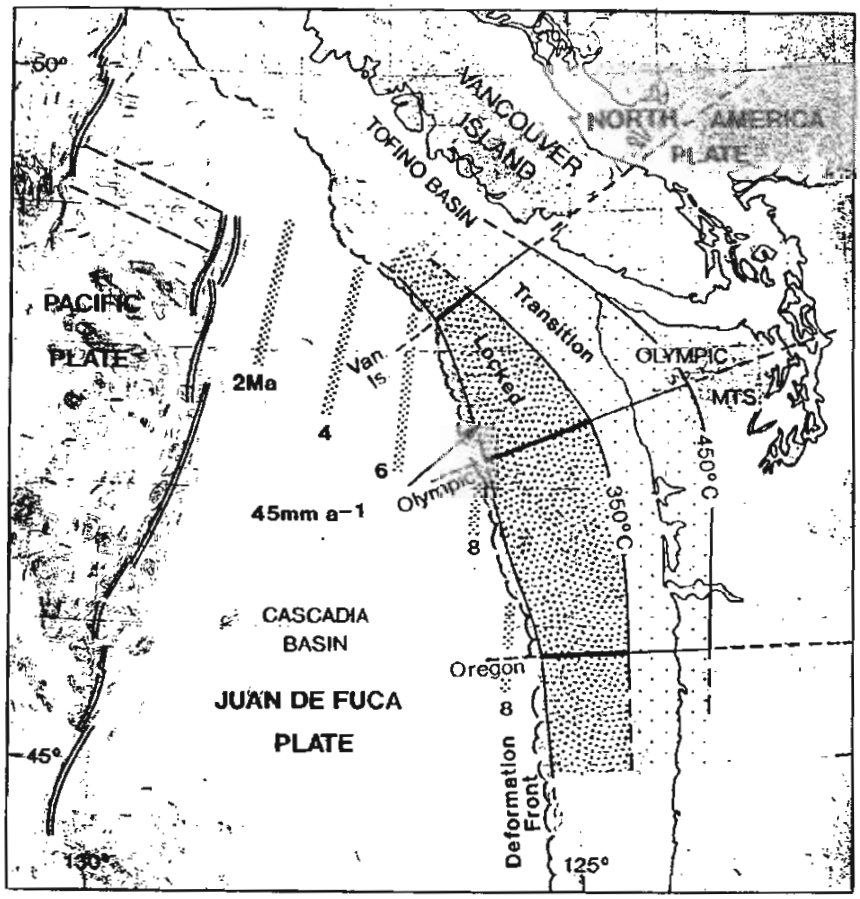


*Figure A2. Map of transects modeled for interseismic deformation rates in the study of Hyndman and Wang (1993). The closely stippled region lies over the fully locked part of the Cascadia subduction zone. The lightly stippled region is partially locked, varying linearly from fully locked at 350 °C to unlocked at 450 °C. Taken from Hyndman and Wang (1993)*

(10 km) difference in the width of the inferred locked zone, well within the ±20 km error in the technique (Hyndman and Wang, 1995). In the following discussion vertical coseismic deformation inferred from interseismic deformation rates of Hyndman and Wang (1993) is referred to as the HW model or HW deformation.

To compare the vertical coseismic deformation of the HW model with Models 1, 2, and 3 of this paper, two extreme cases were examined. In one case the HW rates were multiplied by the time needed to produce uplift matching the maximum uplift of 17 ft (5 m), which occurs in Model 2; in the other case a match was made to the maximum subsidence of 6.6 ± 0.8 feet (2.0 ± 0.25 m) in Model 3. Recall that the Model 3 subsidence is the value inferred from study of buried wetland soils (unpublished 1995 data of Curt D. Peterson). The first HW model requires an earthquake recurrence of about 600 years and produces a zone of maximum uplift much wider than any of the models, while causing maximum subsidence over 50 percent larger than the maximum inferred from the buried soils (Figure A3). The HW model matching the maximum prehistoric (Model 3) coseismic subsidence of 6.6 ± 0.8 feet (2.0 ± 0.25 m) requires an earthquake recurrence of 400 ± 50 years. Multiplying 450 years (mean plus the uncertainty) by the HW deformation rates produces a wide zone of undersea uplift about 3 feet (1 m) higher than that of Model 3, except at the shallow end of the fault, where Model 3 produces a narrow zone about 5 feet (1.5 m) higher than the HW model (Figure A3). This HW model seems to be the most geologically reasonable, approximately matching the east-west location of subsidence inferred from buried soils on the northern coast (Figure A3) and the recurrence of 400 ± 200 years inferred from dating the soils (i.e. Peterson and others, 1991; Darienzo and Peterson, 1995). Hence, when the partially locked zone is taken into account, coseismic subsidence data from buried soils and from temperature data can possibly be accounted for in a single fault dislocation model.

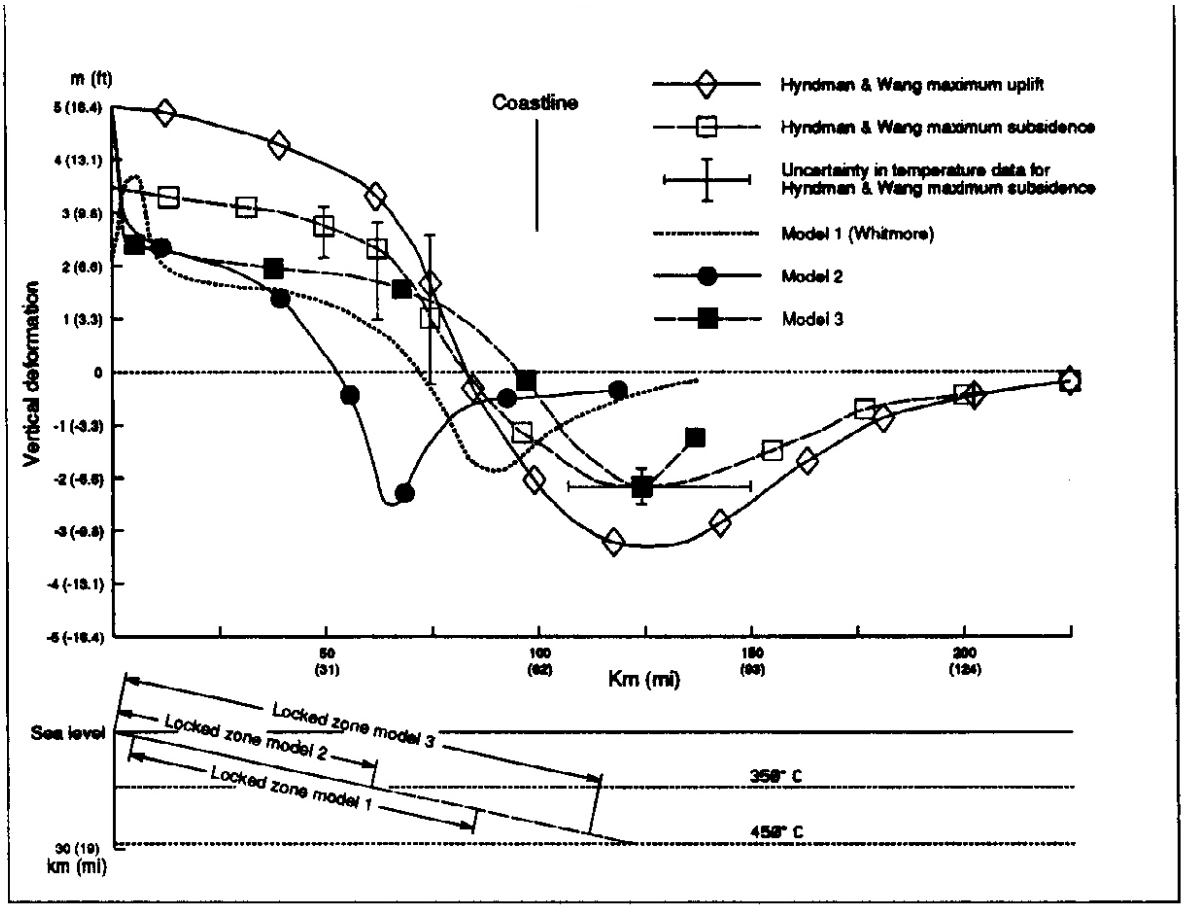


*Figure A3. Upper diagram shows coseismic deformation on the Cascadia subduction zone inferred from Okada (1985) fault dislocation software (Models 1, 2, and 3) and from interseismic deformation rates of Hyndman and Wang (1993)(HW). The two HW deformation patterns are derived by applying enough time between earthquakes for the HW rates to produce the maximum uplift (diamonds) and maximum subsidence (squares) of Model 3. Lower diagram is a cross section of the subduction zone in Oregon showing the locked (solid line) and partially locked (dashed line) zone of Hyndman and Wang (1993) compared to the Okada models*

The most striking feature of the HW model is lack of the narrow zone of extreme uplift that characterizes the Okada (1985) pattern in Models 1, 2, and 3 (Figure A3). In theory the maximum coseismic uplift should not be greater than the fault slip multiplied by the sine of the inclination (dip) angle of the subduction zone fault, unless the fault movement is resisted by an obstacle. An obstacle to movement will force some of the horizontal displacement into a vertical direction. If no obstacle is present, as seems likely for the Cascadia subduction zone, then the maximum uplift for models 1, 2, and 3 should be no more than about 6.5-7.2 feet (2.0-2.2 m), whereas the narrow "spike" of uplift produced by the Okada software is about twice that high.

Paul Whitmore (1996, personal communication) discovered that this "spike" disappears, if the Okada model fault is unlocked all the way to the surface. Hence, the "spike" is in fact produced by the assumption of the Okada model that there is no fault up dip of the locked zone, thereby producing resistance to the coseismic slip and transferal of some horizontal motion upward at the tip of the fault. Since there is a well developed fault up dip of any locked zone on the Cascadia subduction zone, the "spike" of uplift is not a valid representation of the actual deformation. Hence, the HW uplift pattern is probably more geologically reasonable. As explained below, the small volume of the "spike" tsunami wave so generated does not have a significant impact on run-up and may be viewed as adding a small factor of safety to run-up estimates.

EFFECT OF SOURCE UNCERTAINTIES ON PREDICTED TSUNAMI RUN-UP

Using numerical simulation techniques of Models 1, 2, and 3, simulated tsunami waves were produced to evaluate (1) the increase in run-up produced by the anomalous "spike" of uplift in Models 1, 2, and 3, and (2) the differences between run-up from these models and that of the HW model.

Effect of the "Spike" of Uplift Model 2 was chosen to evaluate the effect of the "spike" of uplift on run-up. The "spike" was removed by hand smoothing the predicted bottom deformation, eliminating all uplift greater than 2.2 m, the maximum uplift derived by multiplying slip times the sine of the dip. Using Model 2 as an example, Figure A4 demonstrates that the "spike" of uplift only adds about 3 percent to the run-up elevation in most areas.

[2]Slip for Model 2 = 37.7 ft (11.5m). Dip = 12.1º for thr model dip used in the Okada (1985) technique to correct for sea floor slope. Average dip in the geologic cross section = 10.5º at the seismic line of Trehu and others (1994), so uplift could be calculated as 2.1m (10.5º dip) or 2.4 m (12.1º dip). An intermediate value of 2.2m was chosen.

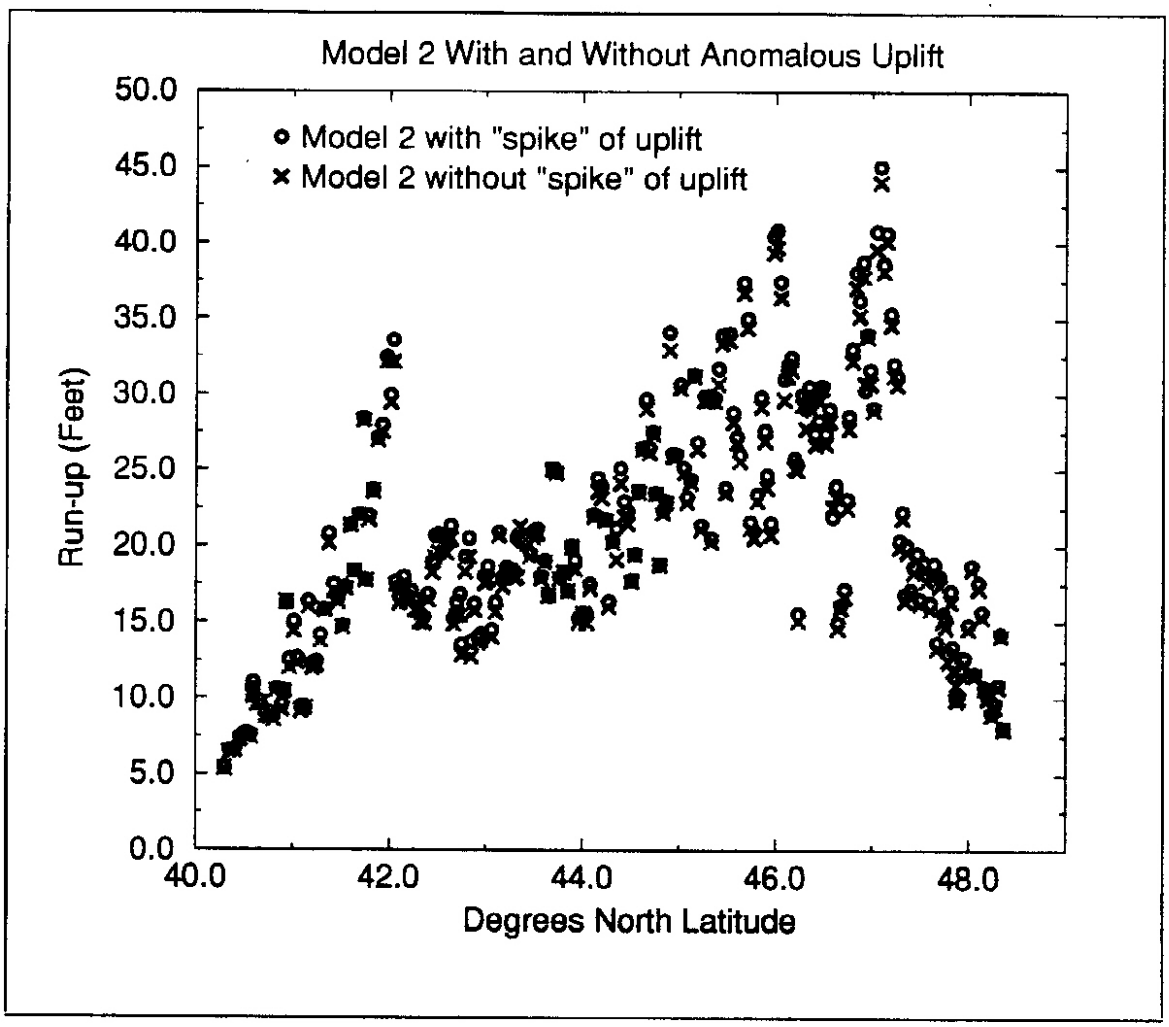


*Figure A4. Comparison of maximum run-up with and without the anomalous "spike" of uplift.*

Effect of the HW Deformation Versus Deformation of Models 2 and 3 A preliminary coseismic deformation for the HW model was computed by (1) using bottom deformation derived from the HW strain rates at two transects perpendicular to the coastlines of Washington and Oregon (Figure A2), (2) assuming 450 years of strain build up before the earthquake, and (3) linearly extrapolating the resulting bottom deformation north-south from the two HW transects. The resulting deformation resembles that of Model 3, but lacks the anomalous "spike" of uplift (Figure A5). Numerical simulation of the resulting tsunami waves yielded HW run-up much larger than that of Model 3 (Figure A6), so run-up was strongly affected by the broad zone of higher uplift in the HW model relative to the same zone in Model 3. The similarity of the bottom deformation between Model 3 and the HW model leads to a similar pattern of variation along the coast (Figure A6). Likewise, the time histories of the HW tsunami simulation are similar to those of Model 3, so there is a leading positive wave in most areas (Figures A7 and A8). This has important implications for evacuation planning (see Appendix C).

[3]The maximum HW uplift of 10.8 feet (3.3 m) requires fault slip of 51.6-59.4 feet (15.7-18.1 m) for a fault dipping 10.5-12.1°; this slip requires a minimum fault length of 800-900 km and Mw of 9.1-9.2, using the empirical data of Scholz (1990). This is a reasonable fault length and magnitude based on an analysis of coseismic subsidence inferred from buried wetland soils (Atwater and others, 1995). The actual fault length used in the simulation (Figure A5) is 700 km, but enlarging the fault length to 800-900 km would not significantly affect the tsunami simulation in Oregon.

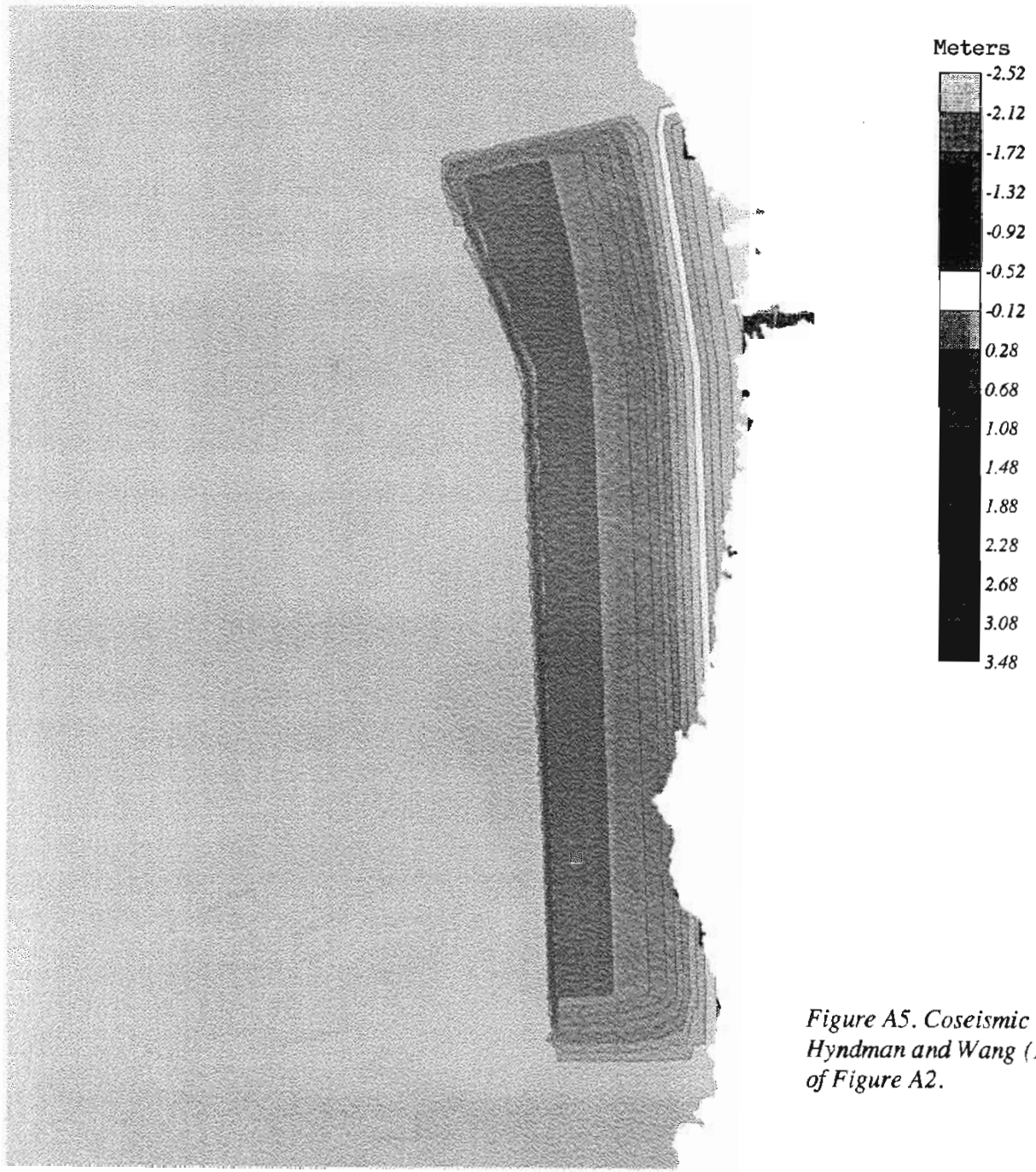


*Figure A5. Coseismic vertical deformation derived from data of Hyndman and Wang (1993) at the Olympic and Oregon transects of Figure A2.*

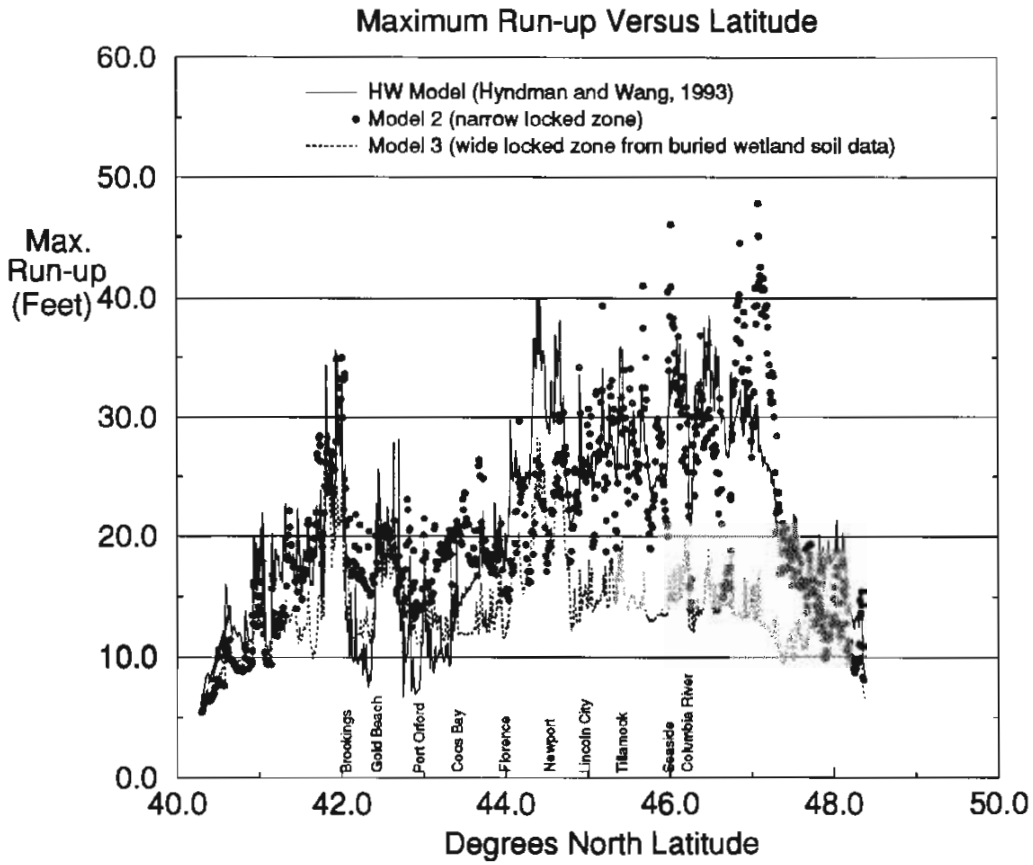


*Figure A6. Maximum run-up of models 2, 3, and the Hyndman and Wang (1993) fault model versus latitude.*

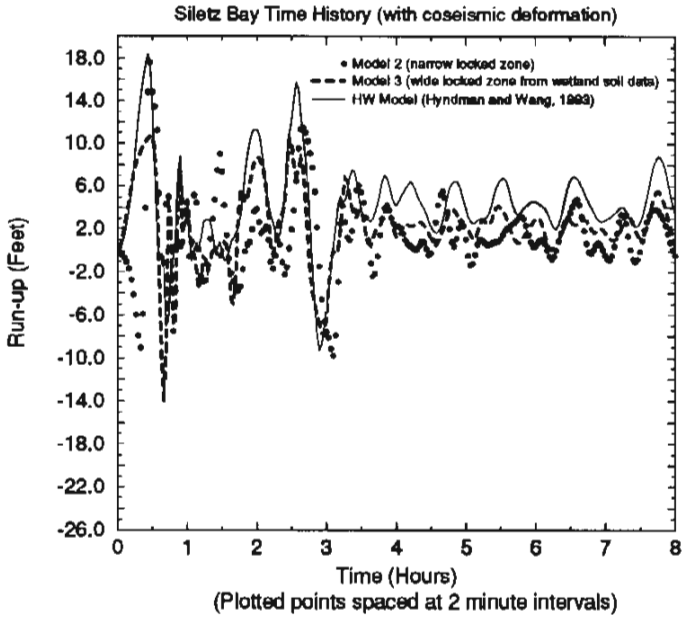


*Figure A7. Time histories for Models 2, 3, and the HW model for a typical north coast site. Note the similarities between the HW model and Model 3.*

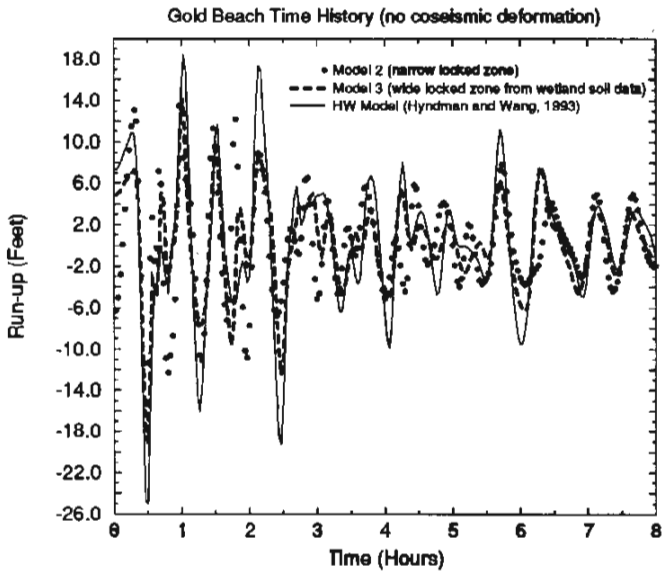


*Figure A8. Time histories for Models 2, 3, and the HW model for a typical south coast site. Note the similarities between the HW model and Model 3.*

The maximum run-up for the HW simulation is most similar to Model 2 (Figure A6). The offshore trough of subsidence in Model 2, which amplifies wave height, compensated for its smaller broad zone of uplift relative to the HW model (Figure A3). From Lincoln City north, the main difference between Model 2 and the HW run-up is a somewhat larger range of run-up elevations for Model 2, leading to slightly higher values where locally higher run-ups occur and lower values where local minimums occur, but the pattern is the same (Figure A6). The HW model run-up is about 10 feet higher than Model 2 at Newport and Waldport, where complex wave interference patterns create higher run-up in the second hour of the simulation for all models. Model 2 is about 3-10 feet higher than the HW model at Brookings and from Coos Bay to the north side of Cape Blanco.

## IMPLICATIONS OF RECENT RESEARCH FOR REVISION OF THE INUNDATION MAPS

A recent paper by Hyndman and Wang (1995) was published too late for incorporation into this study, but their conclusions have important implications for future revision of the Oregon inundation maps. In general, they argue that the width of the locked zone is much narrower than that assumed in any of the models tested here, including the HW model. This conclusion is based primarily on modeling of geodetic uplift data, and making the assumption that uplift rates determined from tide gauge records and resurveying of benchmarks over the last 50 years are representative of the uplift rate for the entire earthquake cycle of 400 ± 200 years. This conclusion may not be valid, at least in central Oregon, since there is abundant evidence of buried wetland soils that developed during periods of significant interseismic uplift, even though many of these same areas have modern geodetic uplift rates near zero (i.e. rates of Goldfinger and others, 1992; Mitchell and others, 1994). Likewise, the narrow locked zone in Oregon inferred by Hyndman and Wang (1995) from geodetic uplift data is narrower than that derived by Hyndman and Wang (1993; 1995) from temperature data alone. This problem leads to a mismatch between the position of coseismic uplift and subsidence simulated by Hyndman and Wang (1995) from geodetic data and that inferred from buried wetland soils on the coast in south central (Figure A9) and in north central Oregon. On the north central coast (Netarts, Tillamook, Nehalem Bay, and Nestucca Bay) Hyndman and Wang (1995) predict 2.6-1.3 feet (0.8-0.4 m) subsidence, assuming a 390 year earthquake recurrence, whereas prehistoric subsidence was about 3-4 feet (unpublished 1995 compilation of Curt D. Peterson; Figure A10). The Hyndman and Wang (1995) deformation may be valid for the subduction zone from Cape Blanco south, where all four models considered here (Figures 4a, b, c and Figure A5) predict coseismic uplift (interseismic subsidence) at the coast, and where all four provide a poor match to the prehistoric data (Figure A10). The reason for the mismatch in southern Oregon is that the prehistoric data supports at least some coseismic subsidence there (Figure A10). For example, Kelsey and others (1993) found buried wetland soils as far west as Cape Blanco. On the other hand, there are some areas with prehistoric uplift (Figure A10), and at Cape Blanco, the 300-year event apparently caused no subsidence, even though a substantial tsunami sand was deposited in the Sixes River marsh (Curt D. Peterson, 1996, personal communication). It may be that the variations are caused by changes in location of Cascadia rupture zone between earthquakes and by the effects of local structures. In any case, there is currently a substantial (4 mm/yr) geodeticly determined coastal uplift rate on the southern Oregon coast (Goldfinger and others, 1992; Mitchell and others, 1994), which implies but does not prove that the next earthquake would reverse this deformation (coseismic subsidence).

The plate tectonic setting argues for narrowing of the locked zone from Cape Blanco south. A narrow locked zone would be more consistent with the Hyndman and Wang (1995) model, based on the geodetic data. Cape Blanco is where the Blanco Fracture Zone separates subducted oceanic plates much hotter to the south than to the north. A hotter subducting plate will raise the temperature at the subduction zone, leading to a shallower, narrower locked zone. The latter hypothesis was not, however, tested by thermal modeling of the southern part of the subduction zone in the Hyndman and Wang (1993; 1995) papers.

As demonstrated by the tsunami simulations of Models 2 and 3, narrower locked zones can cause higher tsunamis, given similar fault slip, so future work may lead to somewhat higher mapped run-up for the coast from Cape Blanco south. Fortunately, this part of the coast is characterized by steep terrain which limits inland inundation, so any change in the horizontal location of the inundation lines on the current maps is likely to be small.

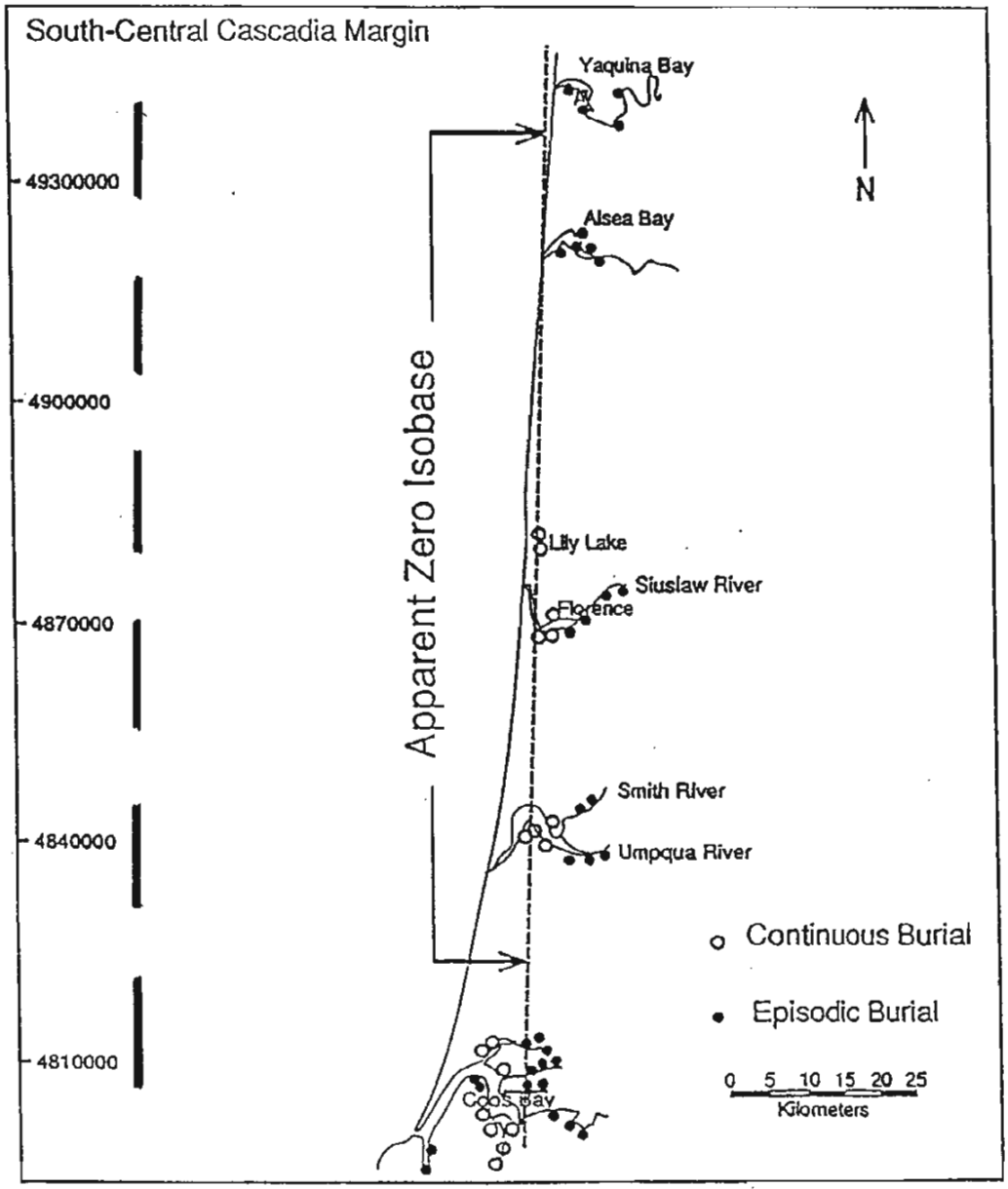


*Figure A9. Comparison of the zero coseismic deformation boundary (zero isobase) determined from buried wetland soils (short dashes) and from modeling of geodetic data by Hyndman and Wang (1995; long dashed lines). Modified from Briggs (1994) and Peterson and Briggs (1992).*

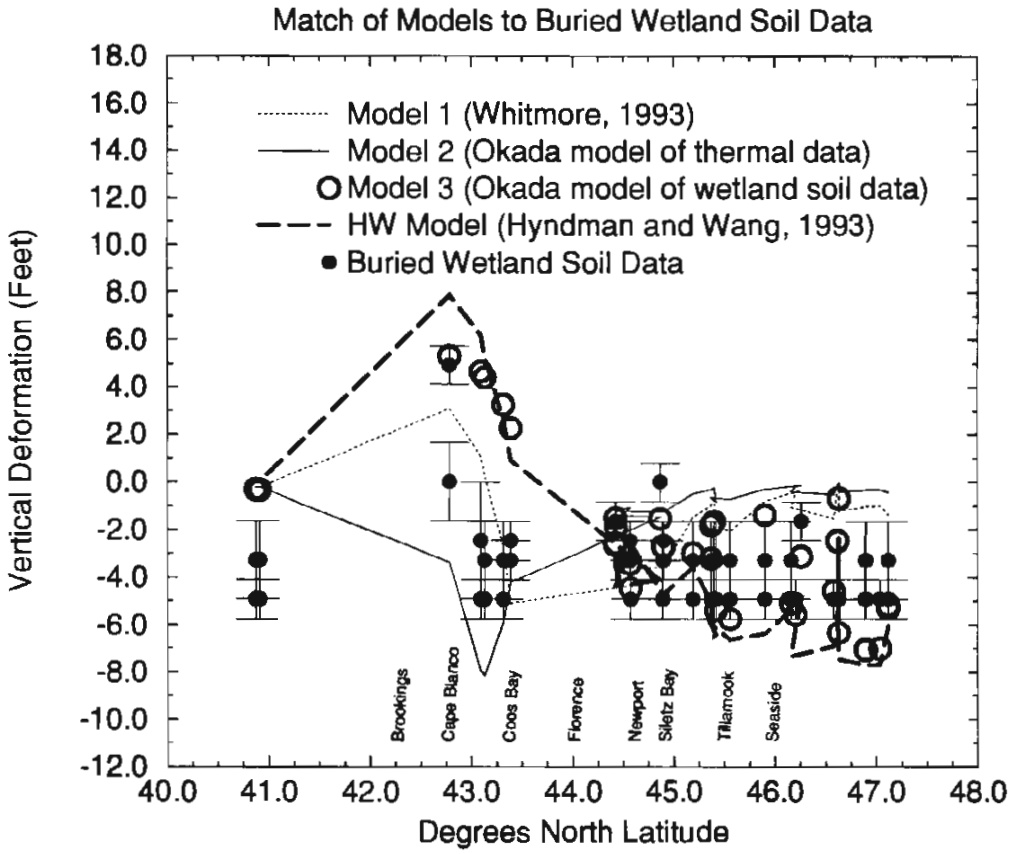


*Figure A10. Coseismic deformation determined from buried wetland soil data versus models. Data points are for matching geographic coordinates.*

## SUMMARY AND RECOMMENDATIONS

The maximum tsunami run-up estimated by Model 2 is similar to that of the preliminary HW model (extrapolated from deformation of Hyndman and Wang, 1993) and is a reasonable inundation boundary for implementation of SB 379 (ORS 455.446 and 455.447). Future revision of the maps may produce somewhat higher run-up in Newport, Waldport, and areas from Cape Blanco south. For evacuation and emergency planning, the sequence and timing of arrival of tsunamis at the coast should be estimated from the time histories of Model 3, which most resemble those of the HW model (see Appendix C).

The next step is to produce a three-dimensional dislocation model that simulates partial locking of the subduction zone, resolves the difference between the Okada (1985) and HW simulation of coseismic uplift, and incorporates rapidly evolving knowledge of coseismic deformation on the Cascadia subduction zone. When this is accomplished, a more accurate simulation of the tsunami hazard will be possible and revision of the inundation maps will be justified.

APPENDIX B

MAXIMUM TSUNAMI RUN-UP ELEVATIONS AT THE OPEN COAST IN OREGON

The following charts show the maximum run-up elevations reached by each of the numerical simulations of Model 1, 2, and 3 during the 8 hours following a great subduction zone earthquake. The run-up ***without coseismic subsidence but with tide at about 4 feet above mean sea level*** is plotted by latitude along the open coastal shoreline. Run-up elevations used in mapping areas north of Florence were adjusted upward by adding a small amount of coseismic subsidence estimated from an unpublished 1995 compilation by C. D. Peterson of Portland State University. Values of 0-1 feet were added from Florence to Waldport 1-2 feet from Waldport to Newport, 2-3 feet from Newport to Siletz Bay, and 3-4 feet from Siletz Bay to the mouth of the Columbia River. These adjustments made only minor differences in the mapped inundation.

Note that the run-up elevations for inland areas are not listed, because, with one exception, no accurate numerical simulation of run-up was done for inland areas. The exception is the Columbia River estuary where run-up in the vicinity of Warrenton was estimated to be approximately 9-10 feet (Model 2) to 4-5 feet (Model 3), decreasing to about half these values at Astoria. Coseismic subsidence in these areas is in the range of 5-6 feet (unpublished data of C. D. Peterson), which was added to the model run-up in order to map inundation. The run-up was generally assumed to be equal to the coseismic subsidence of about 5-7 feet from Tongue Point to Blind Slough, even though little tsunami wave energy is likely to affect those areas.

Each chart presents the data at the open coast for a single USGS 7.5' topographic quadrangle. The quadrangle title is given at the top of the chart. USGS quadrangles have tick marks for each 2.5 minutes of latitude. In order to make cross referencing between chart and quadrangle easy, the only latitude labels on the charts are these same 2.5' latitudes plus the latitude at the south boundary of the quadrangle. The chart latitudes are given in decimal degrees rather than degrees, minutes and seconds, as listed on the USGS quadrangles, so the actual latitude labels on the charts will not look like the ones on the quadrangles. Table B1 lists the decimal equivalents of the minutes and seconds of latitude that bound all 7.5' quadrangles. For example, the quadrangle whose southern boundary is at 44° 37' 30" would have a label at the origin of the equivalent chart of 44.625°. Tick marks on the sides of the quadrangle would be labeled in increments of 2.5' (0.042°). The next quadrangle north would have as its southern boundary 44° 45' (44.75°), etc.

*Table B1. Decimal equivalents of minutes and seconds of latitude bounding 7.5' quadrangles.*

| USGS Quadrangle Boundary | Decimal Degrees |
|---|---|
| 52' 30" | 0.875 |
| 45' | 0.750 |
| 37' 30" | 0.625 |
| 30' | 0.500 |
| 22' 30" | 0.375 |
| 15' | 0.250 |
| 7' 30" | 0.125 |

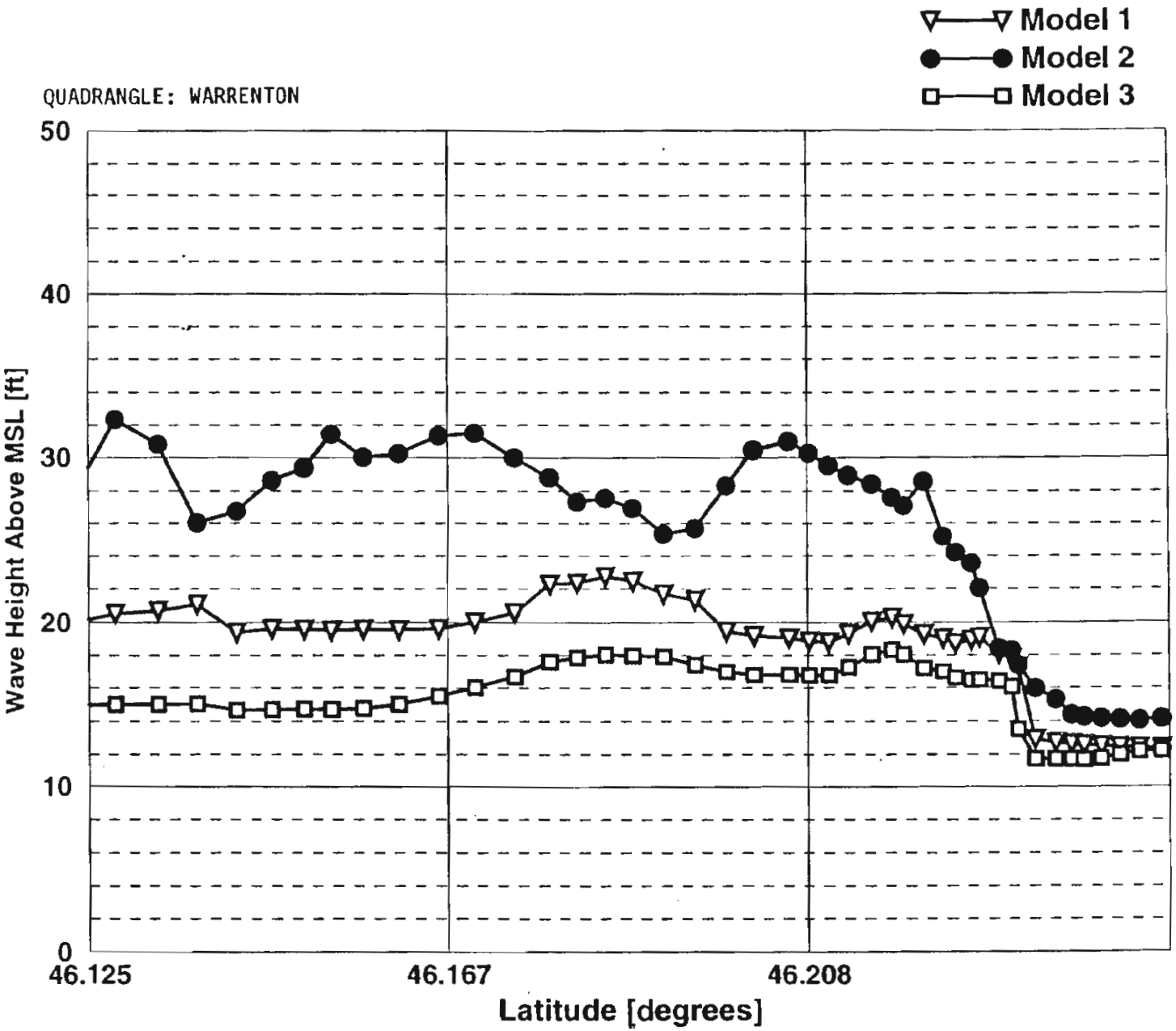
Model 1
Model 2
Model 3
QUADRANGLE: WARRENTON
50
40
30
20
10
0
Wave Height Above MSL [ft]
46.125
46.167
46.208
Latitude [degrees]

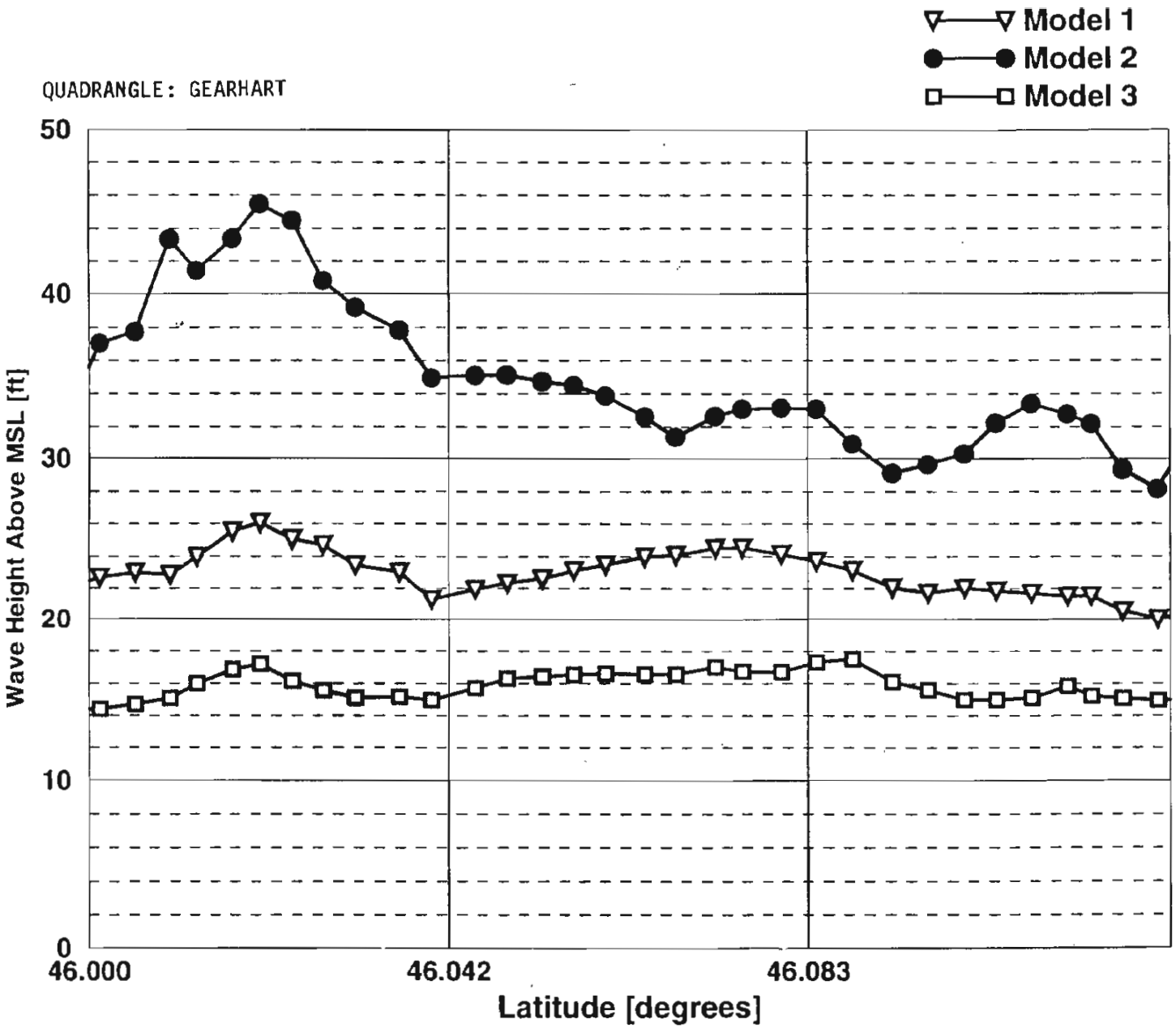
Model 1
Model 2
Model 3
QUADRANGLE: GEARHART
50
40
30
20
10
0
Wave Height Above MSL [ft]
46.000
46.042
46.083
Latitude [degrees]

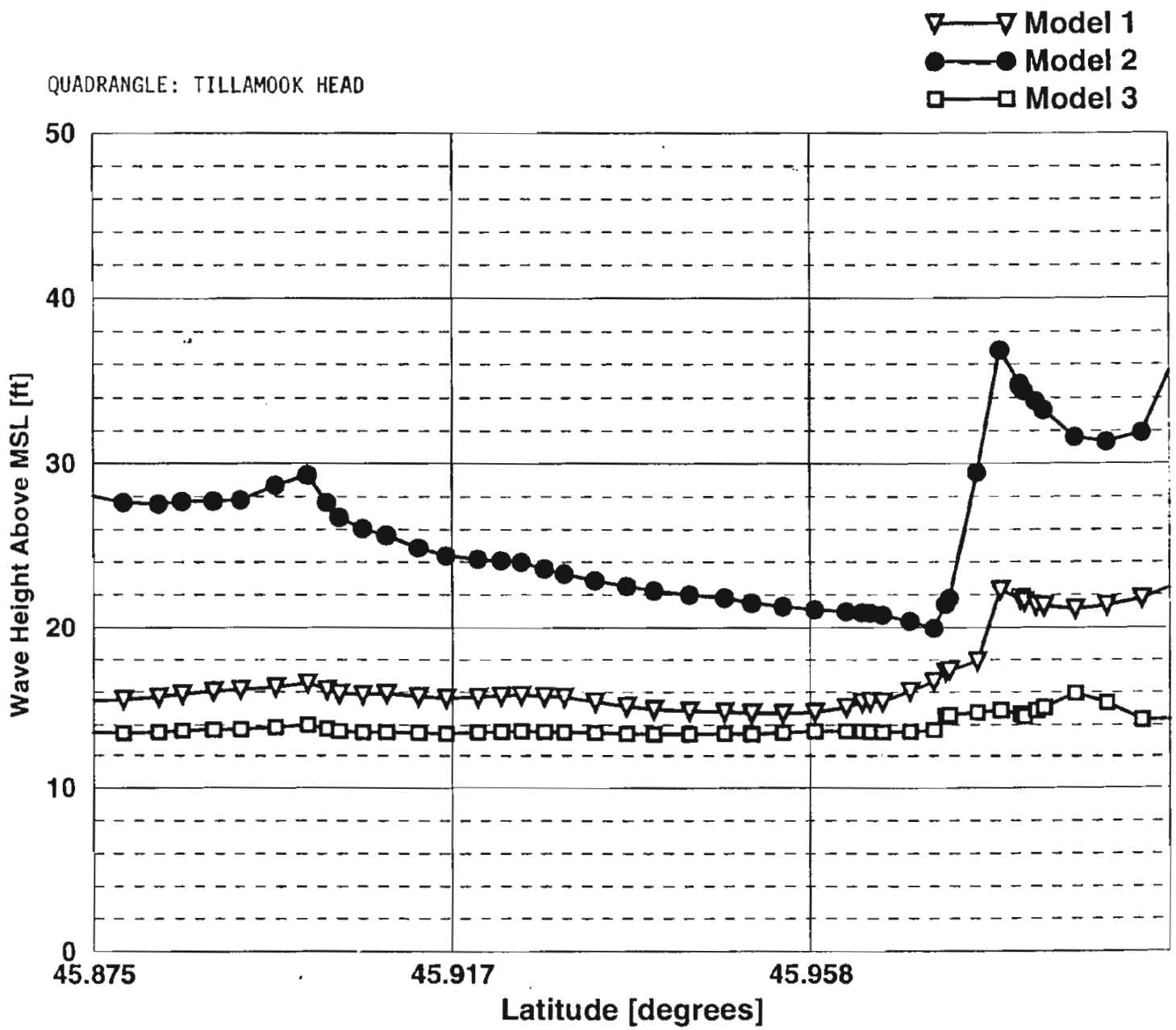
Model 1
Model 2
Model 3
QUADRANGLE: TILLAMOOK HEAD
Wave Height Above MSL [ft]
50
40
30
20
10
0
45.875
45.917
45.958
Latitude [degrees]

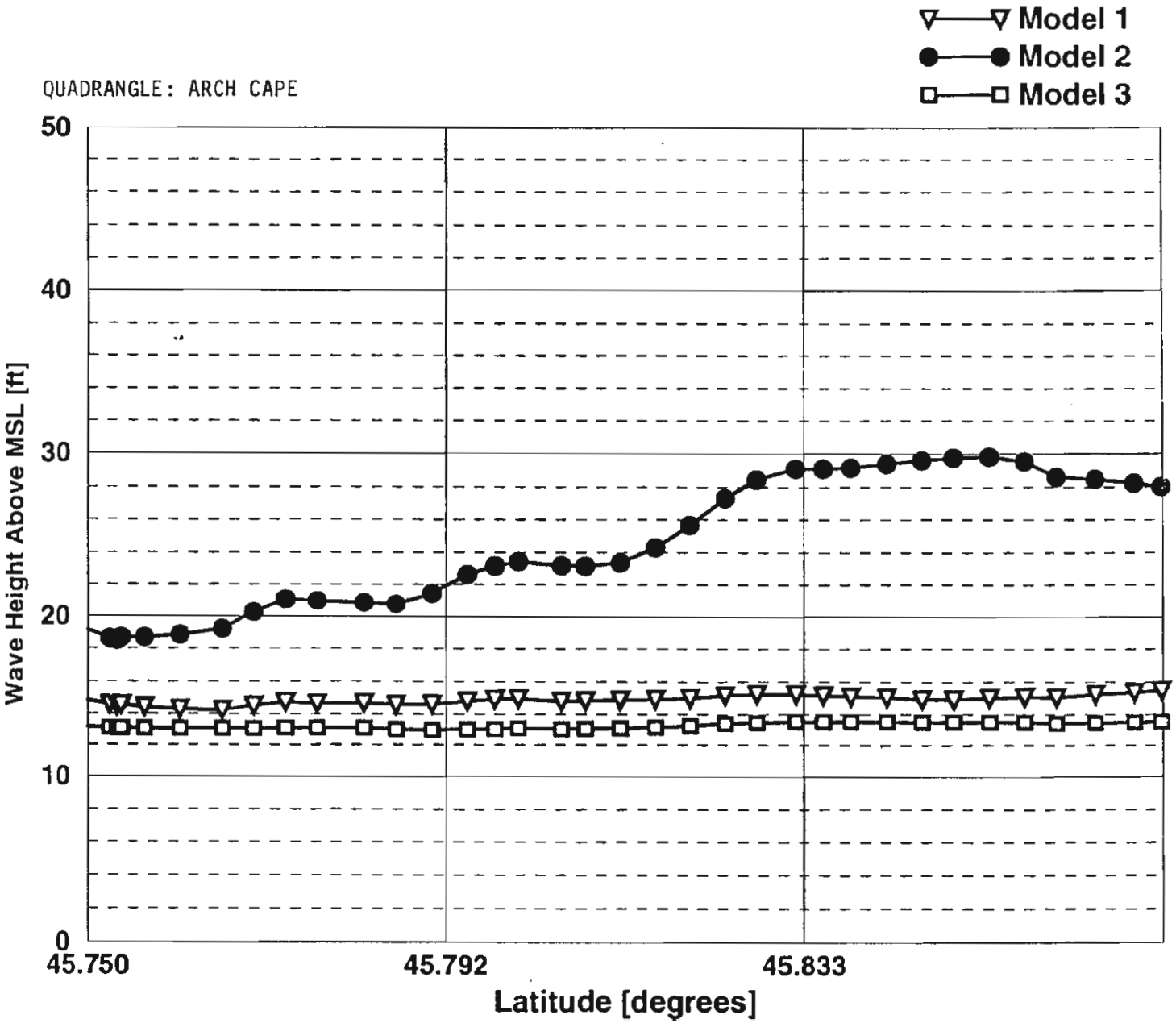
Model 1
Model 2
Model 3
QUADRANGLE: ARCH CAPE
50
40
30
20
10
0
Wave Height Above MSL [ft]
45.750
45.792
45.833
Latitude [degrees]

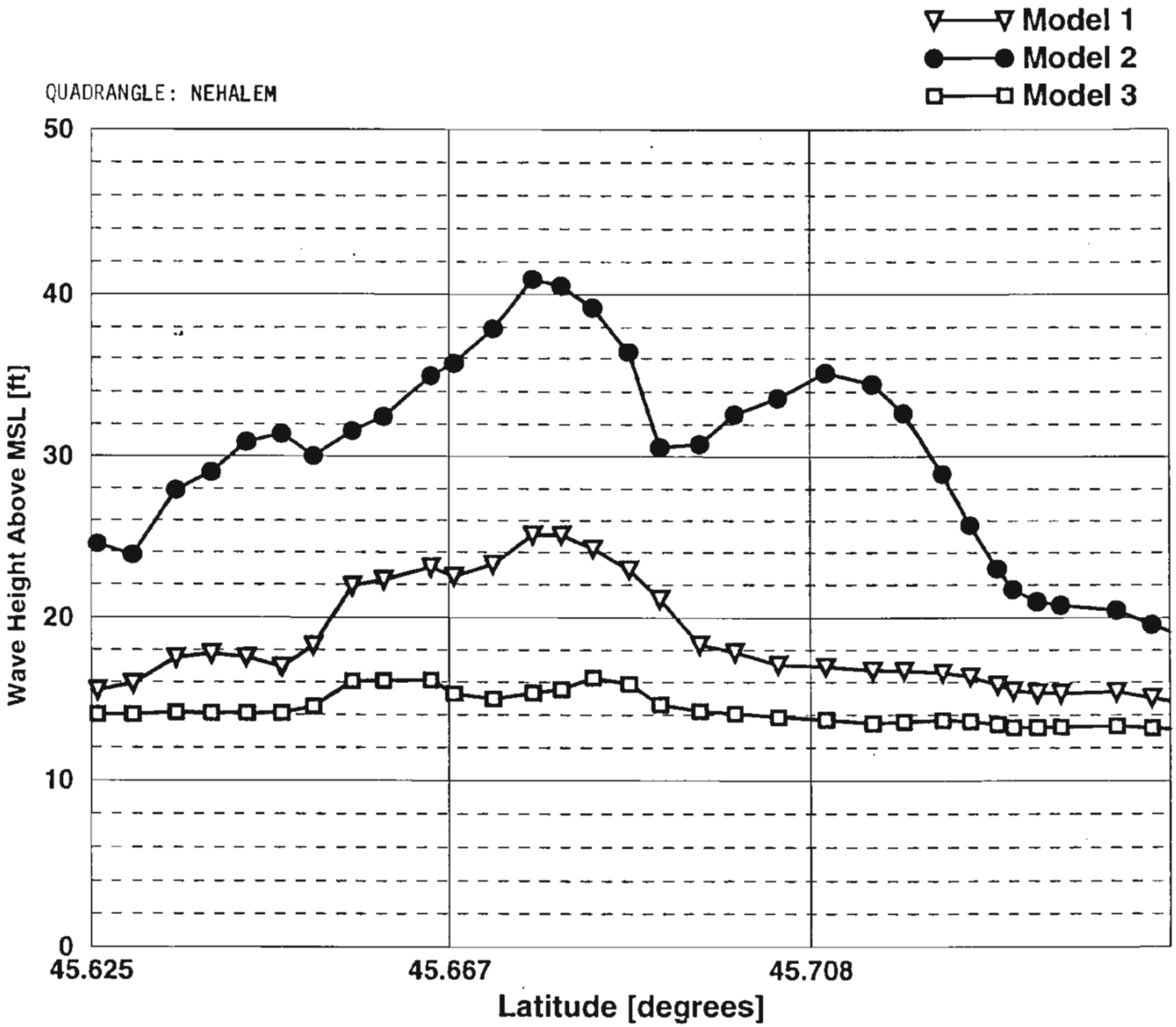
Model 1
Model 2
Model 3
QUADRANGLE: NEHALEM
50
40
30
20
10
0
Wave Height Above MSL [ft]
45.625
45.667
45.708
Latitude [degrees]

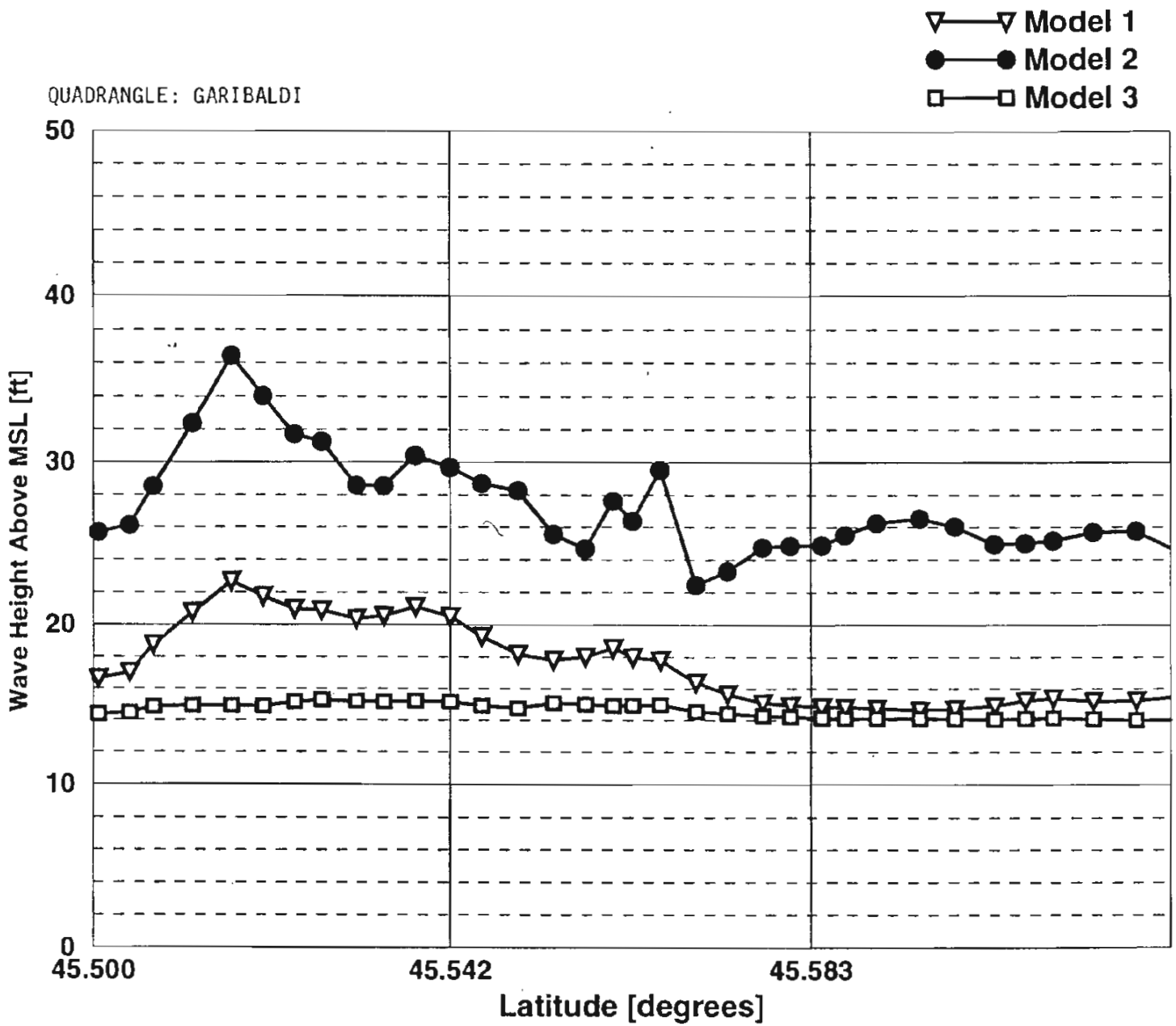
Model 1
Model 2
Model 3
QUADRANGLE: GARIBALDI
Wave Height Above MSL [ft]
50
40
30
20
10
0
45.500
45.542
45.583
Latitude [degrees]

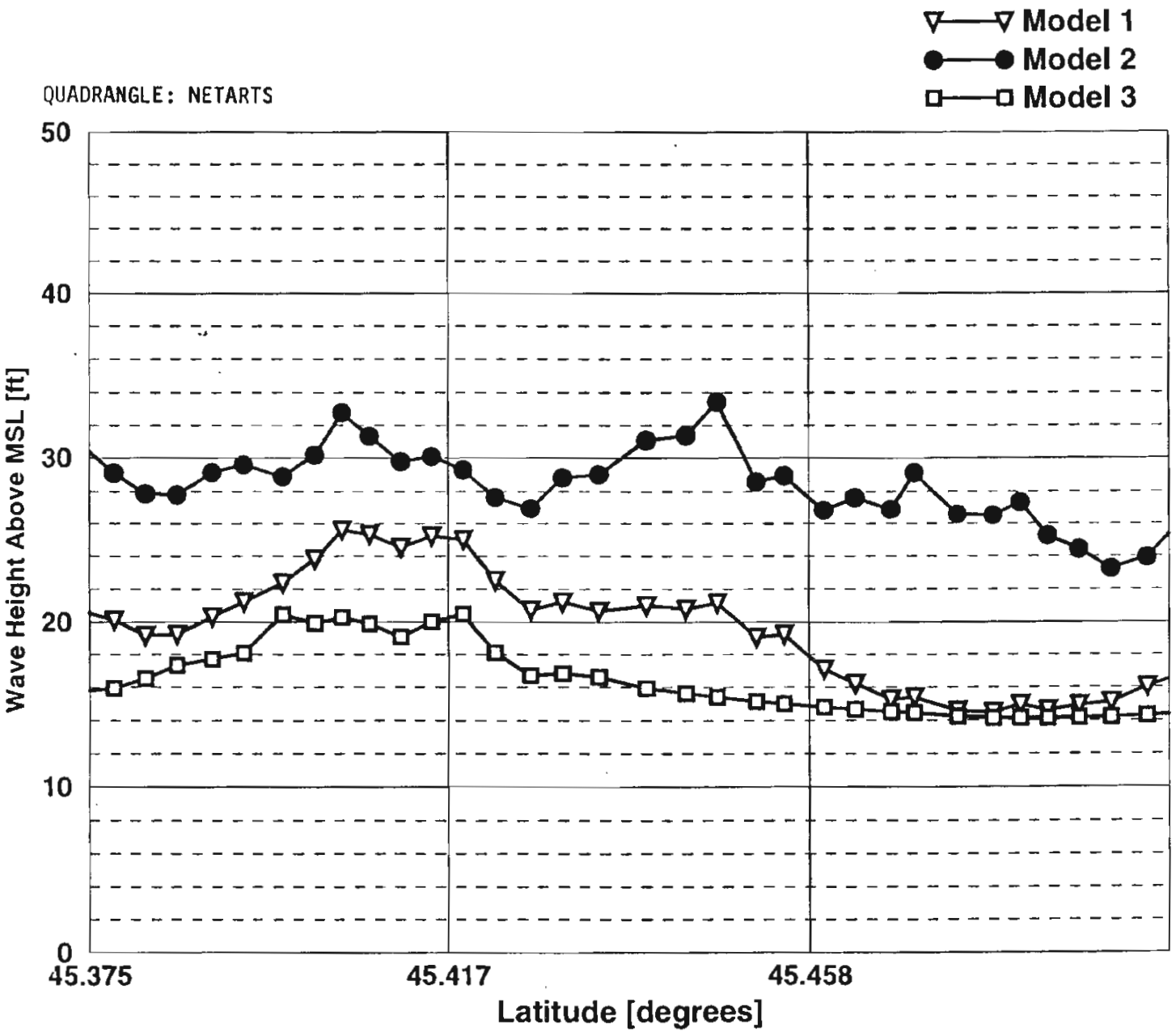
Model 1
Model 2
Model 3
QUADRANGLE: NETARTS
50
40
30
20
10
0
Wave Height Above MSL [ft]
45.375
45.417
45.458
Latitude [degrees]

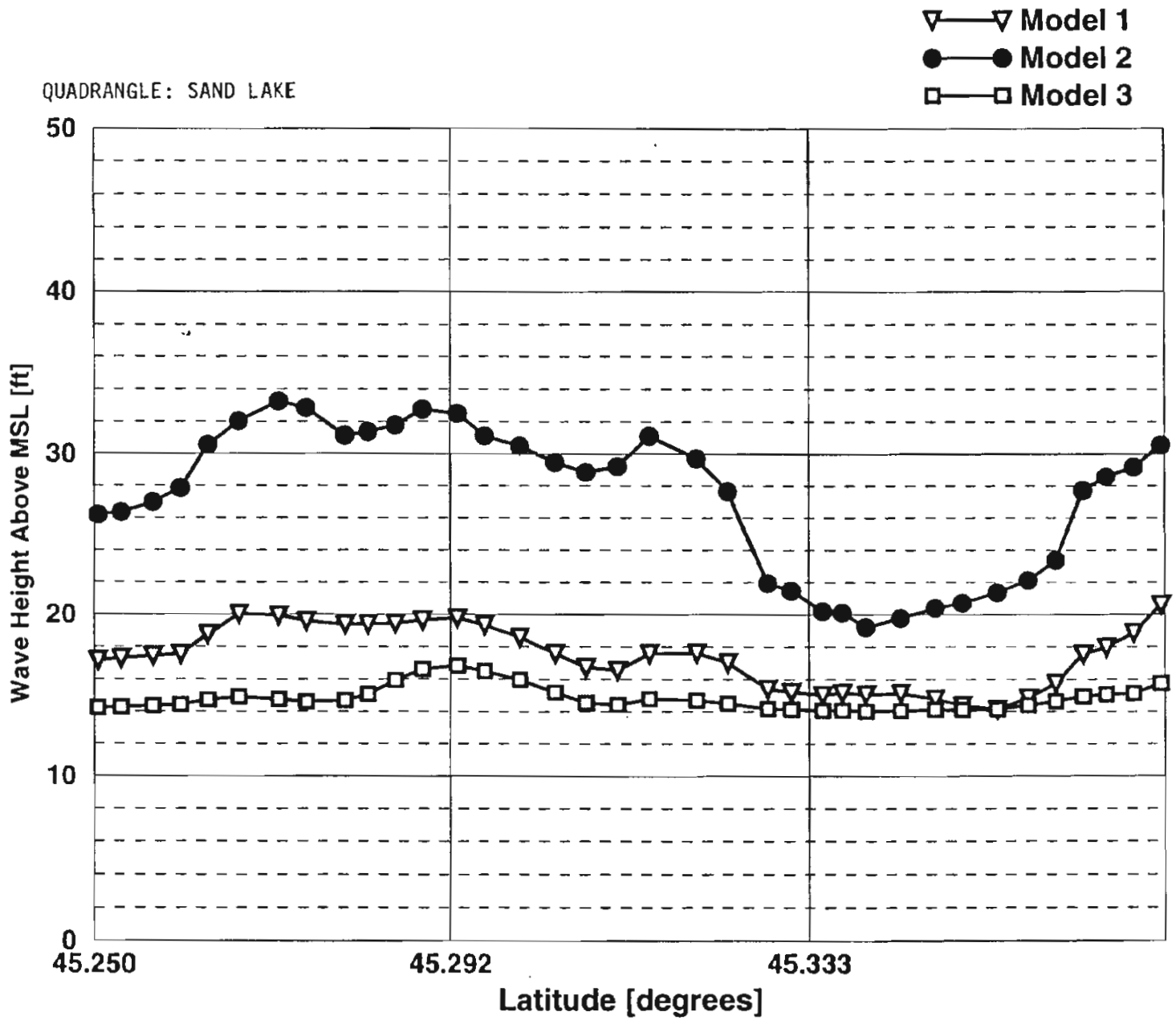
Model 1
Model 2
Model 3
QUADRANGLE: SAND LAKE
Wave Height Above MSL [ft]
50
40
30
20
10
0
45.250
45.292
45.333
Latitude [degrees]

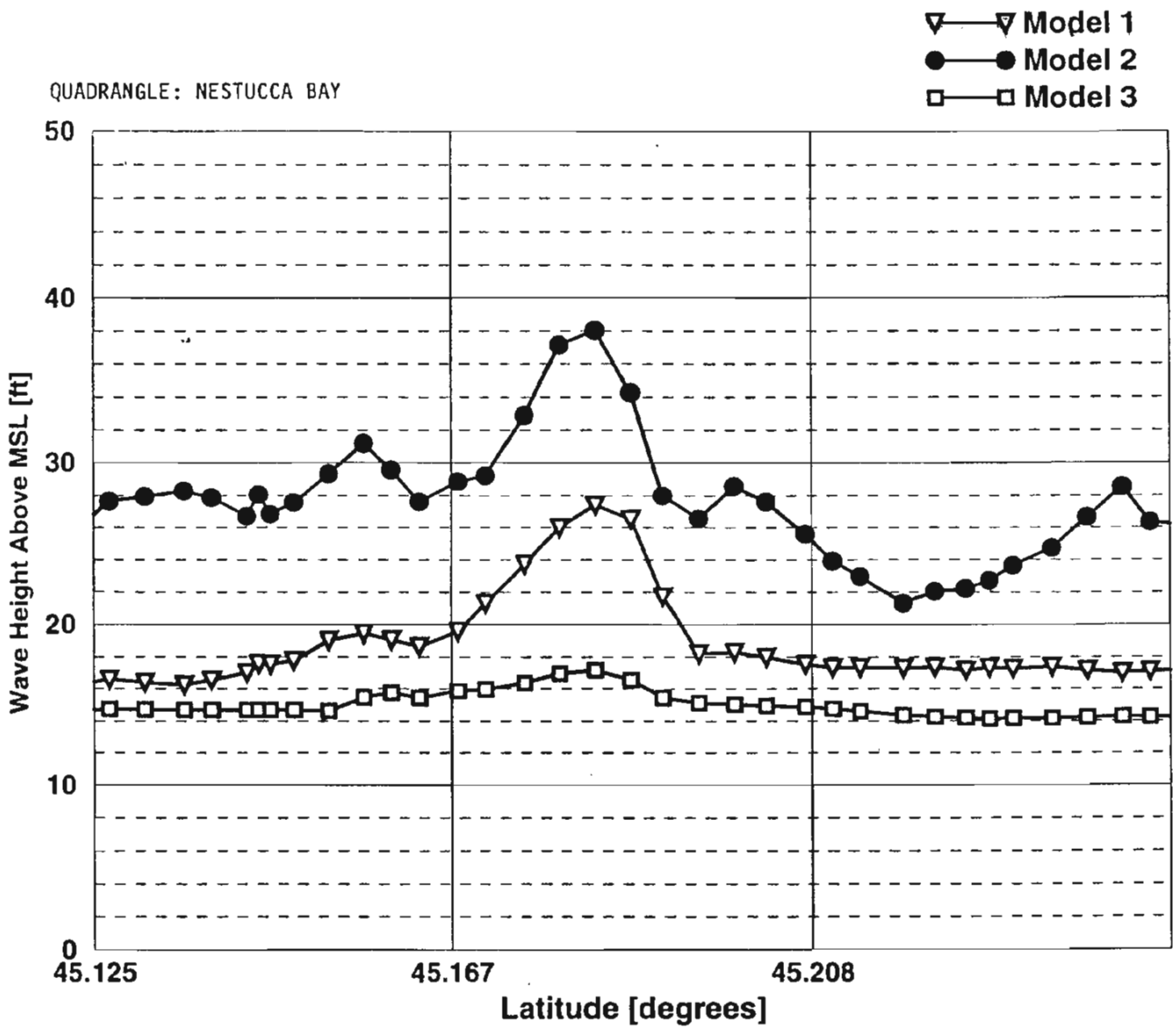
Model 1
Model 2
Model 3
QUADRANGLE: NESTUCCA BAY
Wave Height Above MSL [ft]
50
40
30
20
10
0
45.125
45.167
45.208
Latitude [degrees]

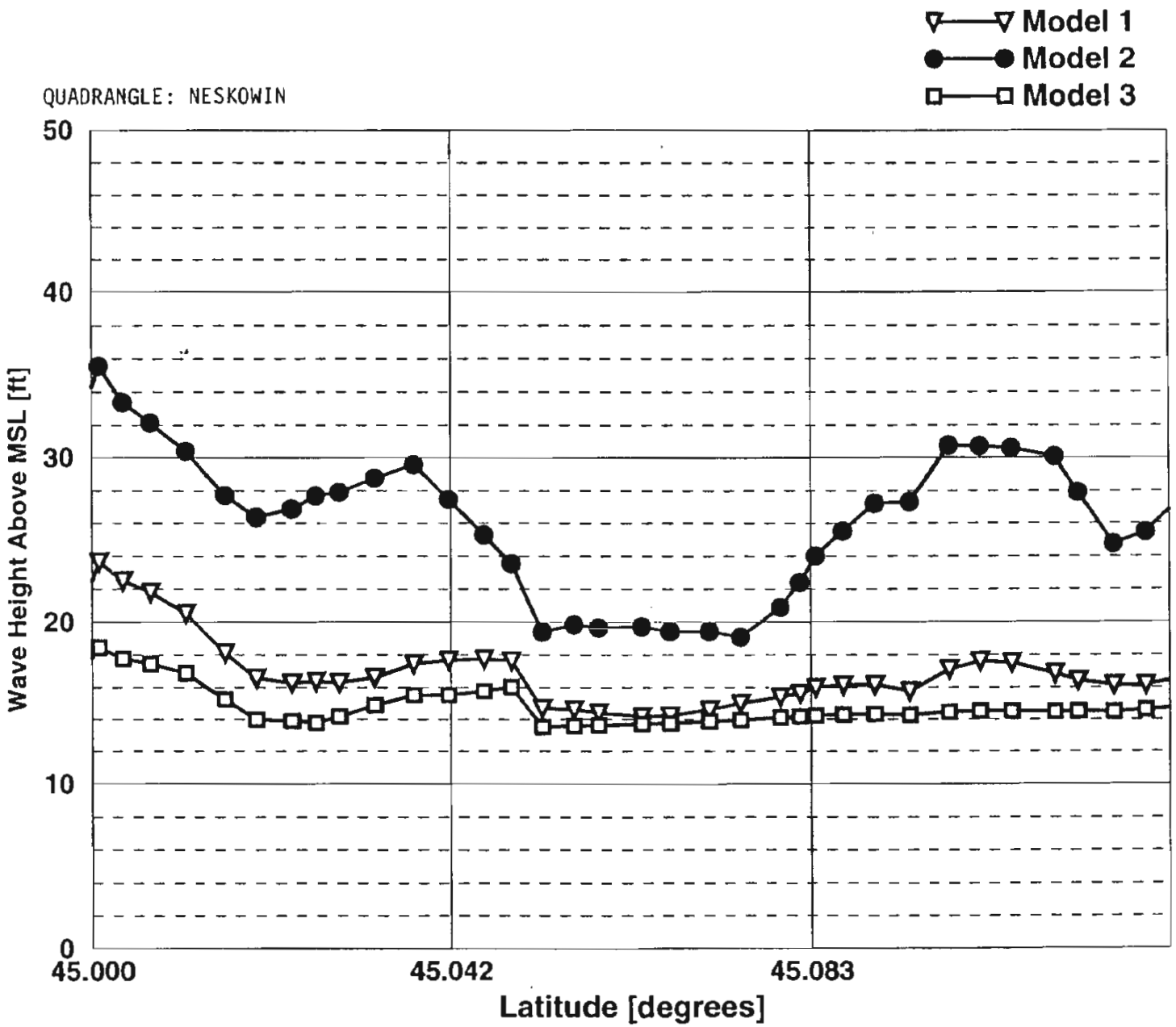
Model 1
Model 2
Model 3
QUADRANGLE: NESKOWIN
50
40
30
20
10
0
Wave Height Above MSL [ft]
45.000
45.042
45.083
Latitude [degrees]

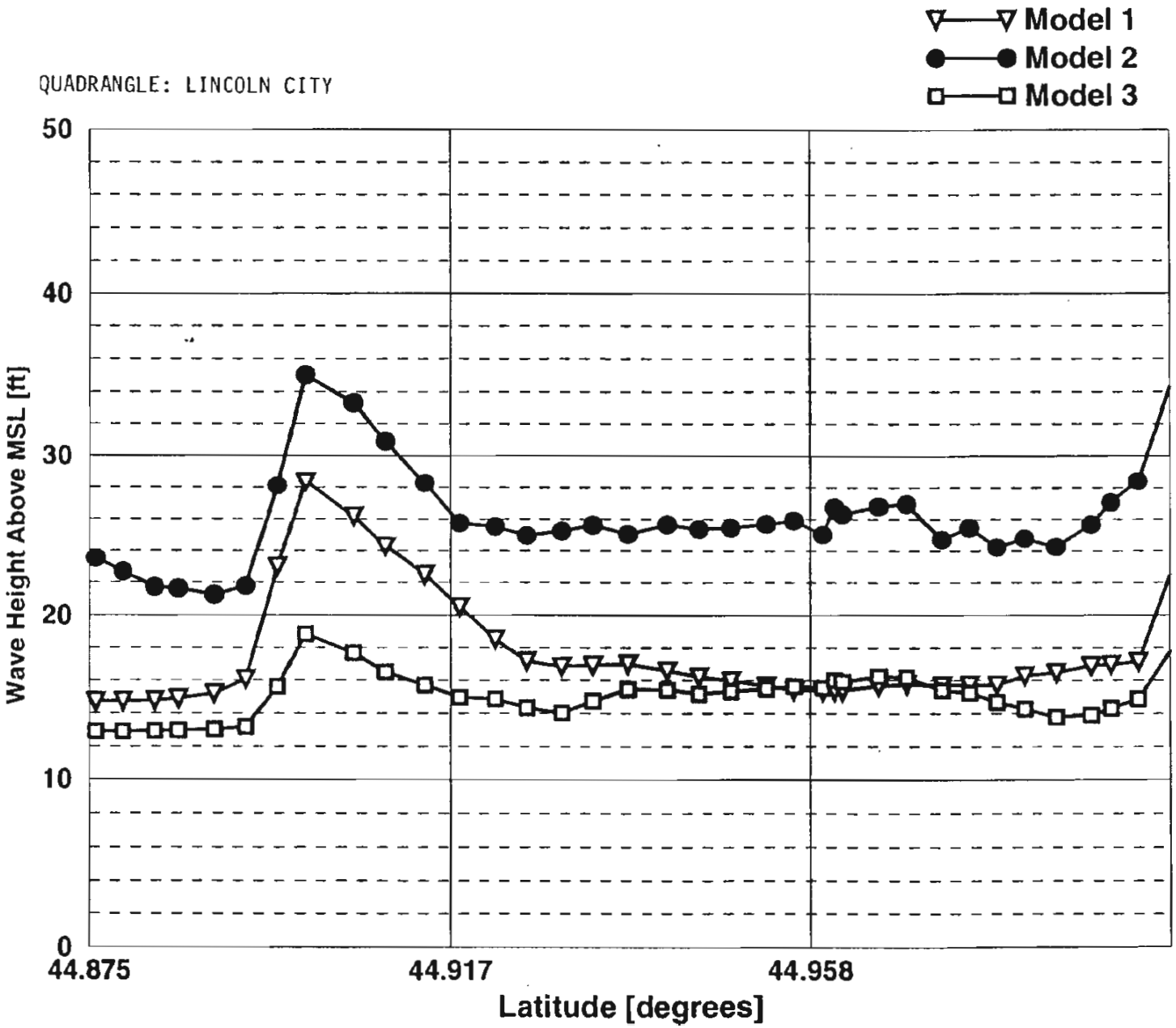
Model 1
Model 2
Model 3
QUADRANGLE: LINCOLN CITY
Wave Height Above MSL [ft]
50
40
30
20
10
0
44.875
44.917
44.958
Latitude [degrees]

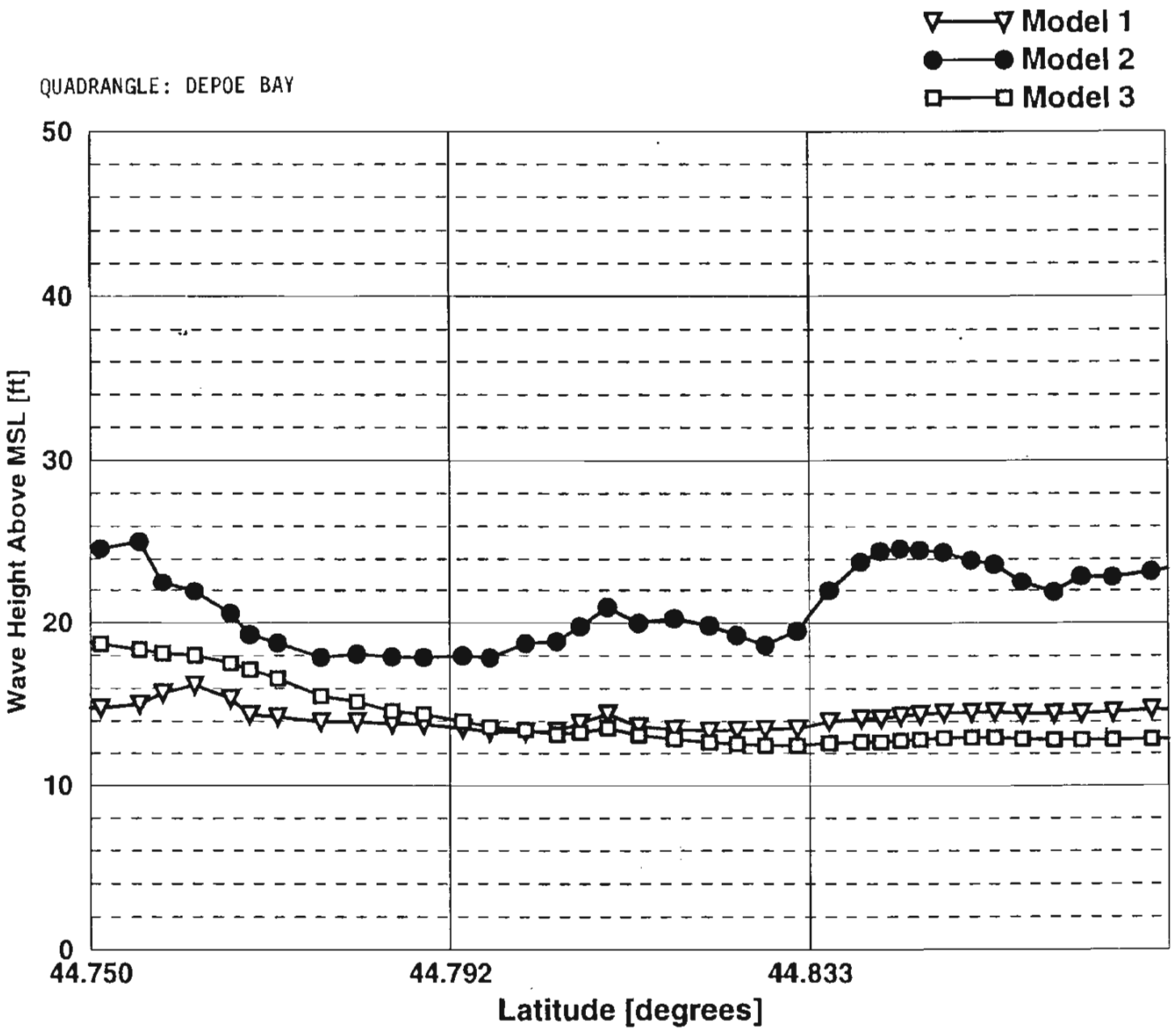
Model 1
Model 2
Model 3
QUADRANGLE: DEPOE BAY
Wave Height Above MSL [ft]
50
40
30
20
10
0
44.750
44.792
44.833
Latitude [degrees]

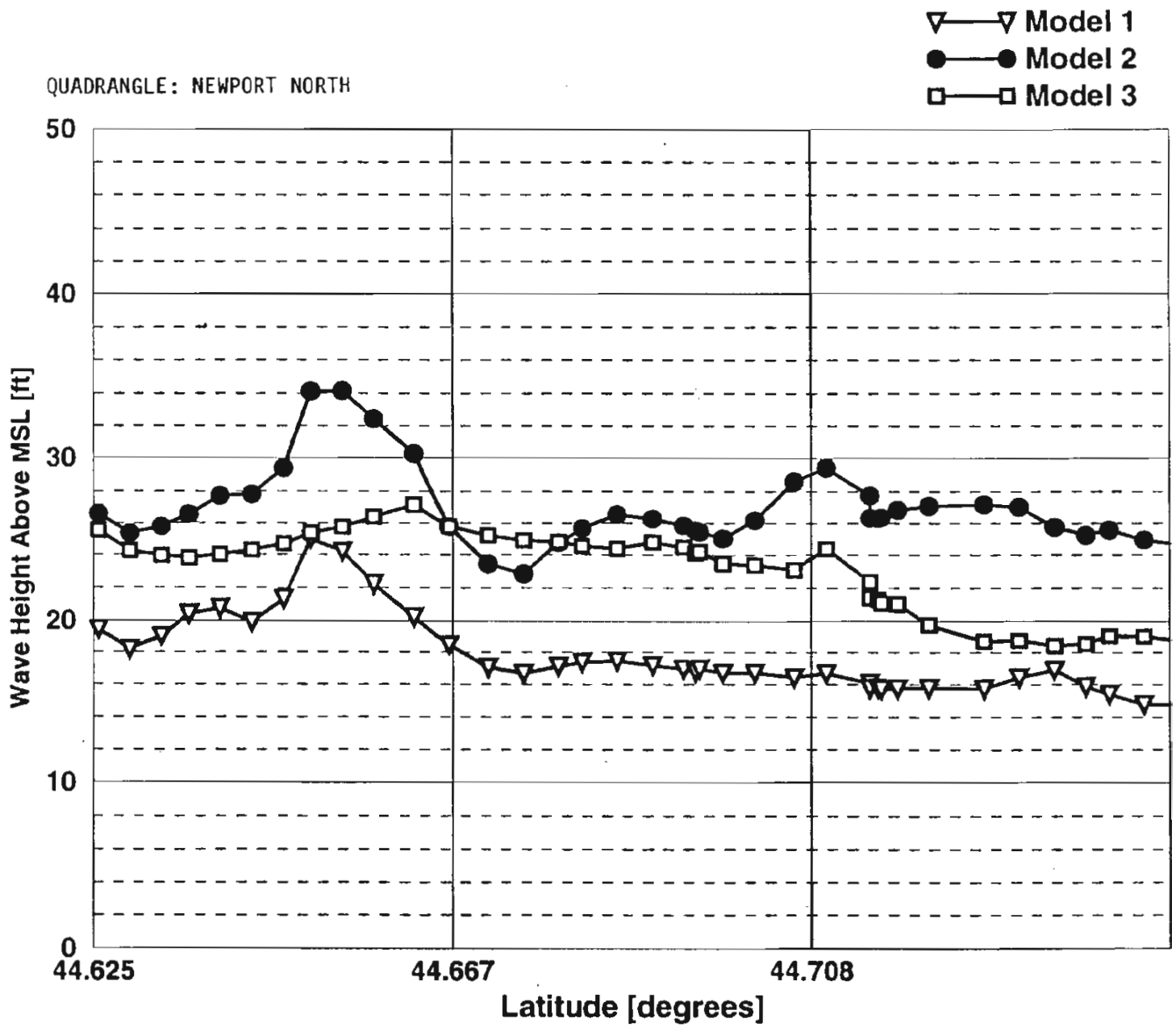
Model 1
Model 2
Model 3
QUADRANGLE: NEWPORT NORTH
50
40
30
20
10
0
Wave Height Above MSL [ft]
44.625
44.667
44.708
Latitude [degrees]

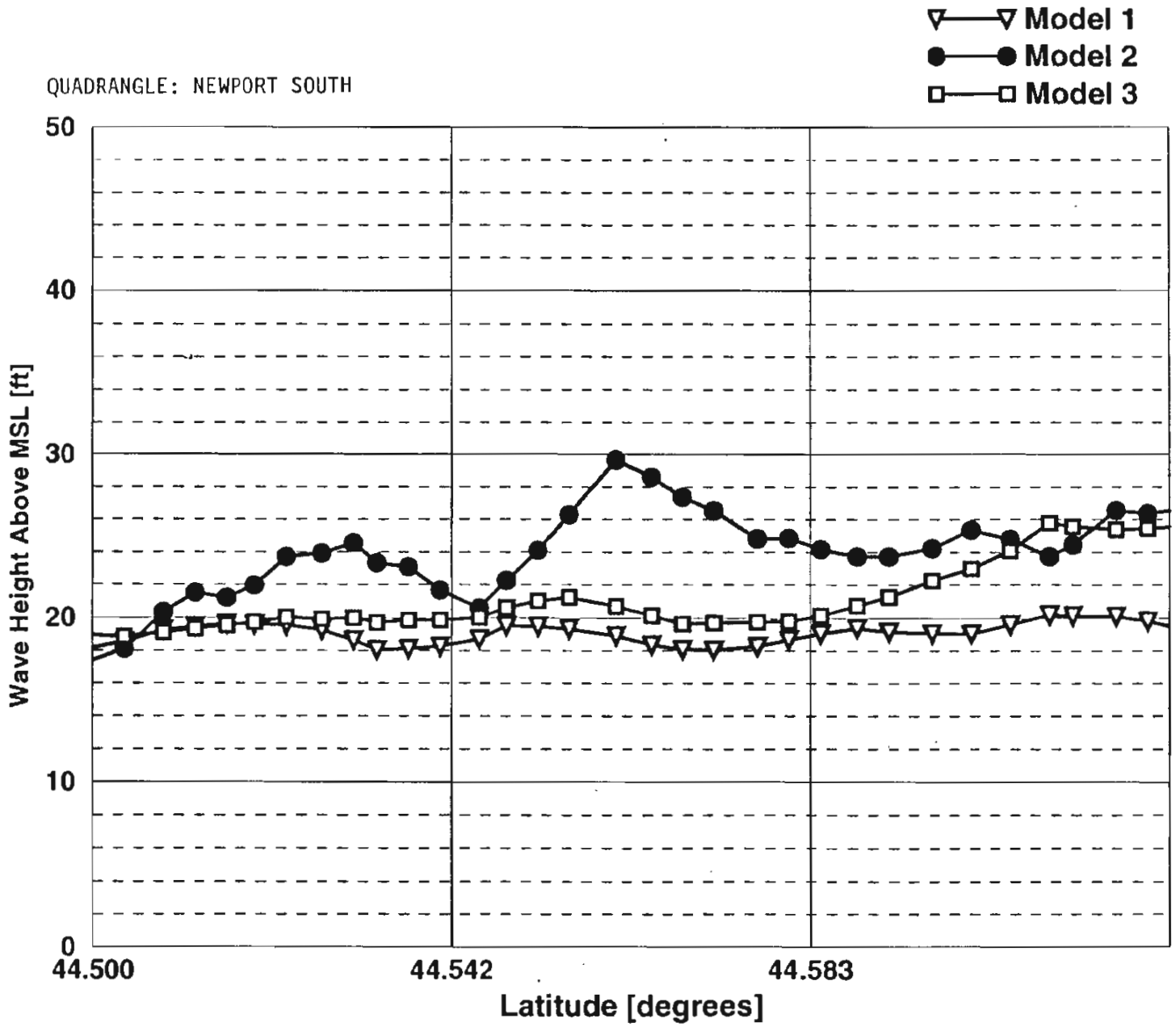
Model 1
Model 2
Model 3
QUADRANGLE: NEWPORT SOUTH
50
40
30
20
10
0
Wave Height Above MSL [ft]
44.500
44.542
44.583
Latitude [degrees]

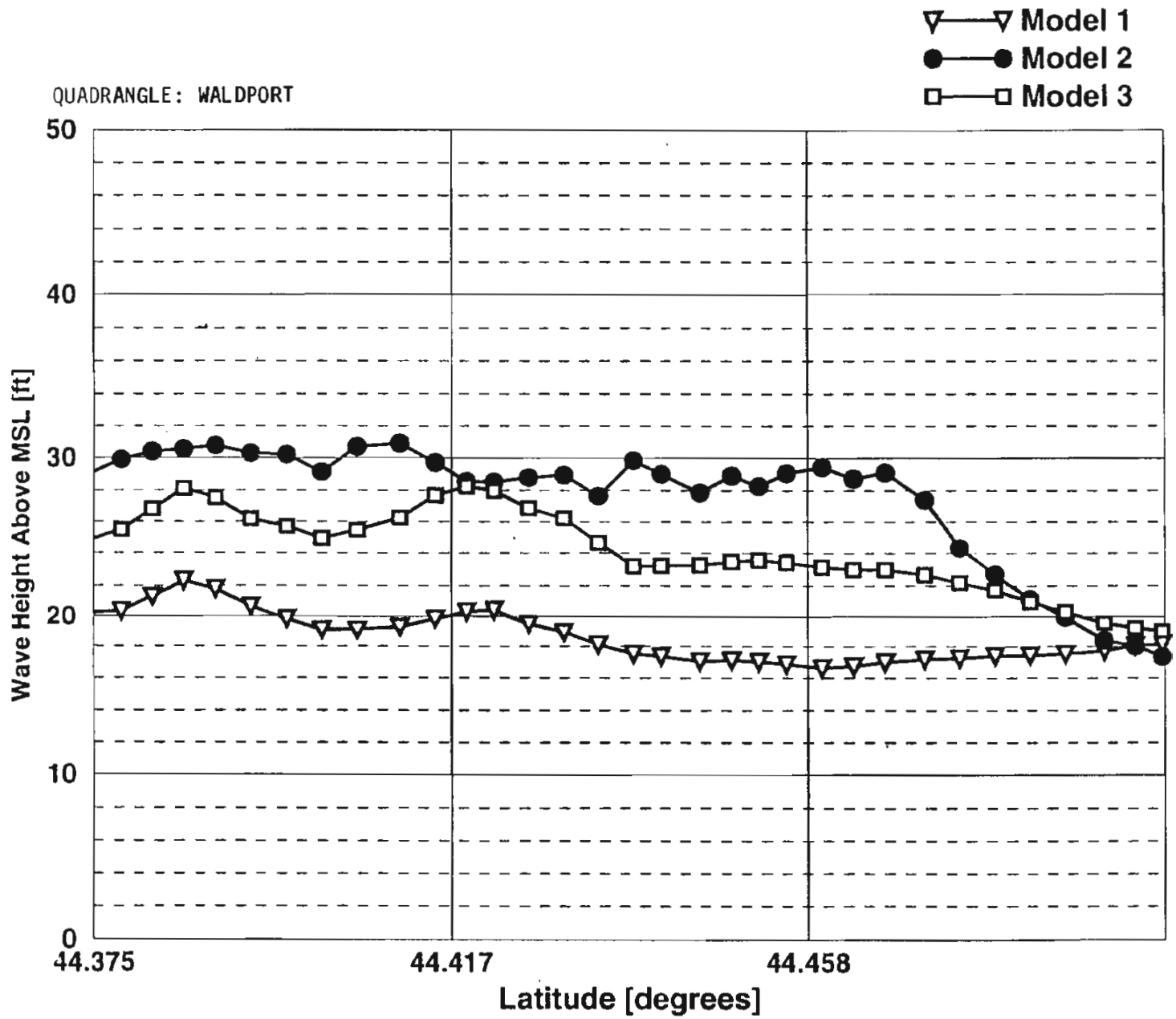
Model 1
Model 2
Model 3
QUADRANGLE: WALDPORT
50
40
30
20
10
0
Wave Height Above MSL [ft]
44.375
44.417
44.458
Latitude [degrees]

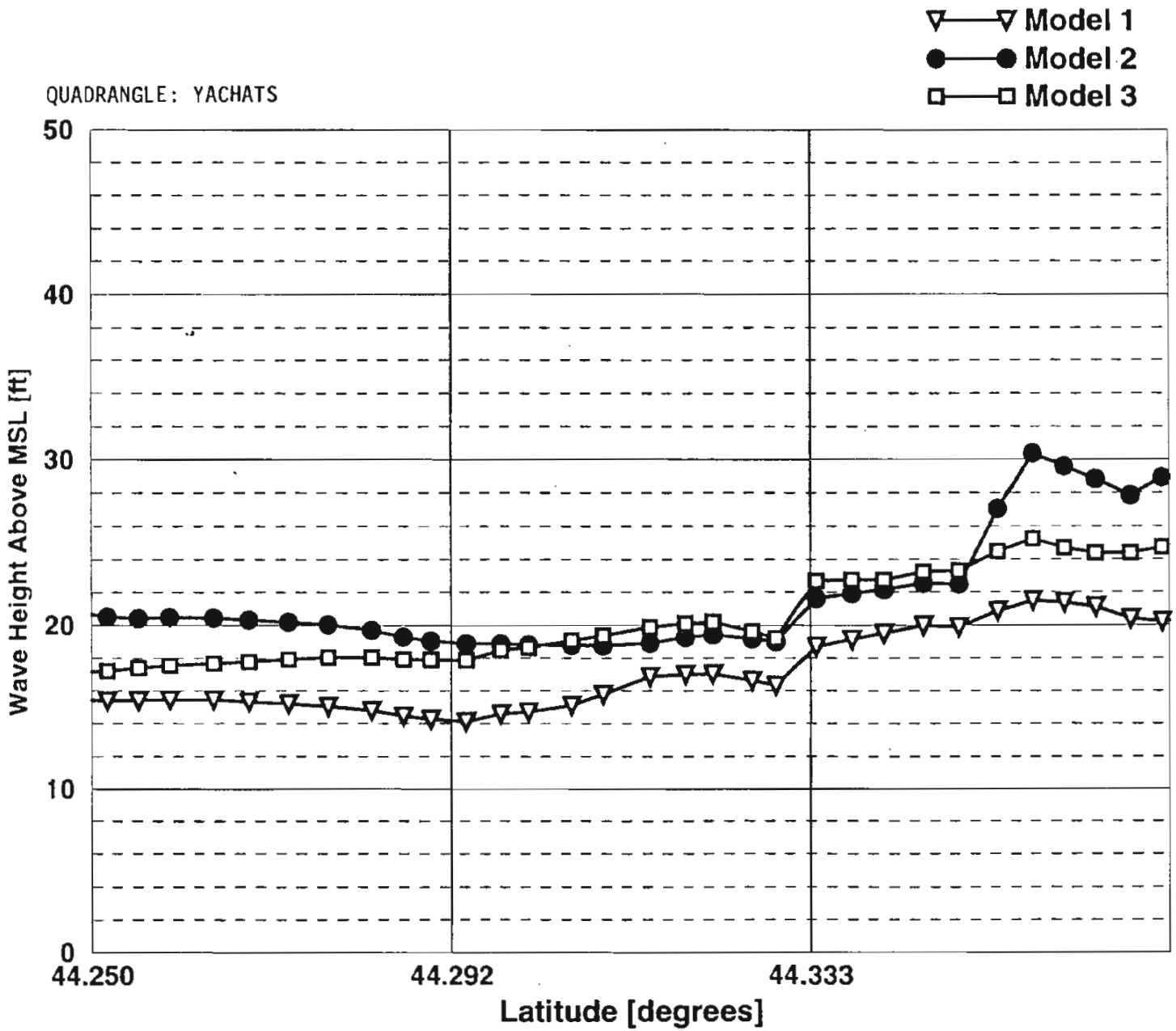
Model 1
Model 2
Model 3
QUADRANGLE: YACHATS
50
40
30
20
10
0
Wave Height Above MSL [ft]
44.250
44.292
44.333
Latitude [degrees]

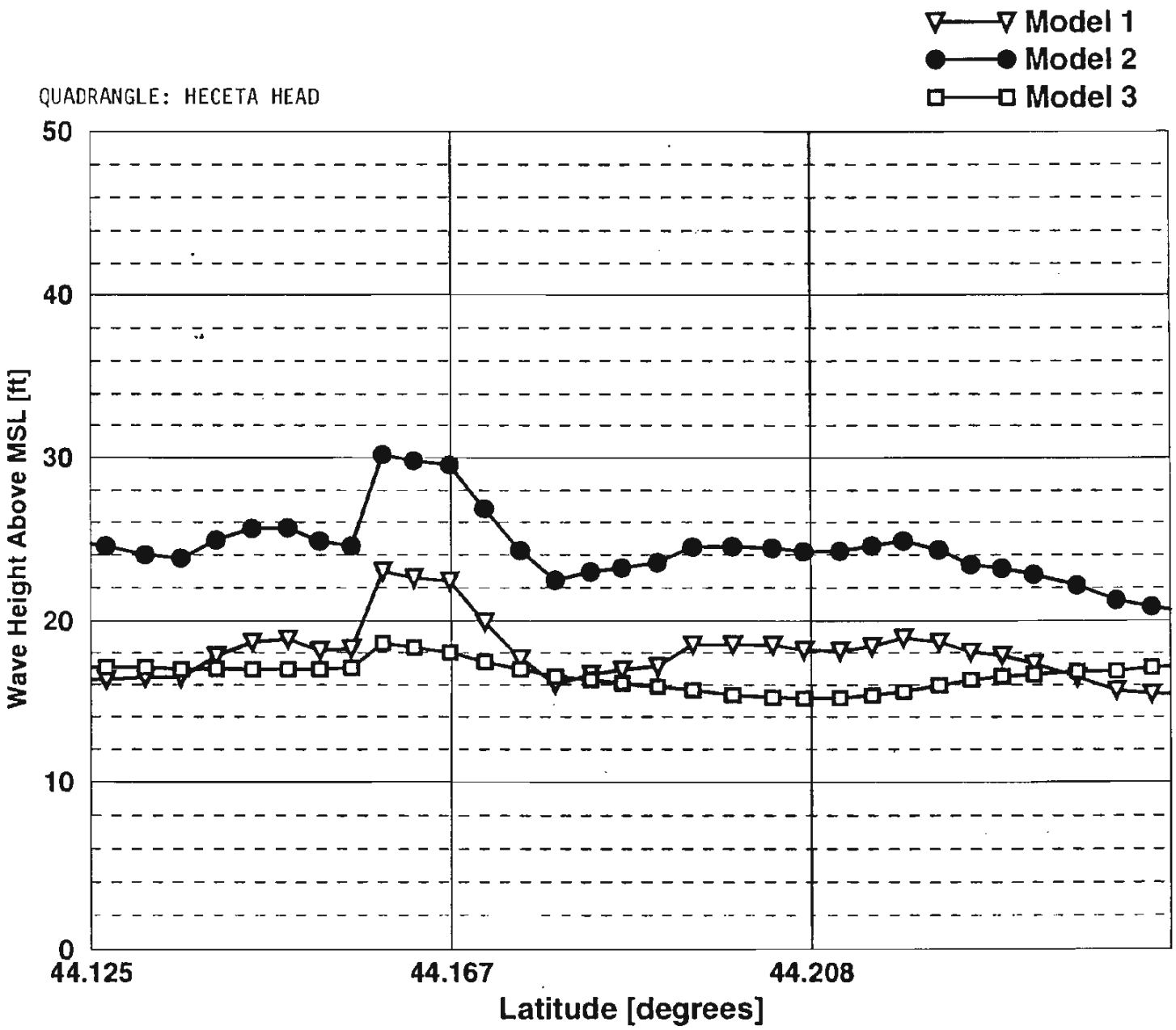
Model 1
Model 2
Model 3
QUADRANGLE: HECETA HEAD
50
40
30
20
10
0
Wave Height Above MSL [ft]
44.125
44.167
44.208
Latitude [degrees]

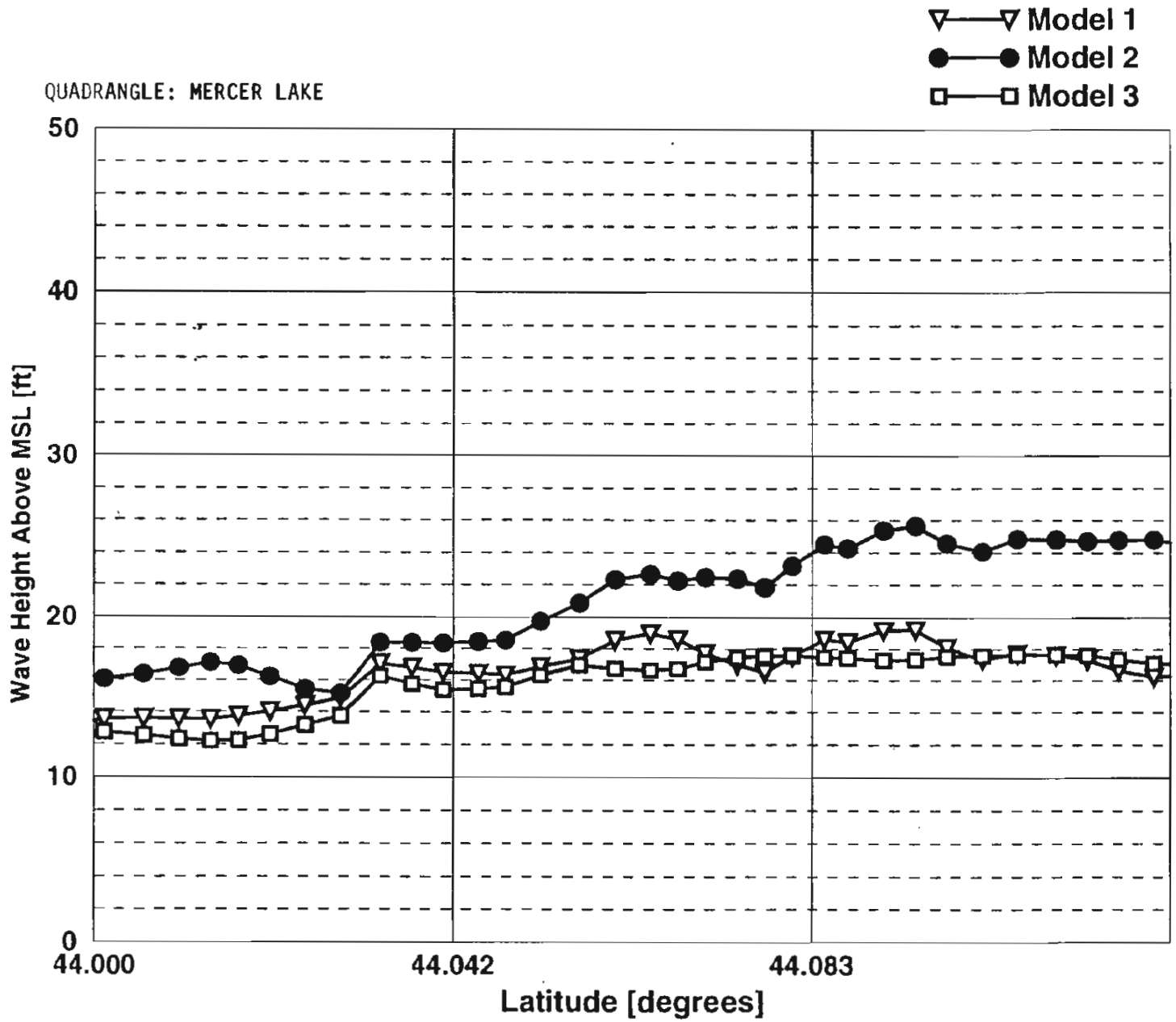
Model 1
Model 2
Model 3
QUADRANGLE: MERCER LAKE
50
40
30
20
10
0
Wave Height Above MSL [ft]
44.000
44.042
44.083
Latitude [degrees]

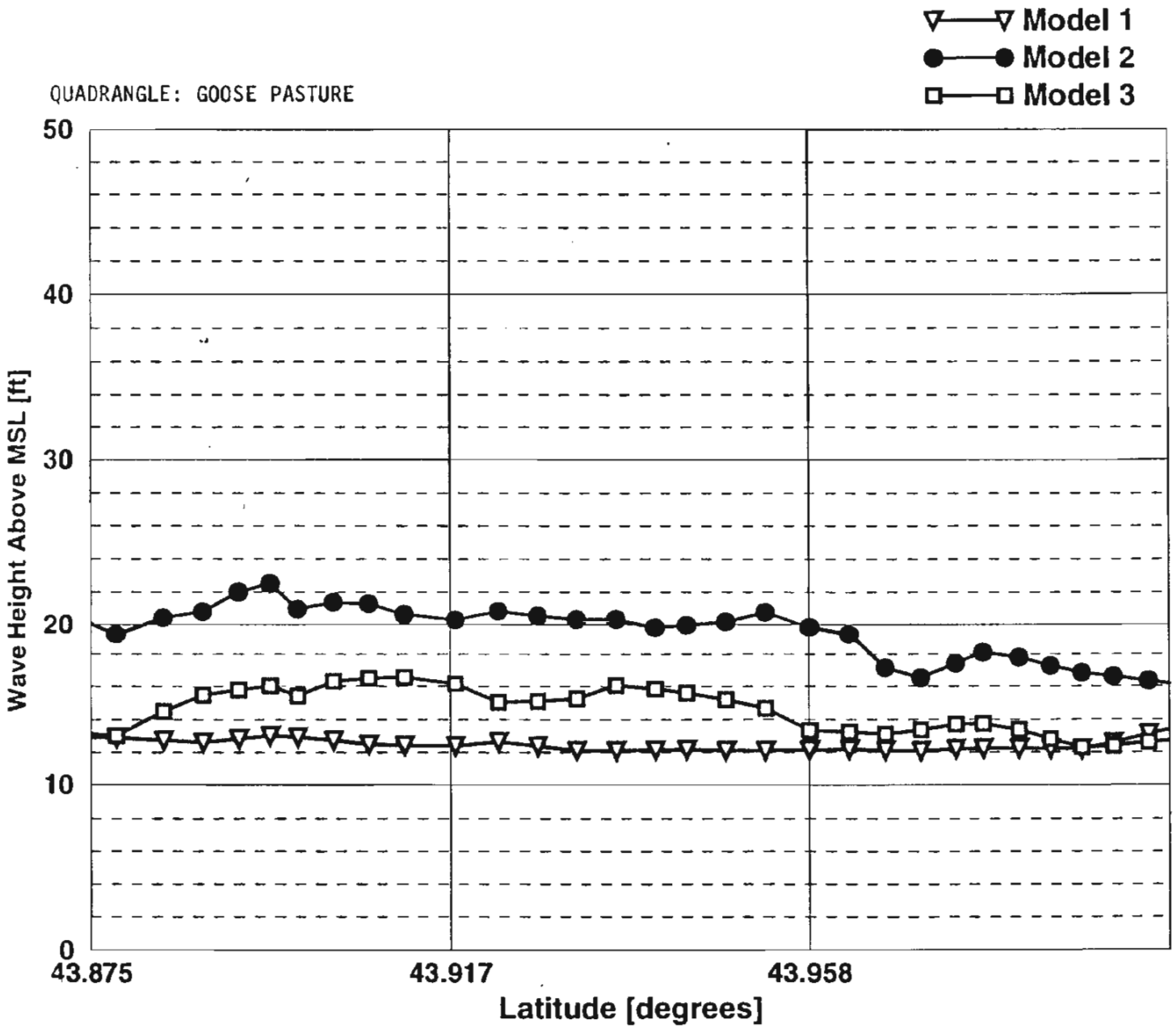
Model 1
Model 2
Model 3
QUADRANGLE: GOOSE PASTURE
50
40
30
20
10
0
Wave Height Above MSL [ft]
43.875
43.917
43.958
Latitude [degrees]

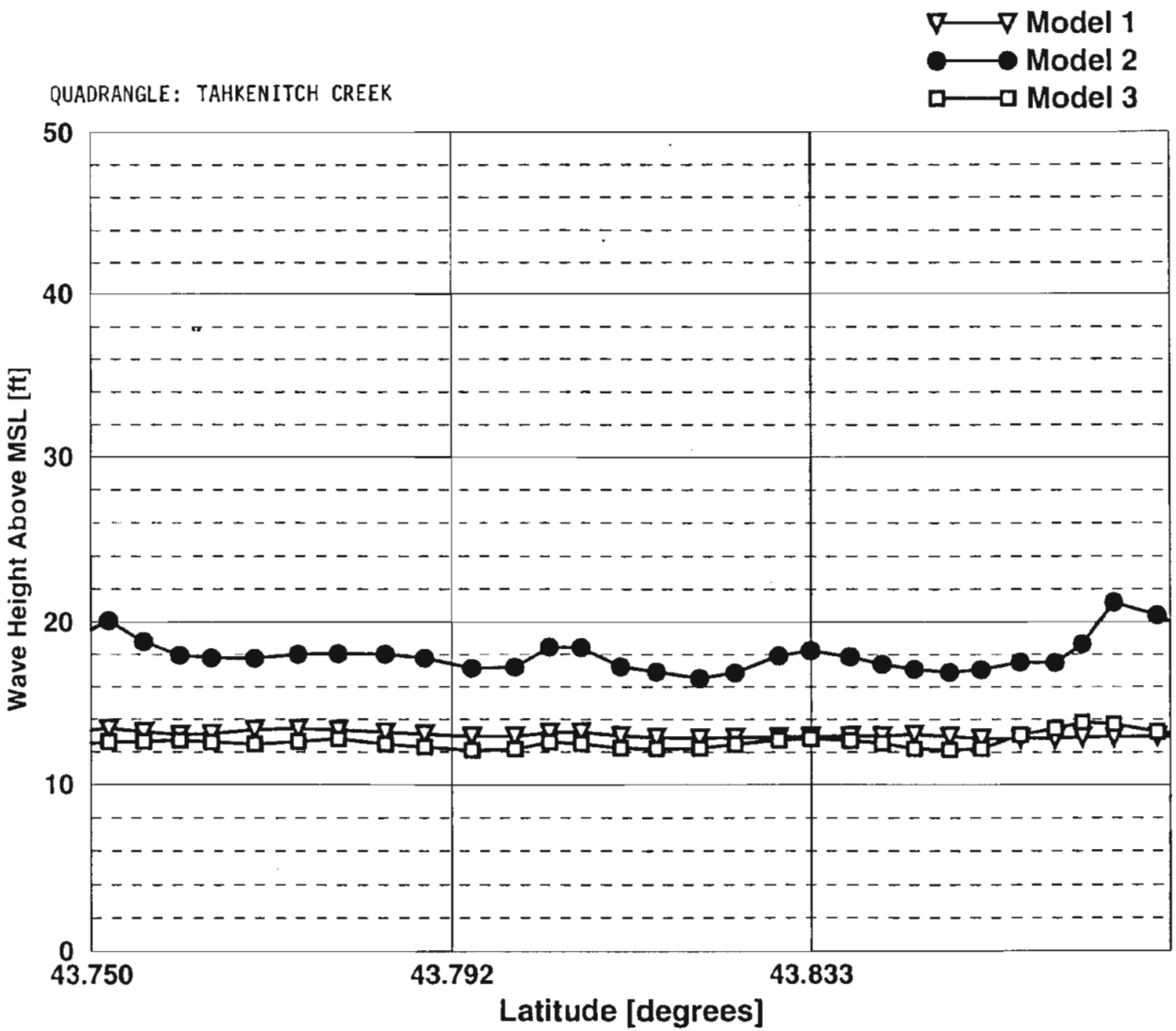
Model 1
Model 2
Model 3
QUADRANGLE: TAHKENITCH CREEK
Wave Height Above MSL [ft]
50
40
30
20
10
0
43.750
43.792
43.833
Latitude [degrees]

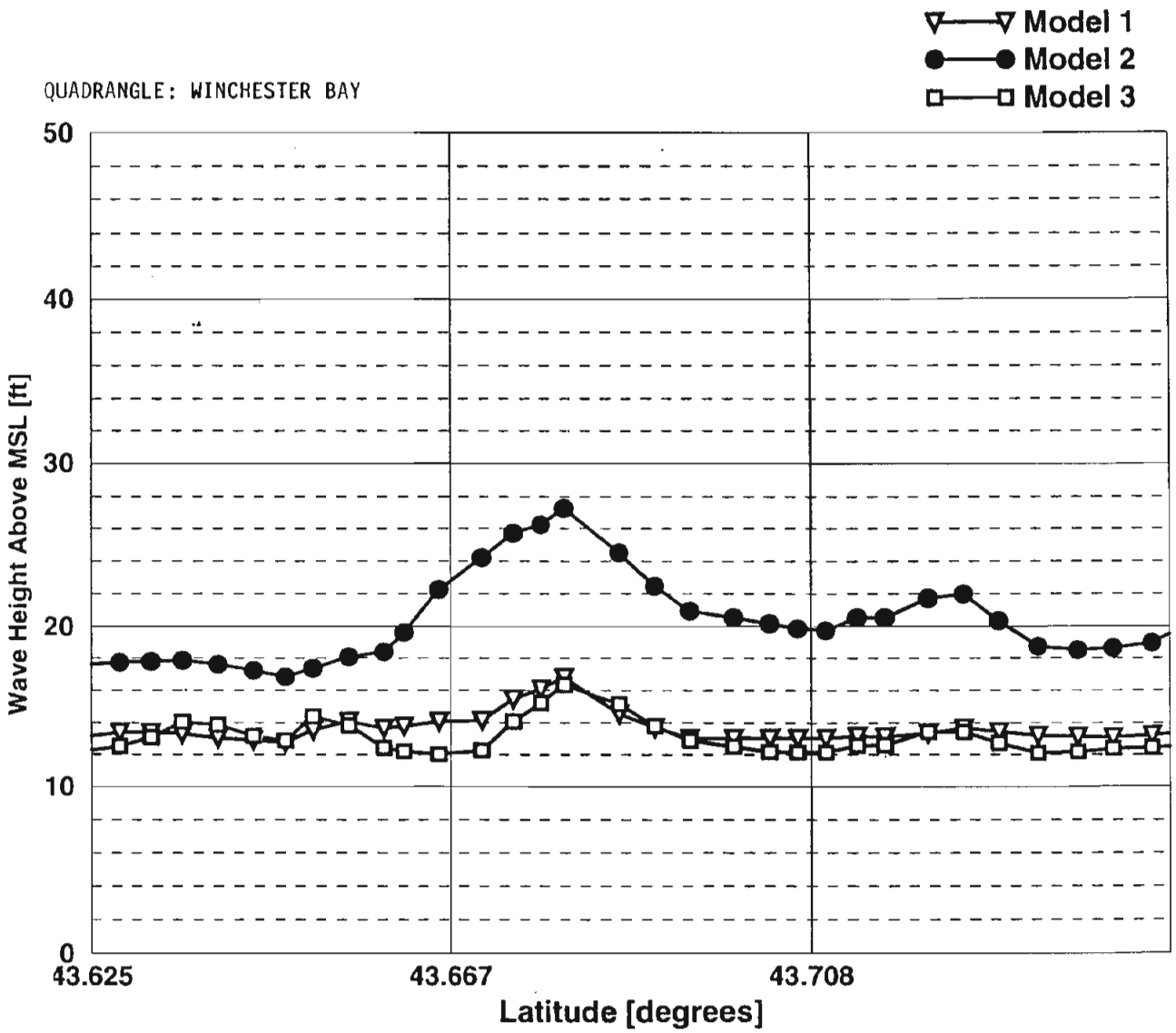
Model 1
Model 2
Model 3
QUADRANGLE: WINCHESTER BAY
50
40
30
20
10
0
Wave Height Above MSL [ft]
43.625
43.667
43.708
Latitude [degrees]

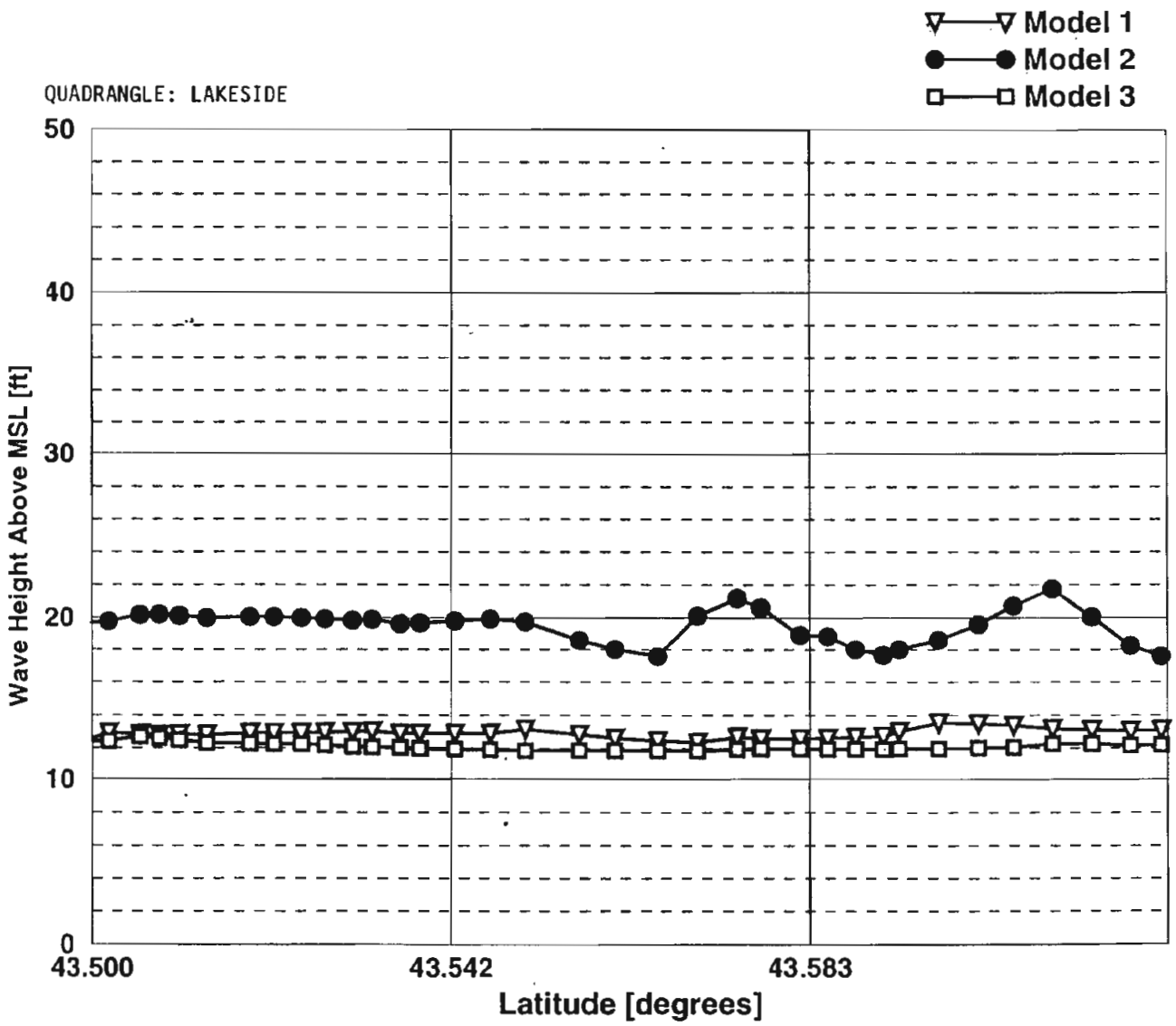
Model 1
Model 2
Model 3
QUADRANGLE: LAKESIDE
50
40
30
20
10
0
Wave Height Above MSL [ft]
43.500
43.542
43.583
Latitude [degrees]

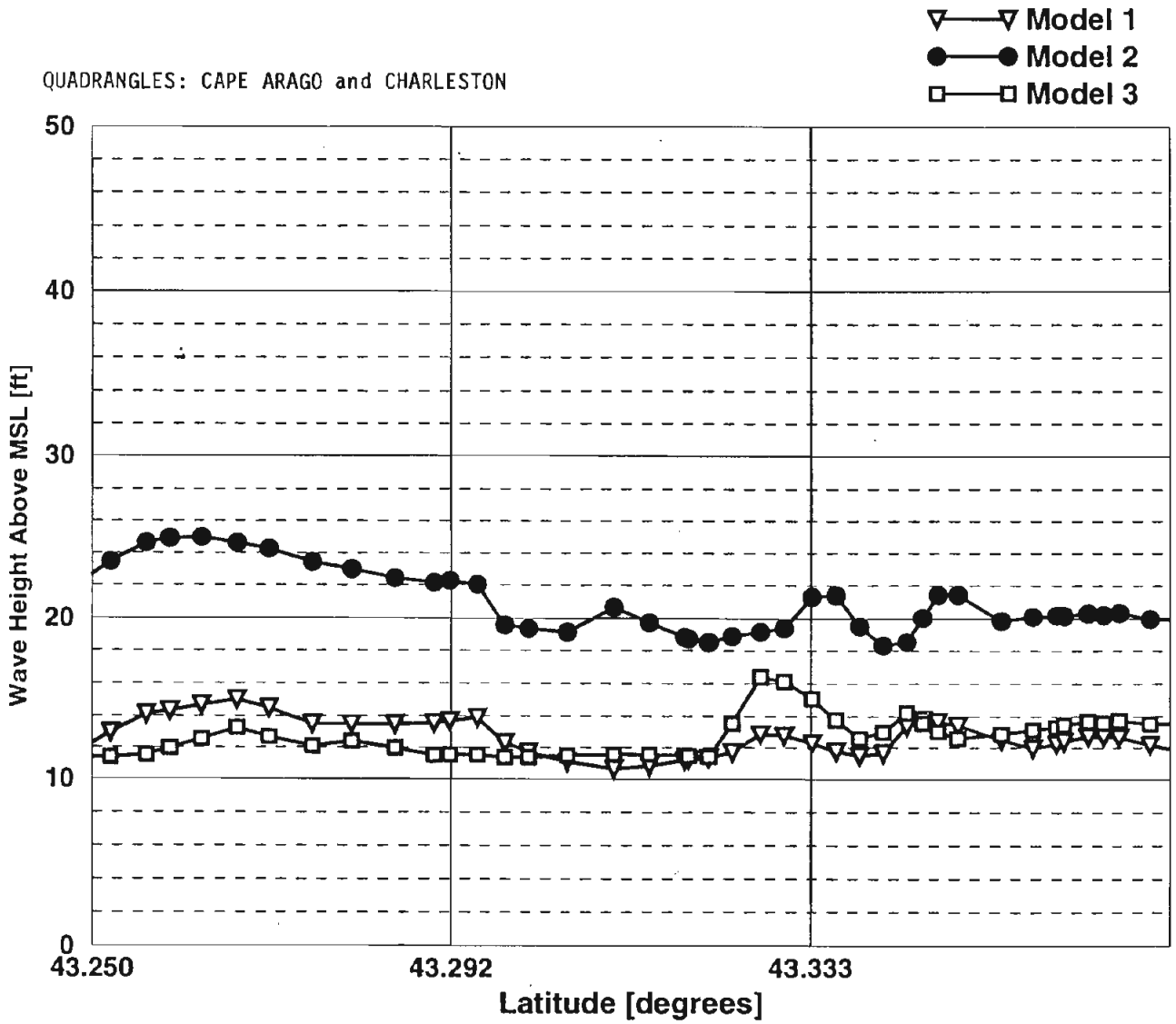
Model 1
Model 2
Model 3
QUADRANGLES: CAPE ARAGO and CHARLESTON
Wave Height Above MSL [ft]
50
40
30
20
10
0
43.250
43.292
43.333
Latitude [degrees]

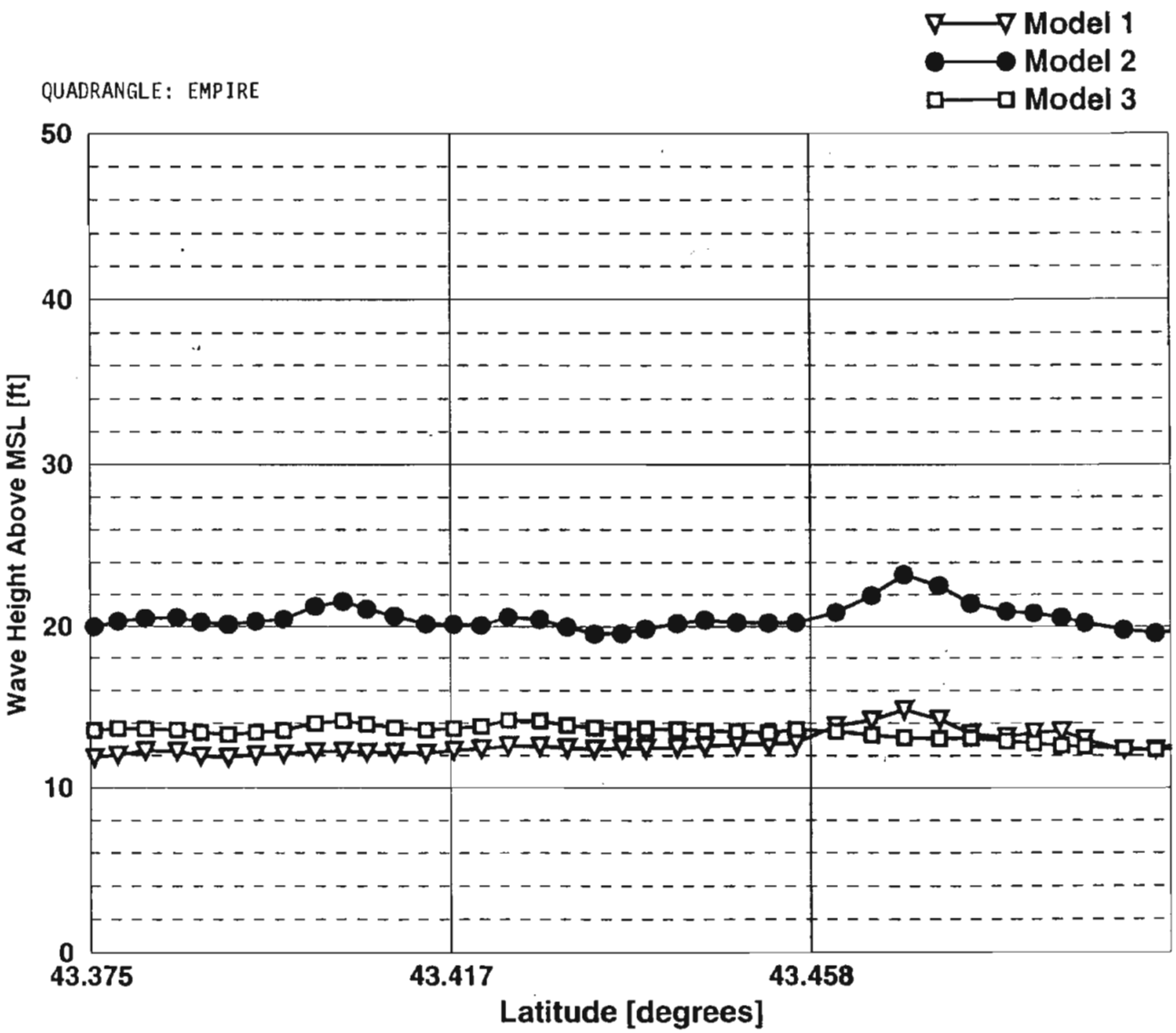
Model 1
Model 2
Model 3
QUADRANGLE: EMPIRE
50
40
30
20
10
0
Wave Height Above MSL [ft]
43.375
43.417
43.458
Latitude [degrees]

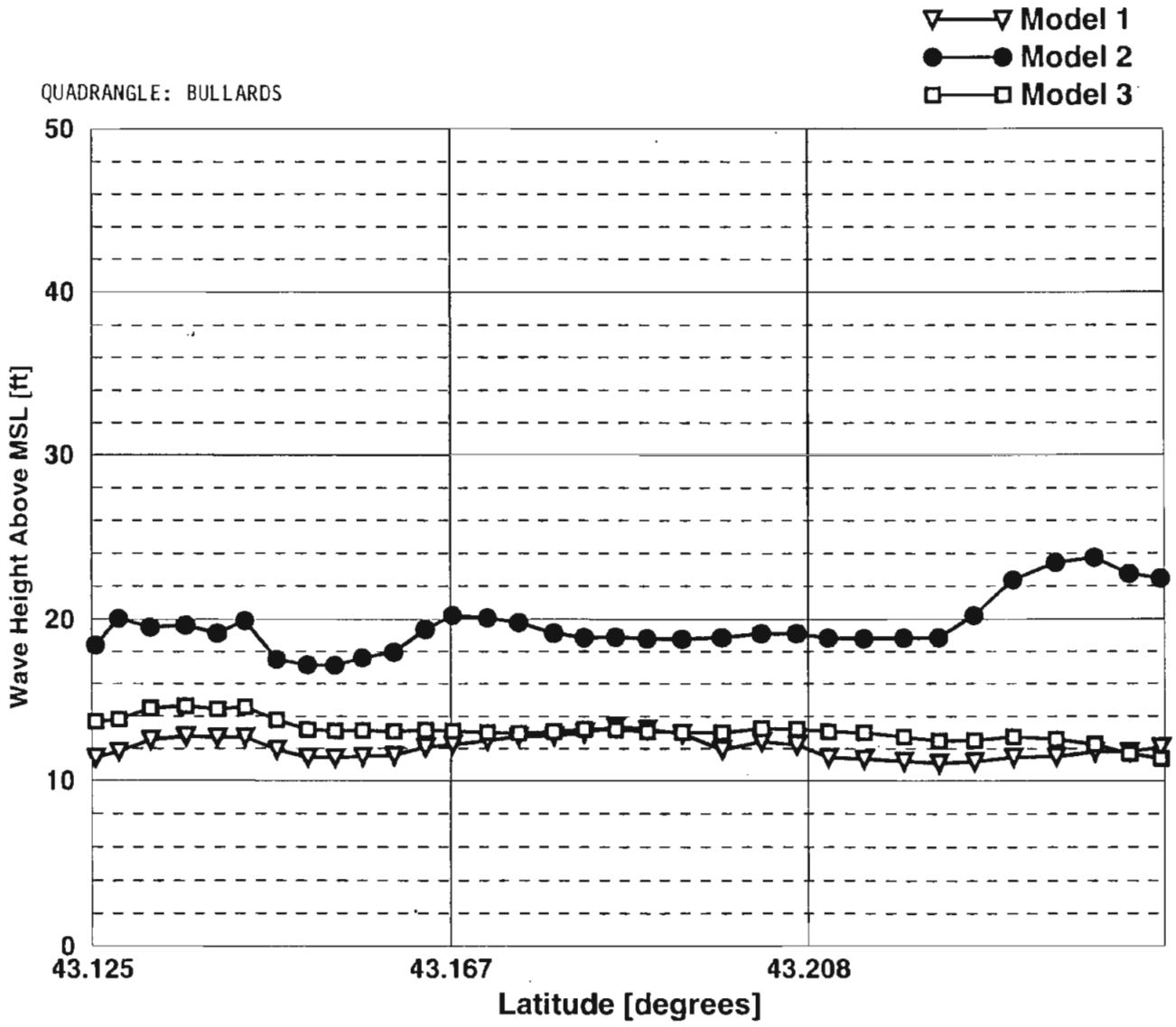
Model 1
Model 2
Model 3
QUADRANGLE: BULLARDS
50
40
30
20
10
0
Wave Height Above MSL [ft]
43.125
43.167
43.208
Latitude [degrees]

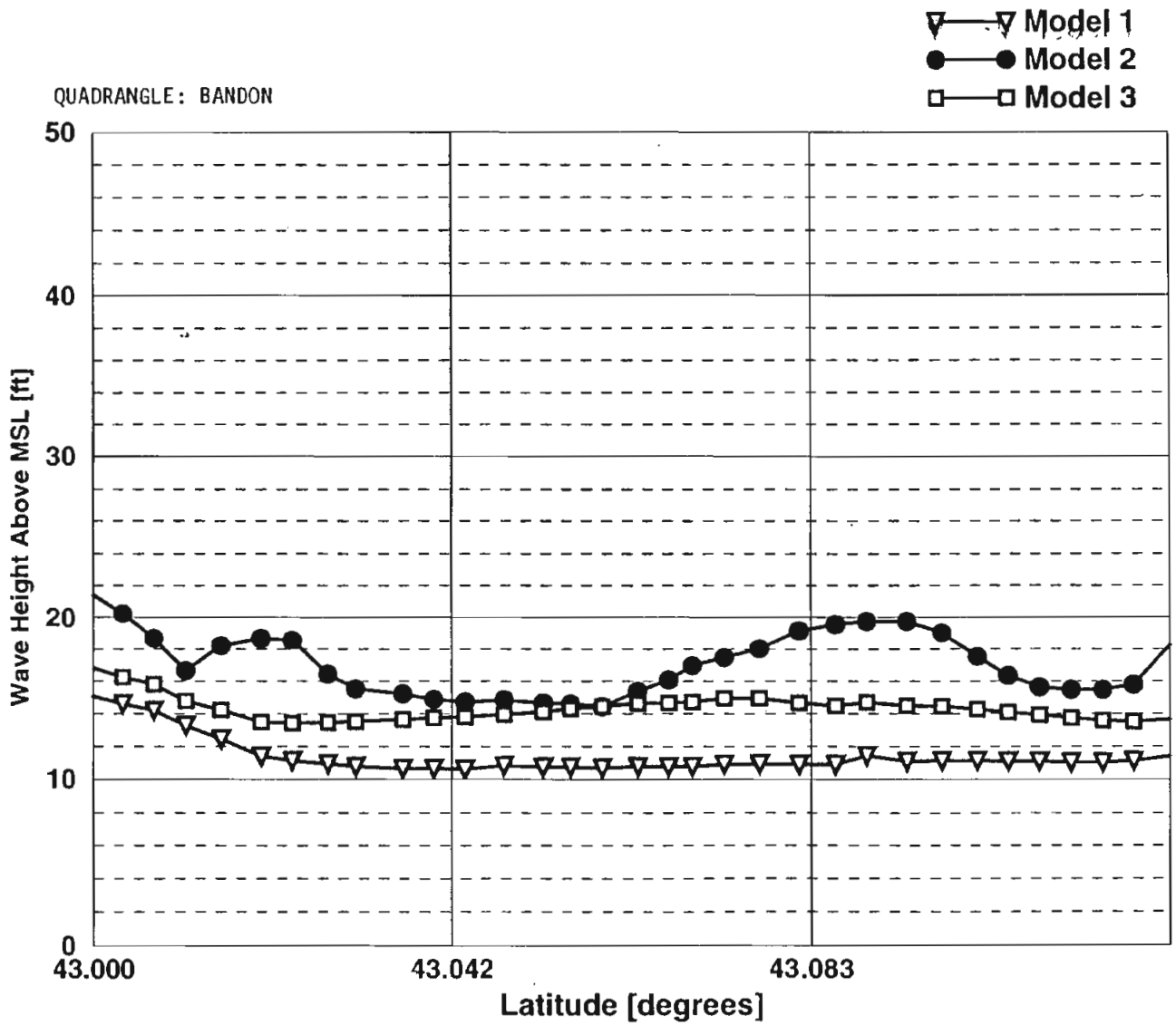
Model 1
Model 2
Model 3
QUADRANGLE: BANDON
Wave Height Above MSL [ft]
50
40
30
20
10
0
43.000
43.042
43.083
Latitude [degrees]

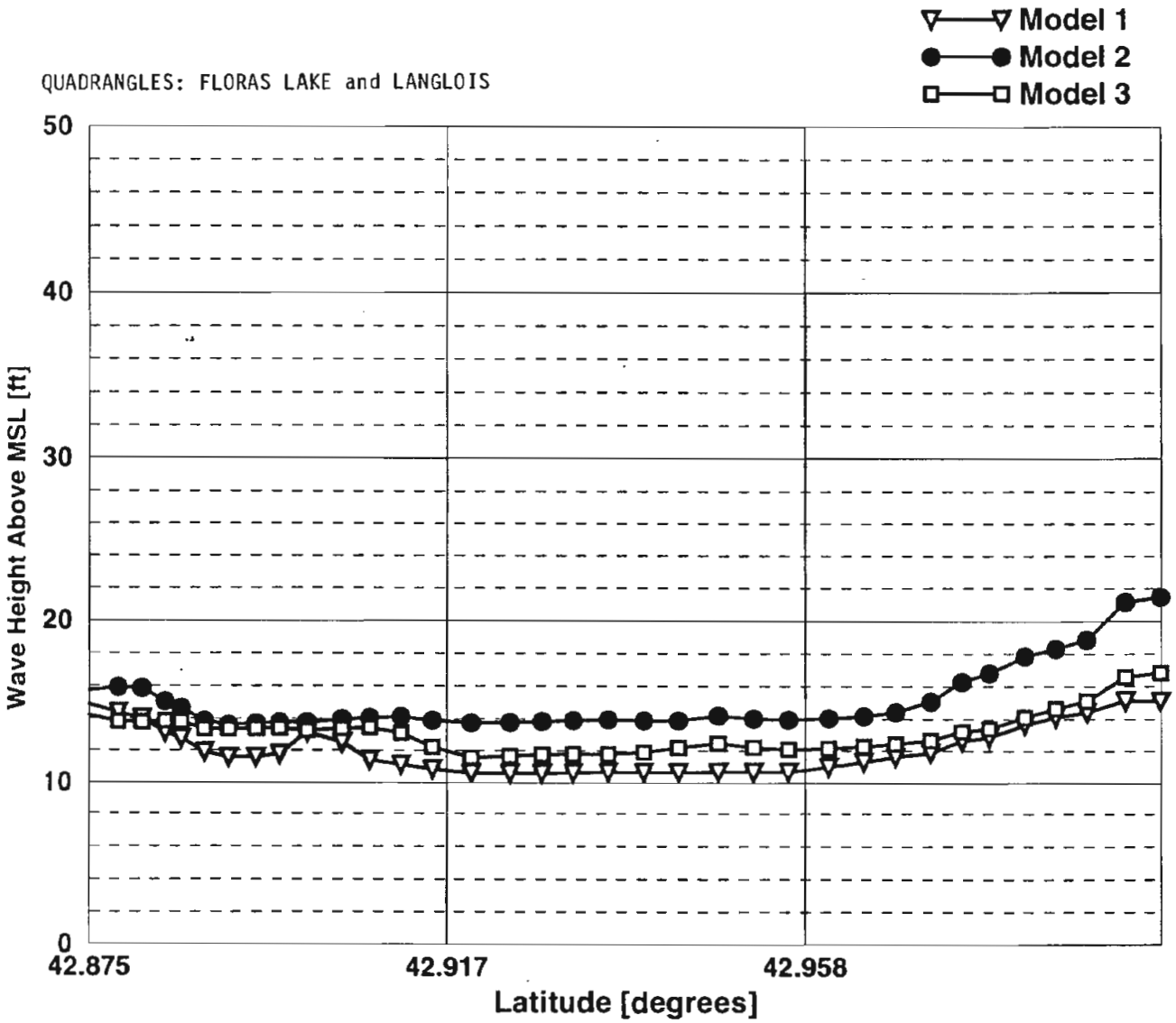
Model 1
Model 2
Model 3
QUADRANGLES: FLORAS LAKE and LANGLOIS
Wave Height Above MSL [ft]
50
40
30
20
10
0
42.875
42.917
42.958
Latitude [degrees]

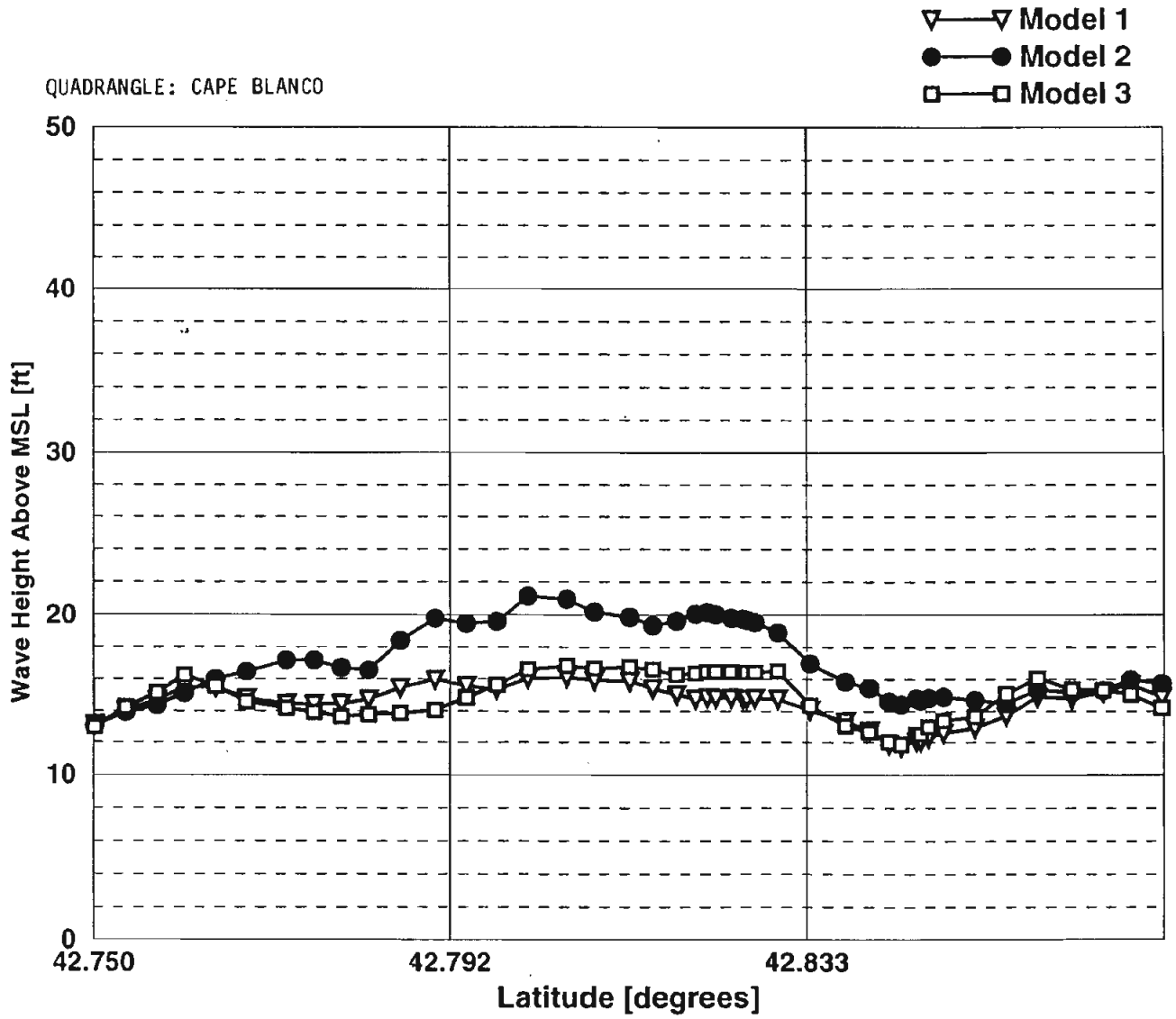
Model 1
Model 2
Model 3
QUADRANGLE: CAPE BLANCO
Wave Height Above MSL [ft]
50
40
30
20
10
0
42.750
42.792
42.833
Latitude [degrees]

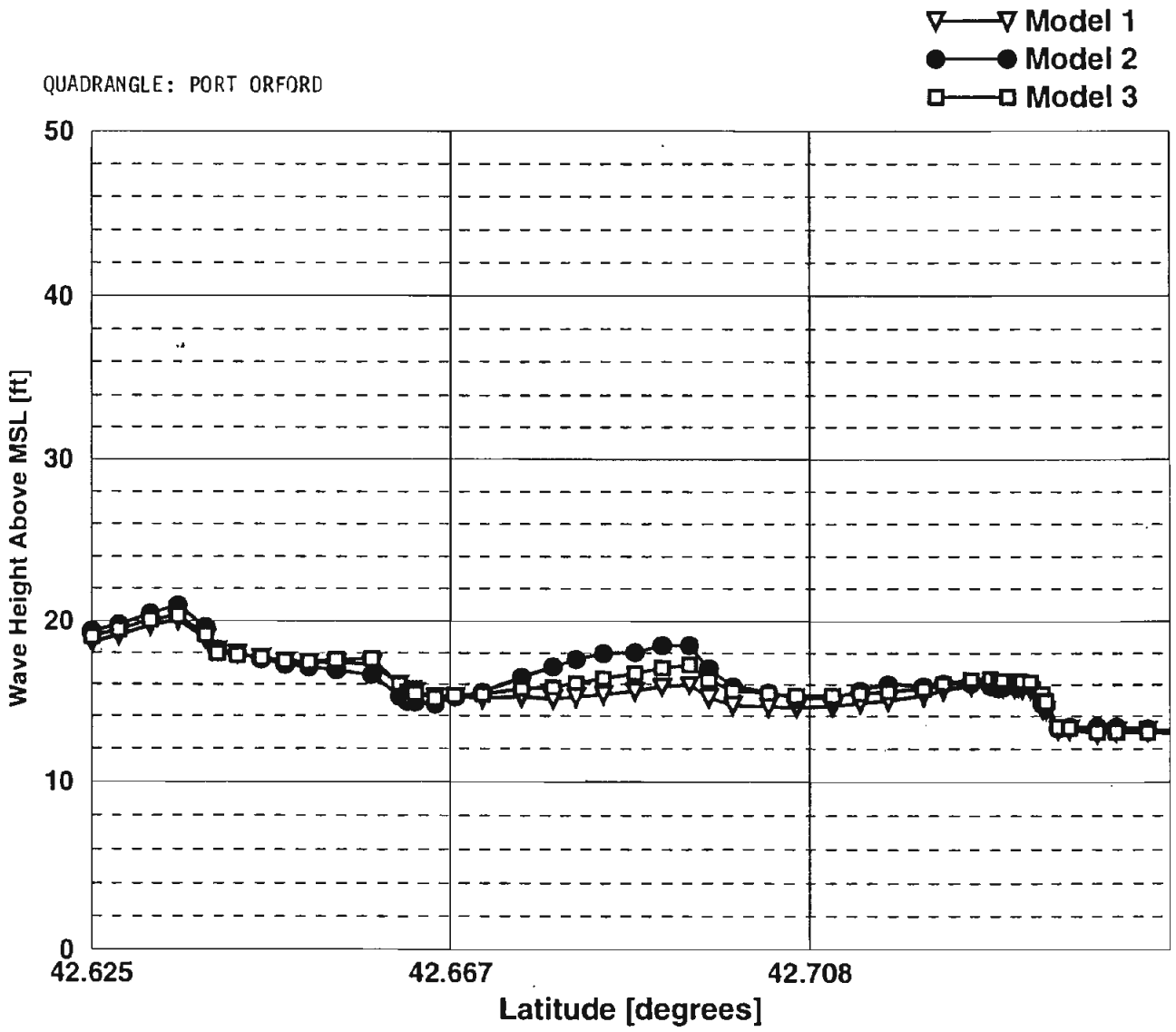
Model 1
Model 2
Model 3
QUADRANGLE: PORT ORFORD
Wave Height Above MSL [ft]
50
40
30
20
10
0
42.625
42.667
42.708
Latitude [degrees]

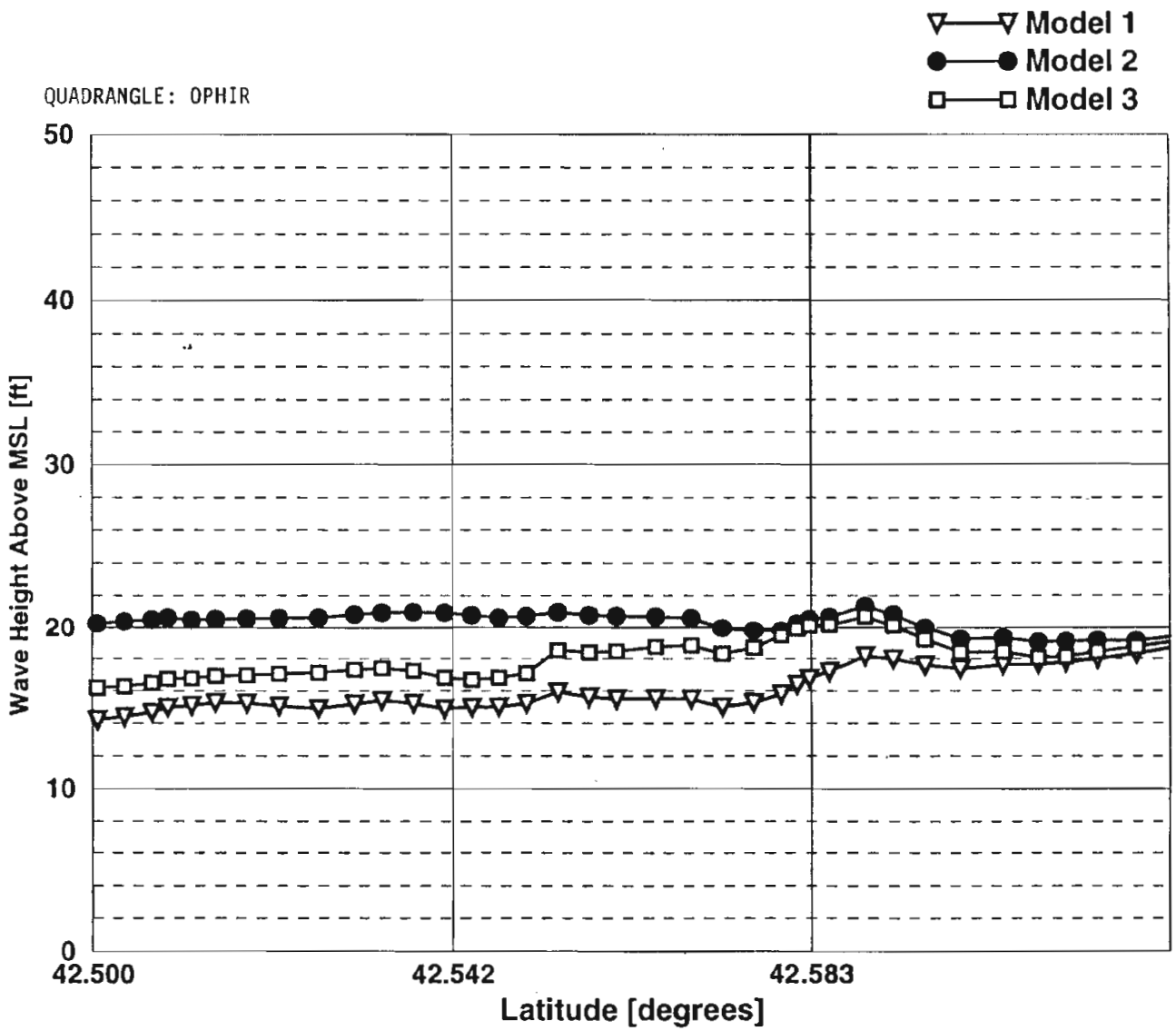
Model 1
Model 2
Model 3
QUADRANGLE: OPHIR
50
40
30
20
10
0
Wave Height Above MSL [ft]
42.500
42.542
42.583
Latitude [degrees]

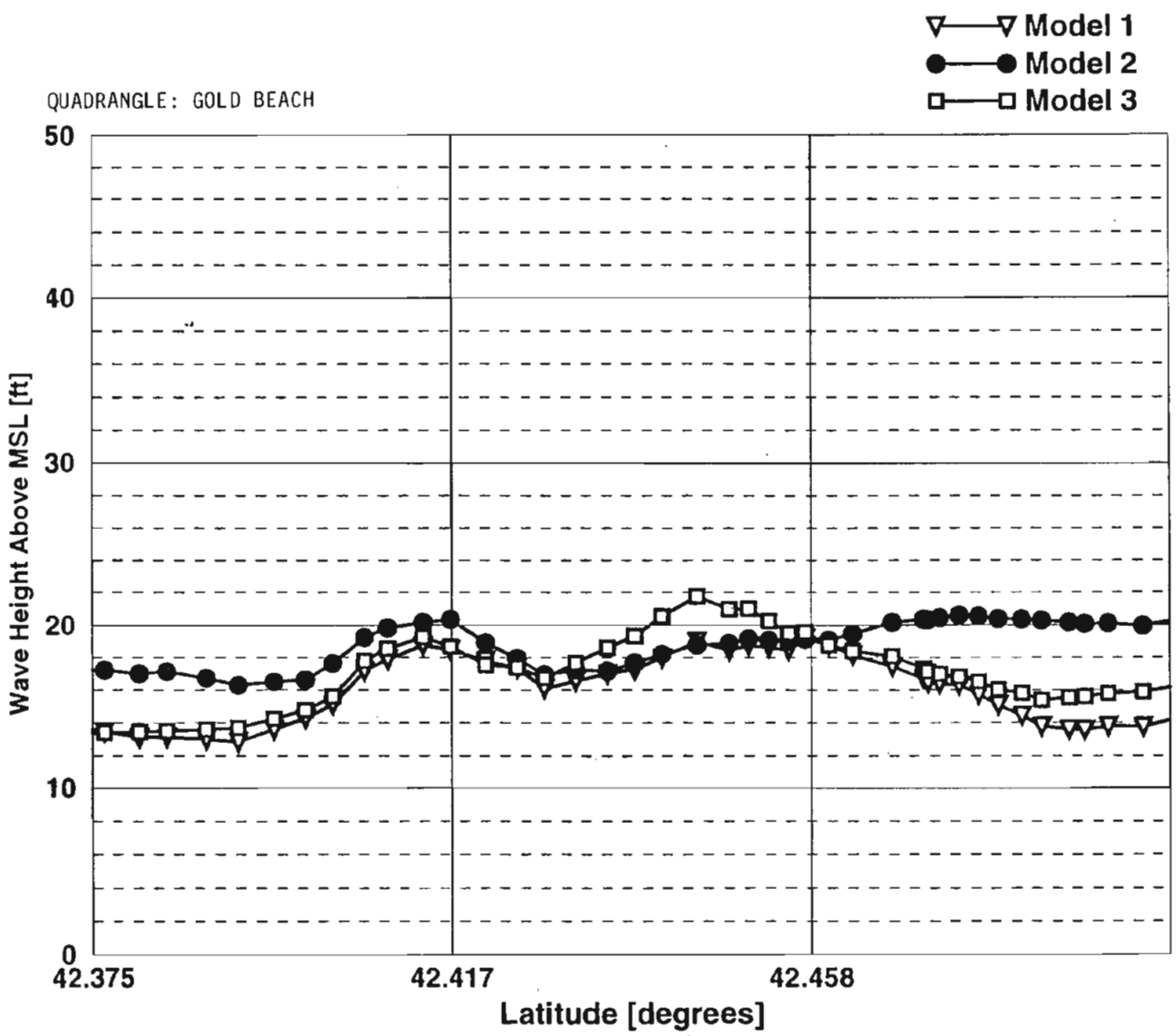
Model 1
Model 2
Model 3
QUADRANGLE: GOLD BEACH
50
40
30
20
10
0
Wave Height Above MSL [ft]
42.375
42.417
42.458
Latitude [degrees]

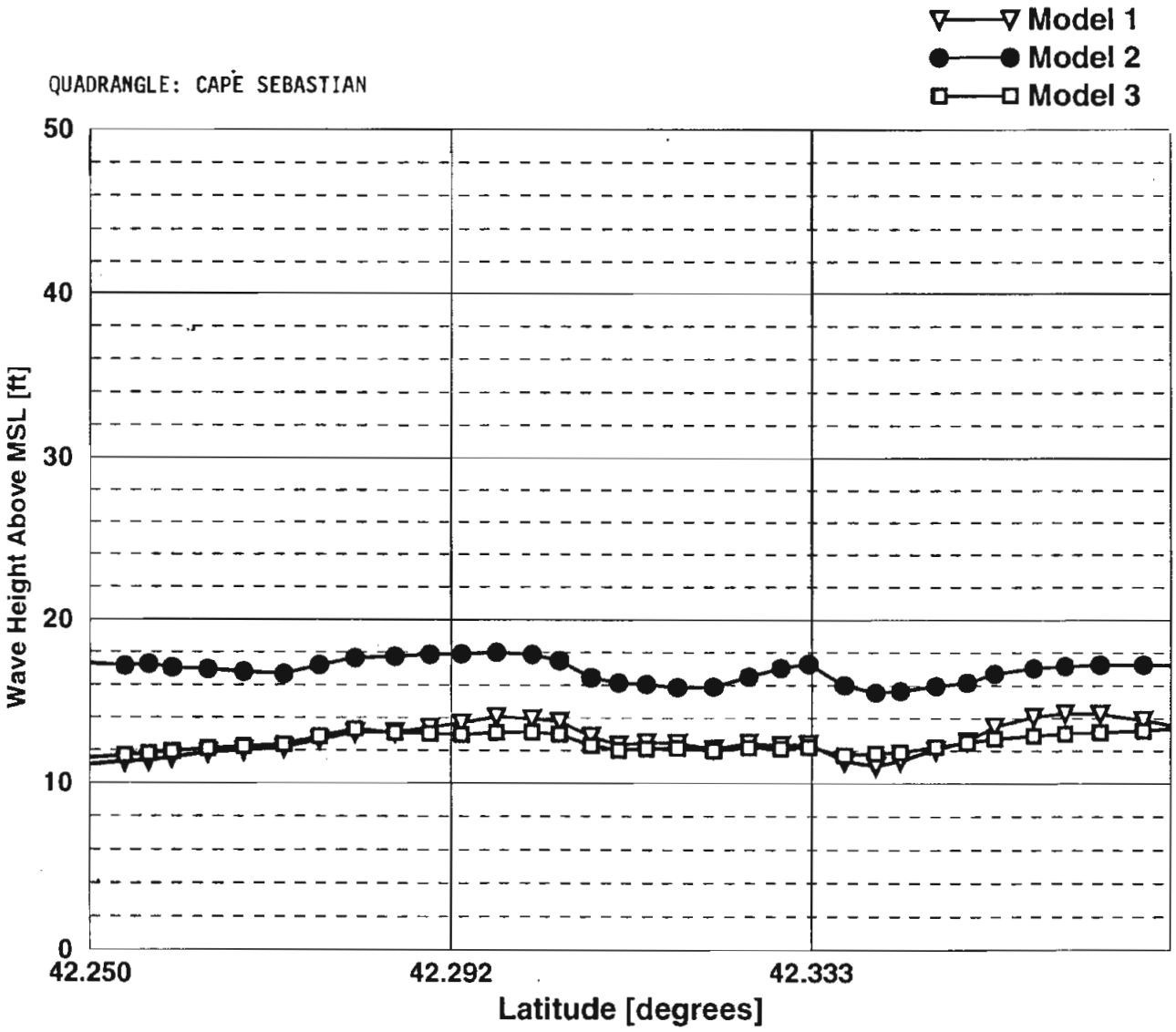
Model 1
Model 2
Model 3
QUADRANGLE: CAPE SEBASTIAN
Wave Height Above MSL [ft]
50
40
30
20
10
0
42.250
42.292
42.333
Latitude [degrees]

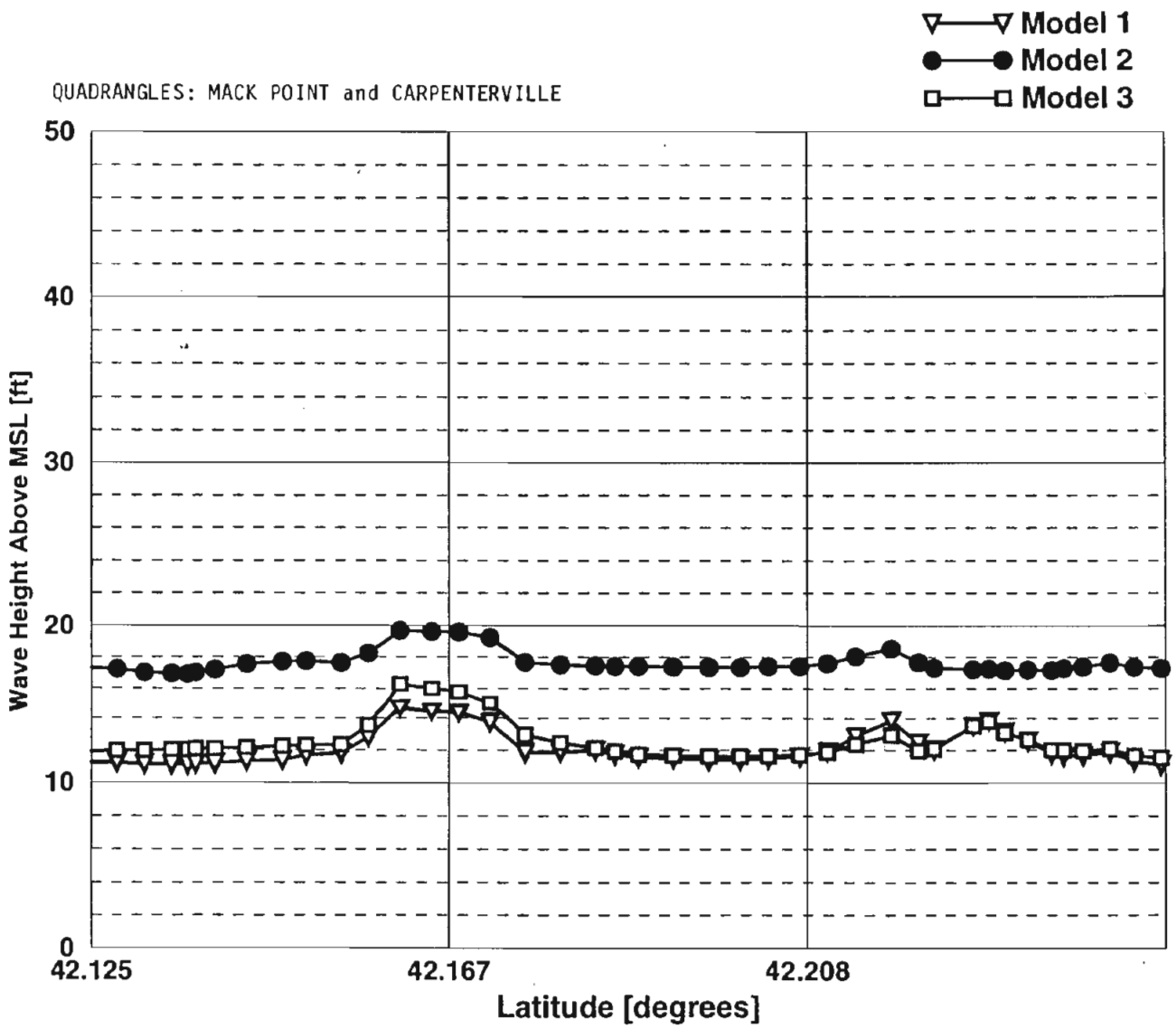
Model 1
Model 2
Model 3
QUADRANGLES: MACK POINT and CARPENTERVILLE
Wave Height Above MSL [ft]
50
40
30
20
10
0
42.125
42.167
42.208
Latitude [degrees]

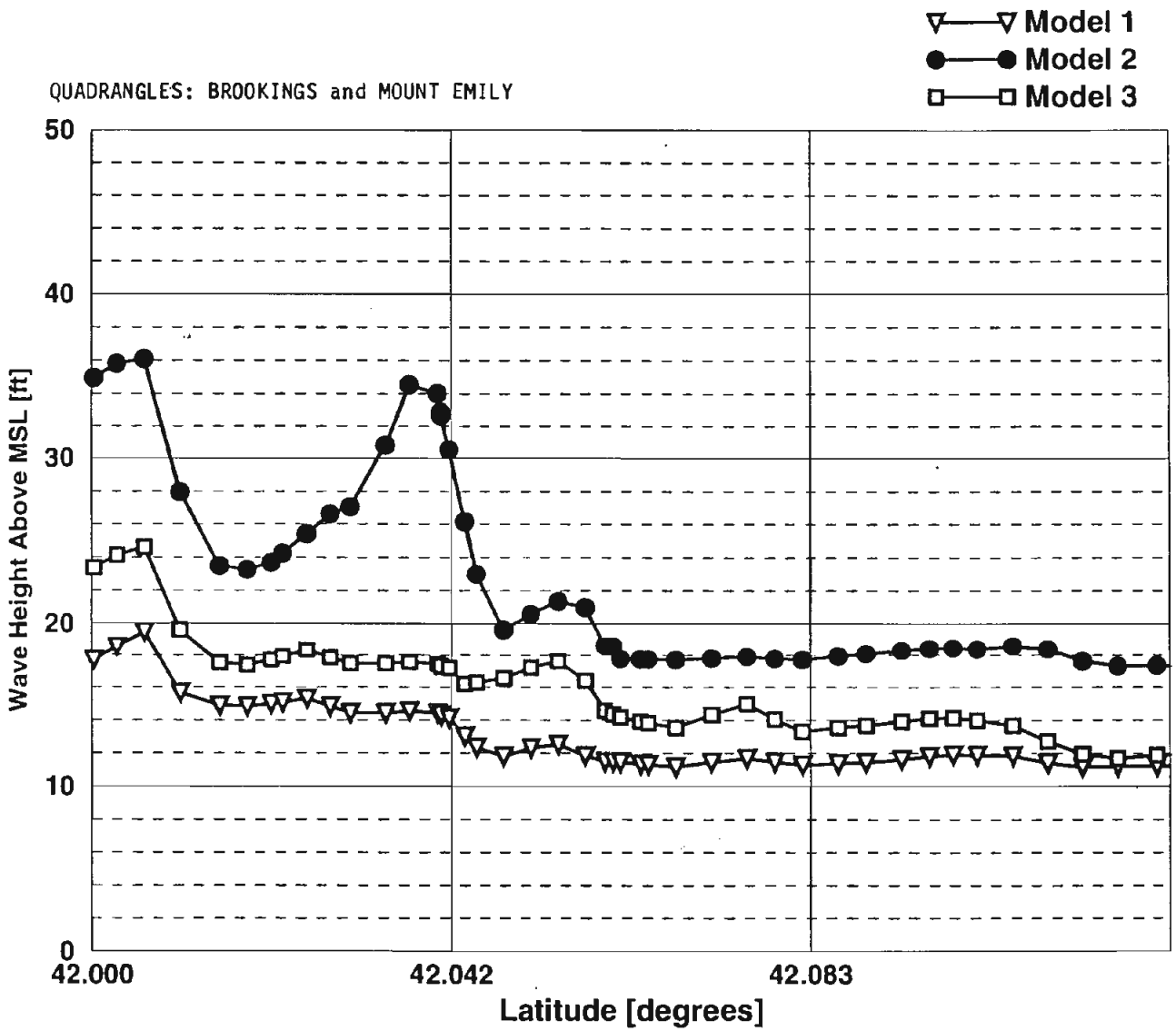
Model 1
Model 2
Model 3
QUADRANGLES: BROOKINGS and MOUNT EMILY
Wave Height Above MSL [ft]
50
40
30
20
10
0
42.000
42.042
42.083
Latitude [degrees]

APPENDIX C

TIME HISTORIES OF RUN-UP AT SELECTED SITES

The following charts show the general pattern and timing of 8 hours of tsunami waves for Models 2 and 3 at selected sites, mainly population centers. The charts are arranged in alphabetical order as follows:

Astoria, Bandon, Brookings, Cape Blanco, Cannon Beach, Columbia River Mouth, Coos Bay Mouth, Depoe Bay, Gold Beach, Nehalem Bay, Neskowin, Nestucca Bay, Netarts Bay, Newport, Otter Rock, Port Orford, Roads End, Seaside, Siletz Bay (Lincoln City-Taft), Siuslaw River (Florence), Tillamook Bay Mouth, Umpqua Bay Mouth (Reedsport-Winchester Bay), Waldport, and Warrenton.

*The absolute run-up elevations are not representative of dry land run-up*, since the nature of the digital technique used to produce the charts requires that the observation point for each chart be located offshore in an area that is not "dry" at any point in the simulation. *This leads to generally lower absolute run-up than actual* and a number of high frequency waves (lots of variation over a few minutes time) that will not be very important for actual inundation observed at the shoreline. The absolute value of the run-up at zero minutes may be a negative or positive value, but this is an artifact of the numerical modeling technique and should not be used to infer actual run-up height being suddenly high or low. It is the pattern of waves and relative differences in the models that is important, not the absolute values read on the vertical axis. The charts should be utilized to:

1. See the difference in the models with respect to wave pattern, particularly during the first 10-15 minutes after the earthquake. For example, Model 2 produces falling water levels and Model 3 rising levels immediately after the earthquake on the north coast.

2. Note that the first positive wave is higher when preceded by withdrawing versus rising water.

3. Observe the time to arrival of the first positive tsunami wave.

4. Observe how long significant wave activity persists.

The charts are presented to aid emergency planners to understand the time constraints for evacuation and recovery after an undersea earthquake. Note that many of the time histories predict some modest flooding beginning even in the first minute after the earthquake, particularly for Model 3 and for all models on the south coast. As explained in Appendix A, the time history for Model 3 may be the most likely scenario, even though the predicted maximum wave height for Model 3 is probably somewhat low relative to the maximum height of a likely scenario tsunami. ***Therefore plan on an initial wave as high as Model 2 but arriving more like Model 3***. This method of planning is the most conservative of life safety. Observation 2 above is important, since it is a direct way of anticipating a particularly high initial wave should rapidly withdrawing sea water be observed immediately after an earthquake.

# Time History Without Coseismic Subsidence Correction
## ASTORIA AREA

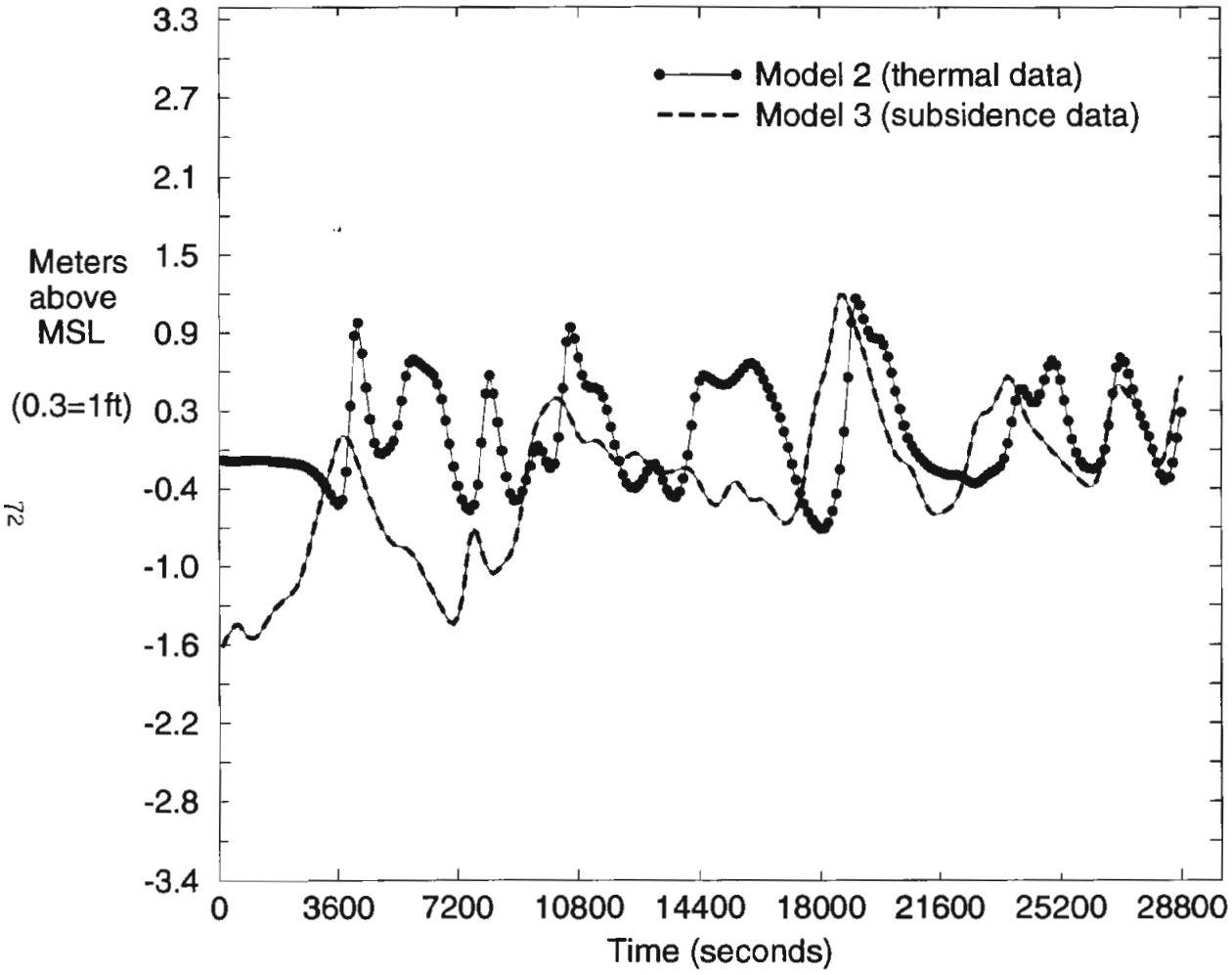


(3600 seconds = 1 hour)
(Plotted points spaced at 2 minute intervals)

# Time History Without Coseismic Subsidence Correction
# BANDON

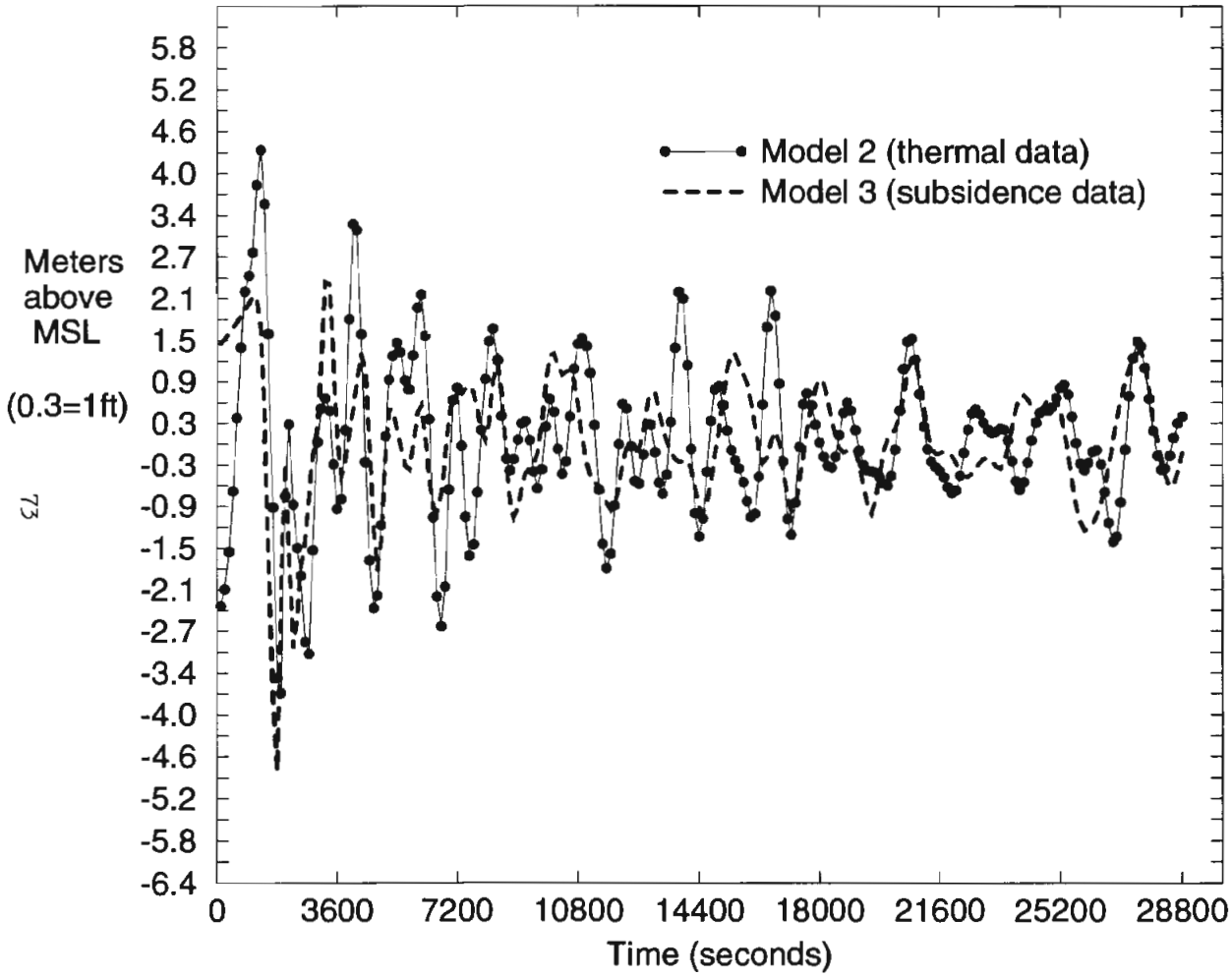


(3600 seconds = 1 hour)
(Plotted points spaced at 2 minute intervals)

# Time History Without Coseismic Subsidence Correction
# BROOKINGS

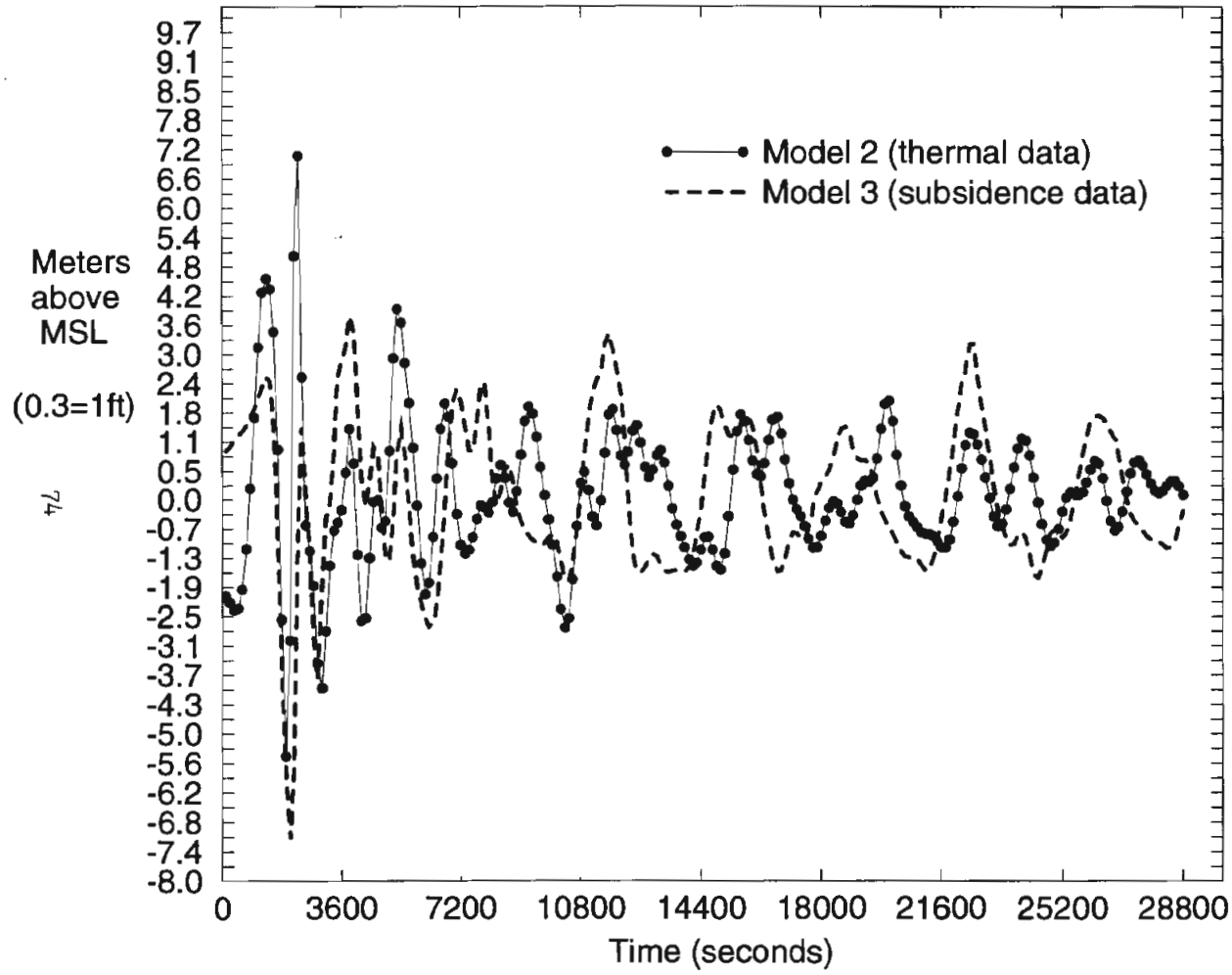


(3600 seconds = 1 hour)
(Plotted points spaced at 2 minute intervals)

# Time History Without Coseismic Subsidence Correction
# CAPE BLANCO AREA

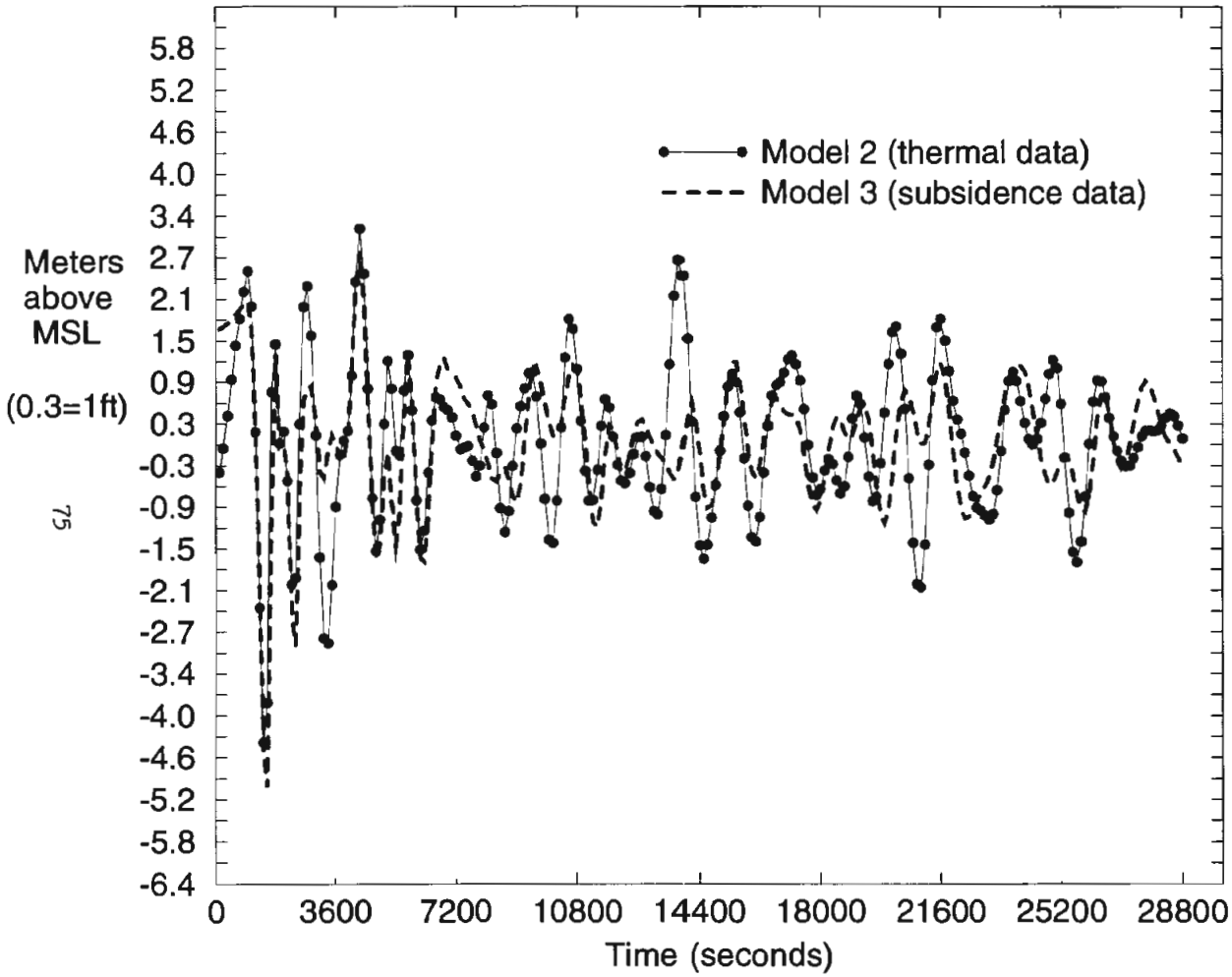


(3600 seconds = 1 hour)
(Plotted points spaced at 2 minute intervals)

# Time History Without Coseismic Subsidence Correction
# CANNON BEACH AREA

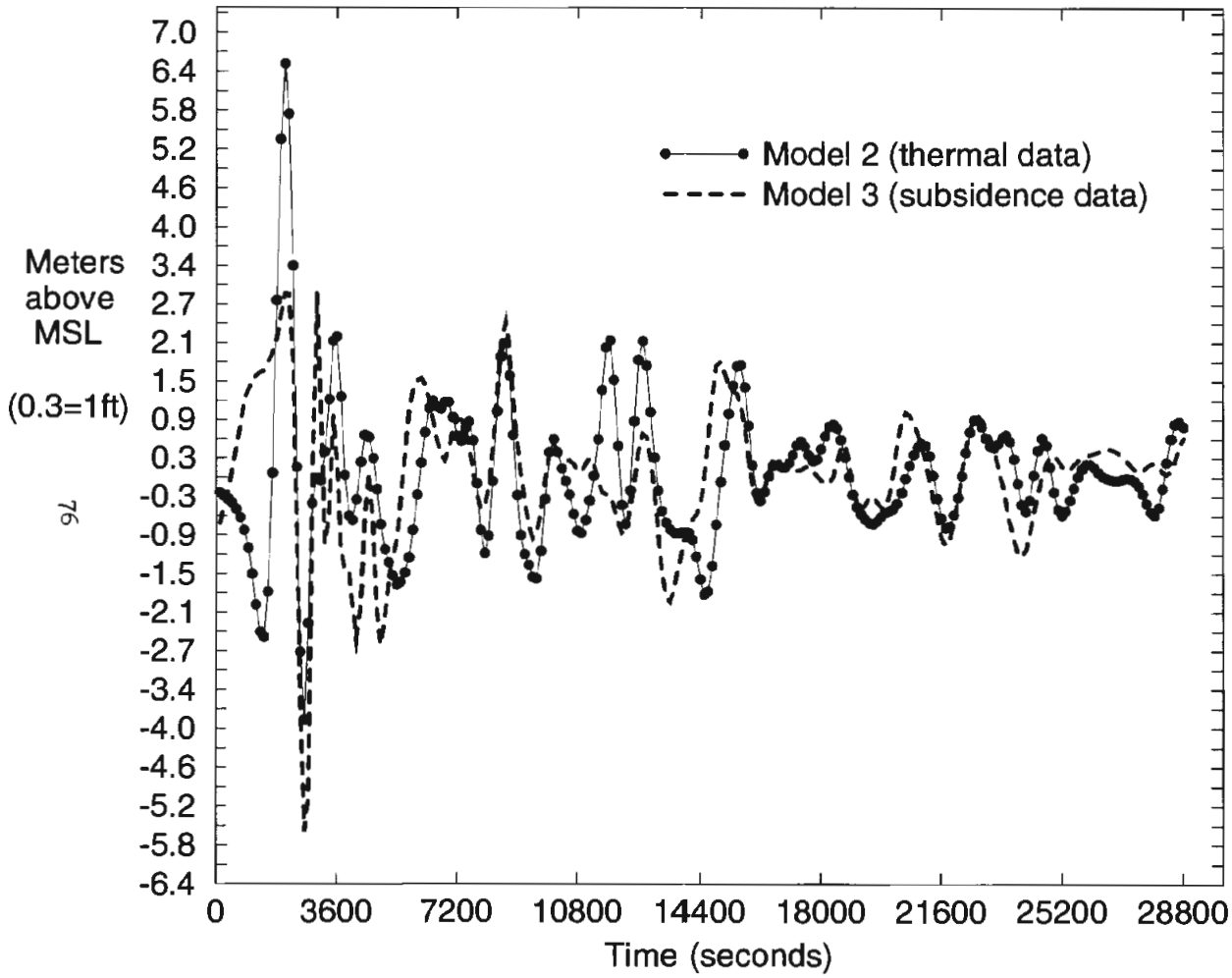


(3600 seconds = 1 hour)
(Plotted points spaced at 2 minute intervals)

# Time History Without Coseismic Subsidence Correction
# COLUMBIA RIVER MOUTH

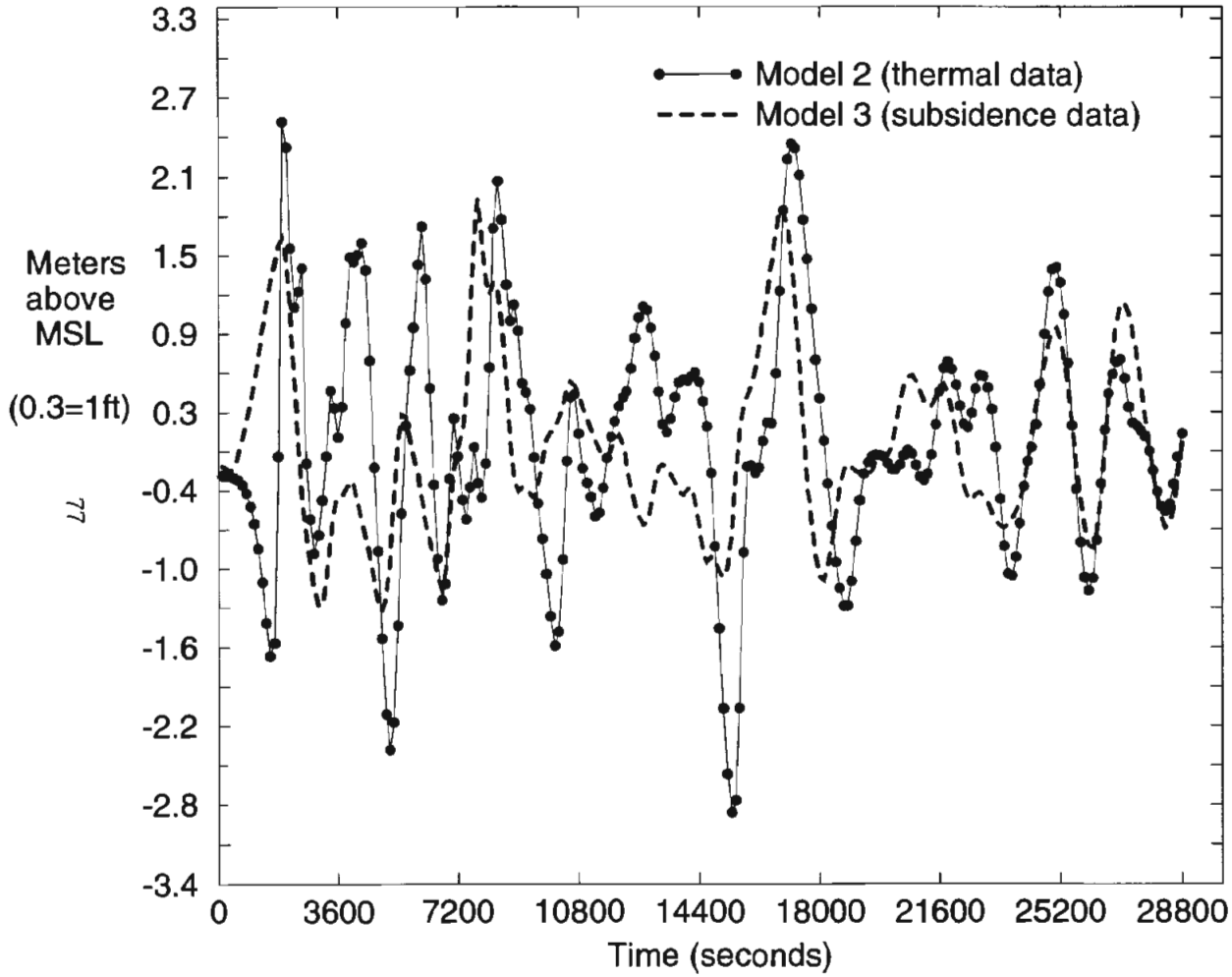


(3600 seconds = 1 hour)
(Plotted points spaced at 2 minute intervals)

# Time History Without Coseismic Subsidence Correction
# COOS BAY MOUTH

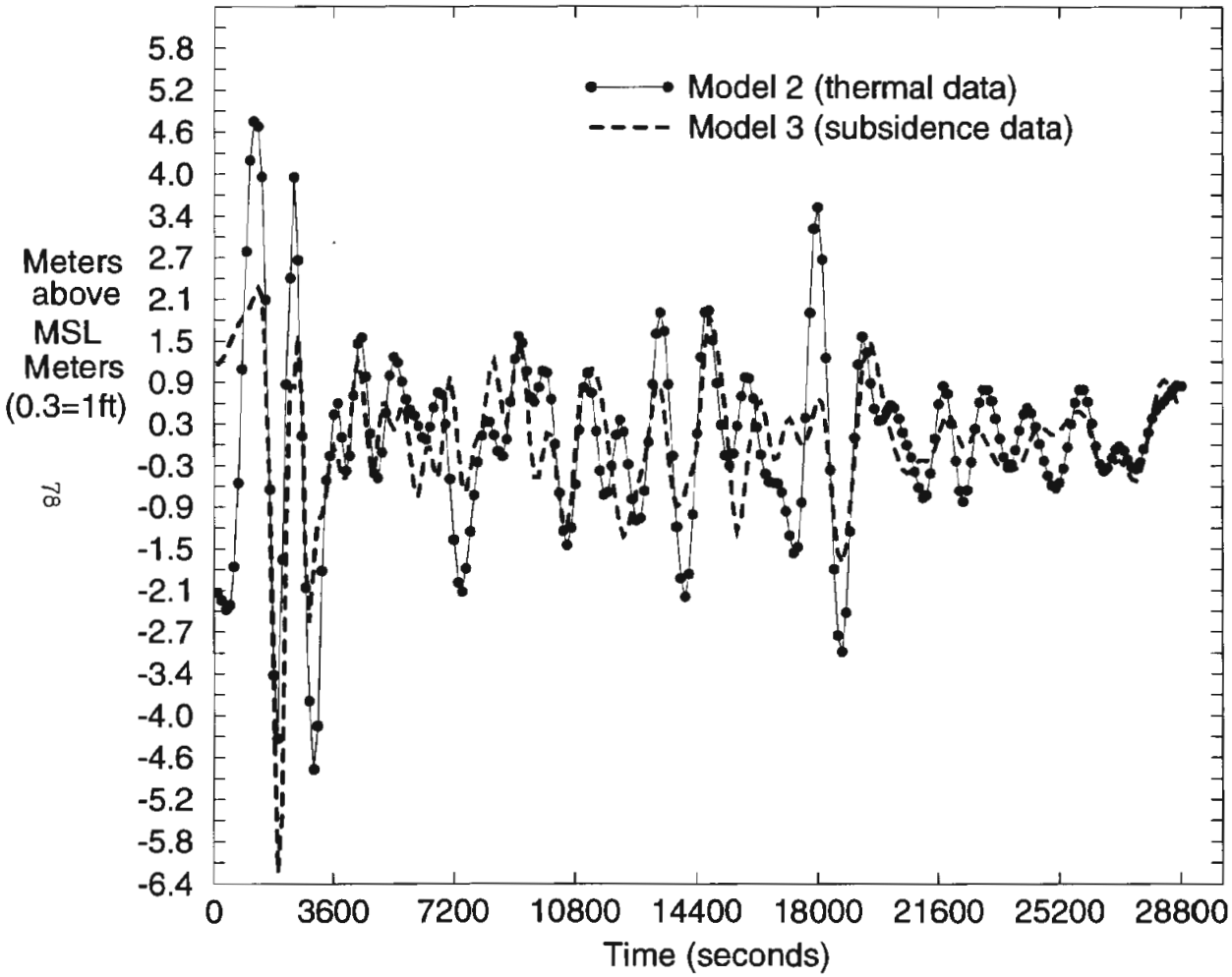


(3600 seconds = 1 hour)
(Plotted points spaced at 2 minute intervals)

# Time History Without Coseismic Subsidence Correction
# DEPOE BAY

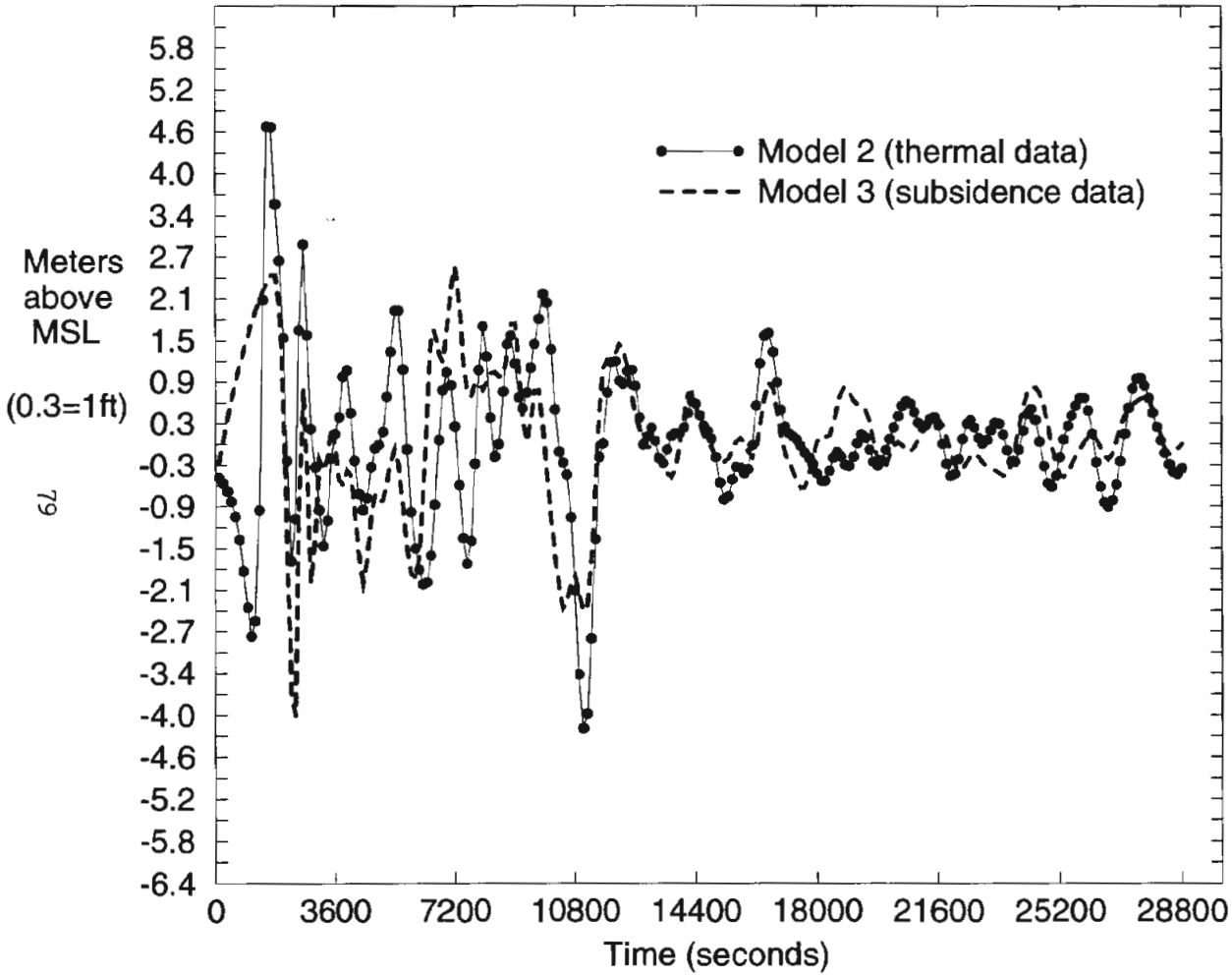


(3600 seconds = 1 hour)
(Plotted points spaced at 2 minute intervals)

# Time History Without Coseismic Subsidence Correction
## GOLD BEACH

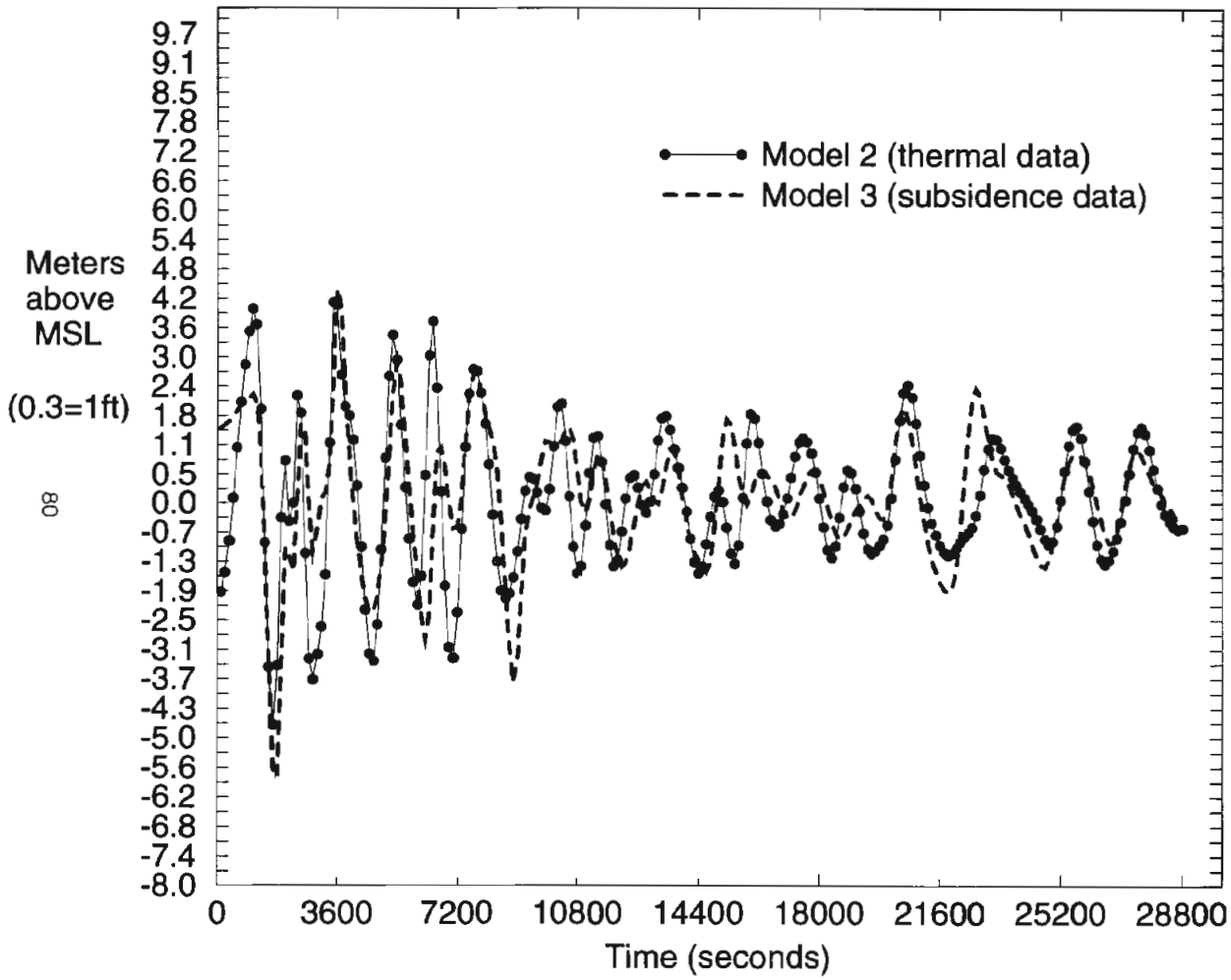


(3600 seconds = 1 hour)
(Plotted points spaced at 2 minute intervals)

# Time History Without Coseismic Subsidence Correction
## NEHALEM BAY AREA

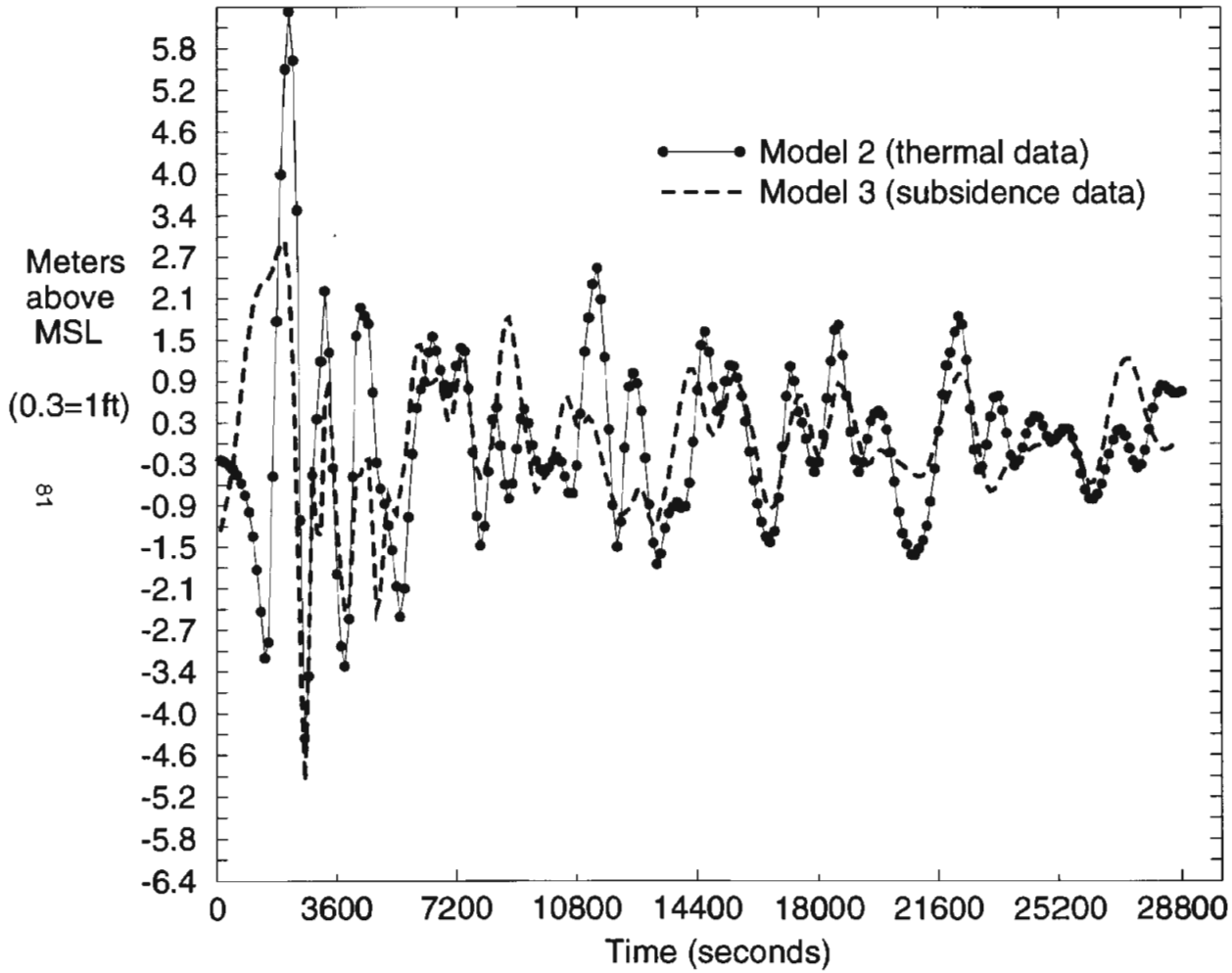


(3600 seconds = 1 hour)
(Plotted points spaced at 2 minute intervals)

# Time History Without Coseismic Subsidence Correction
# NESKOWIN AREA

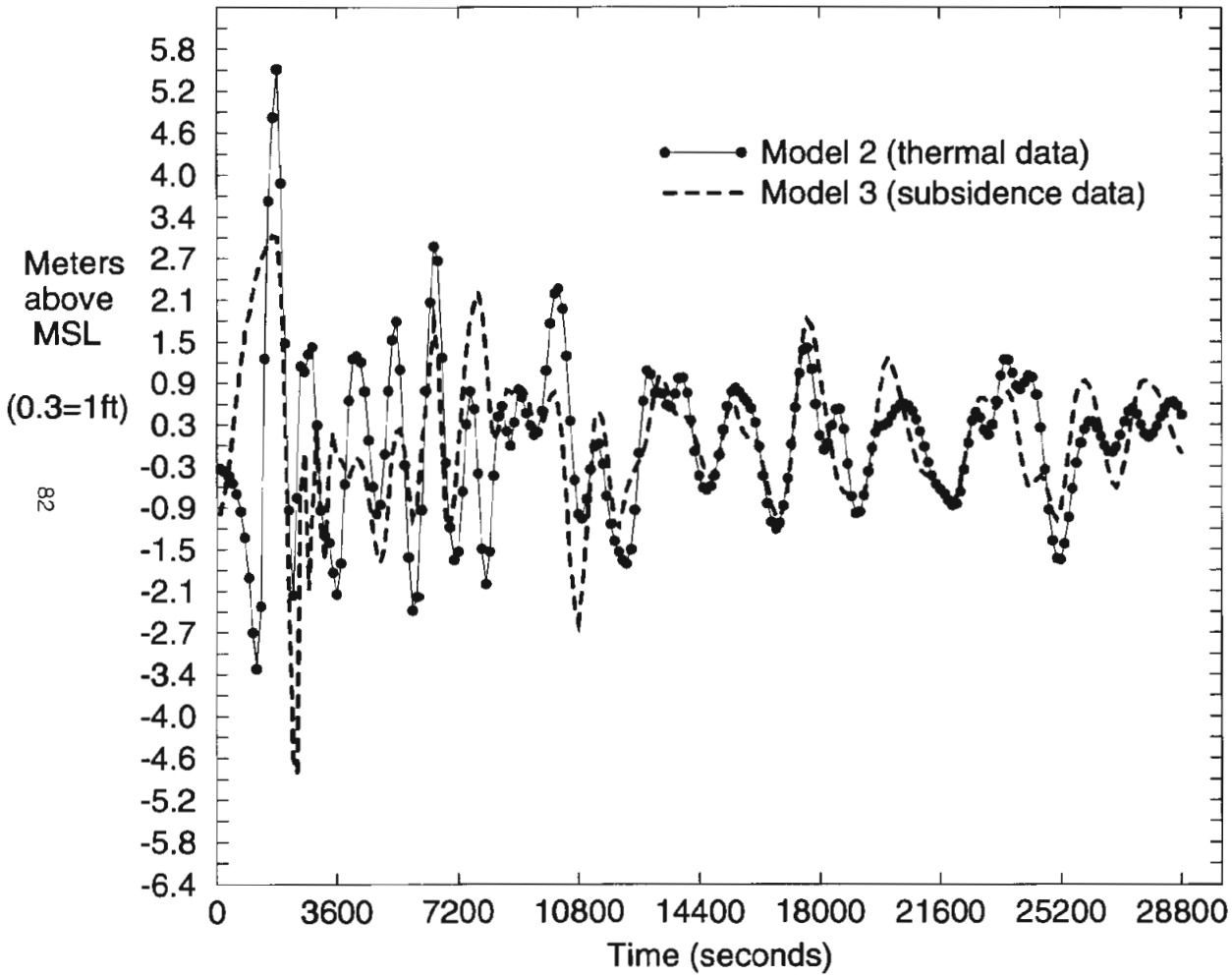


(3600 seconds = 1 hour)
(Plotted points spaced at 2 minute intervals)

# Time History Without Coseismic Subsidence Correction
## NESTUCCA BAY AREA

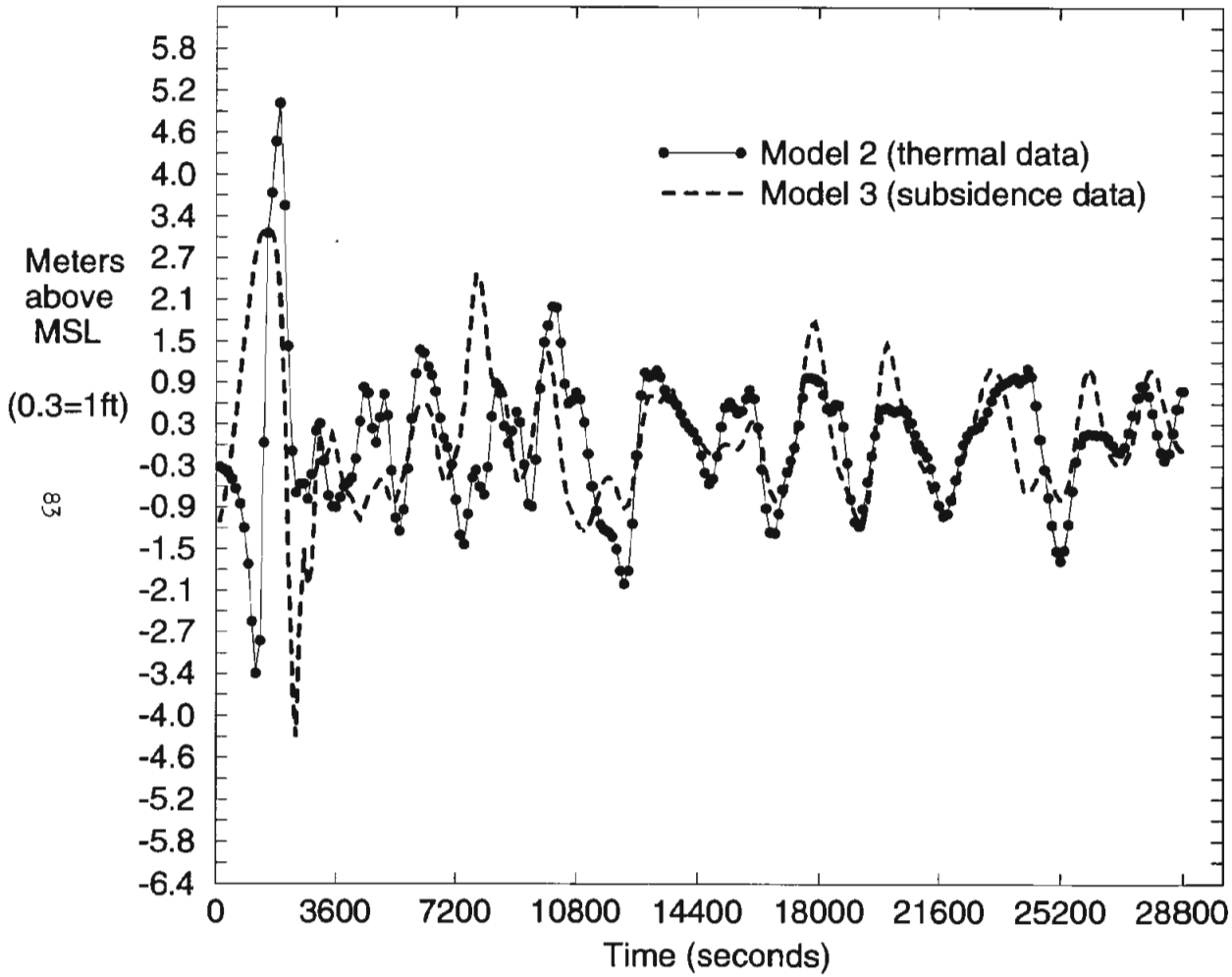


(3600 seconds = 1 hour)
(Plotted points spaced at 2 minute intervals)

# Time History Without Coseismic Subsidence Correction
# NETARTS BAY

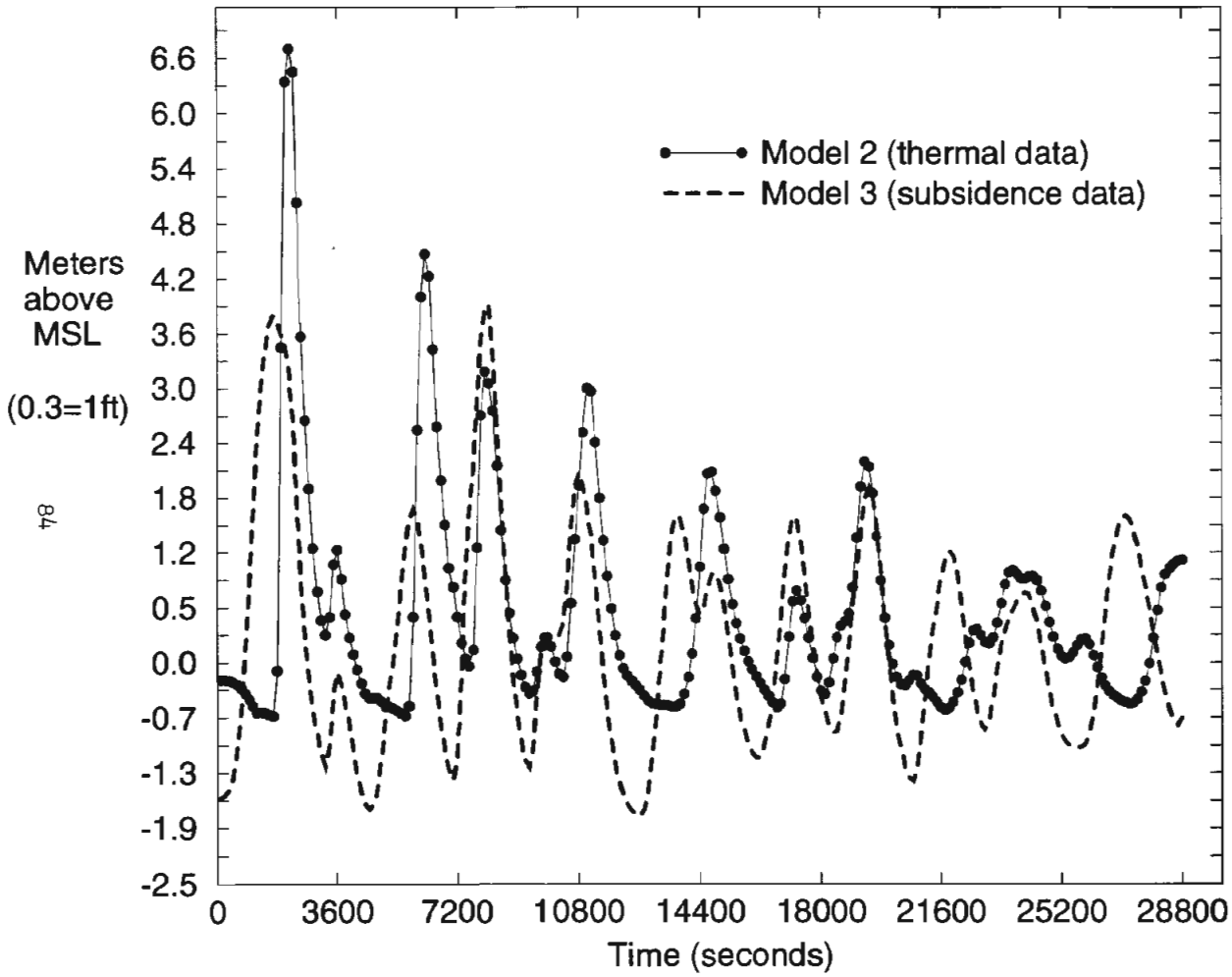


(3600 seconds = 1 hour)
(Plotted points spaced at 2 minute intervals)

# Time History Without Coseismic Subsidence Correction
# NEWPORT AREA

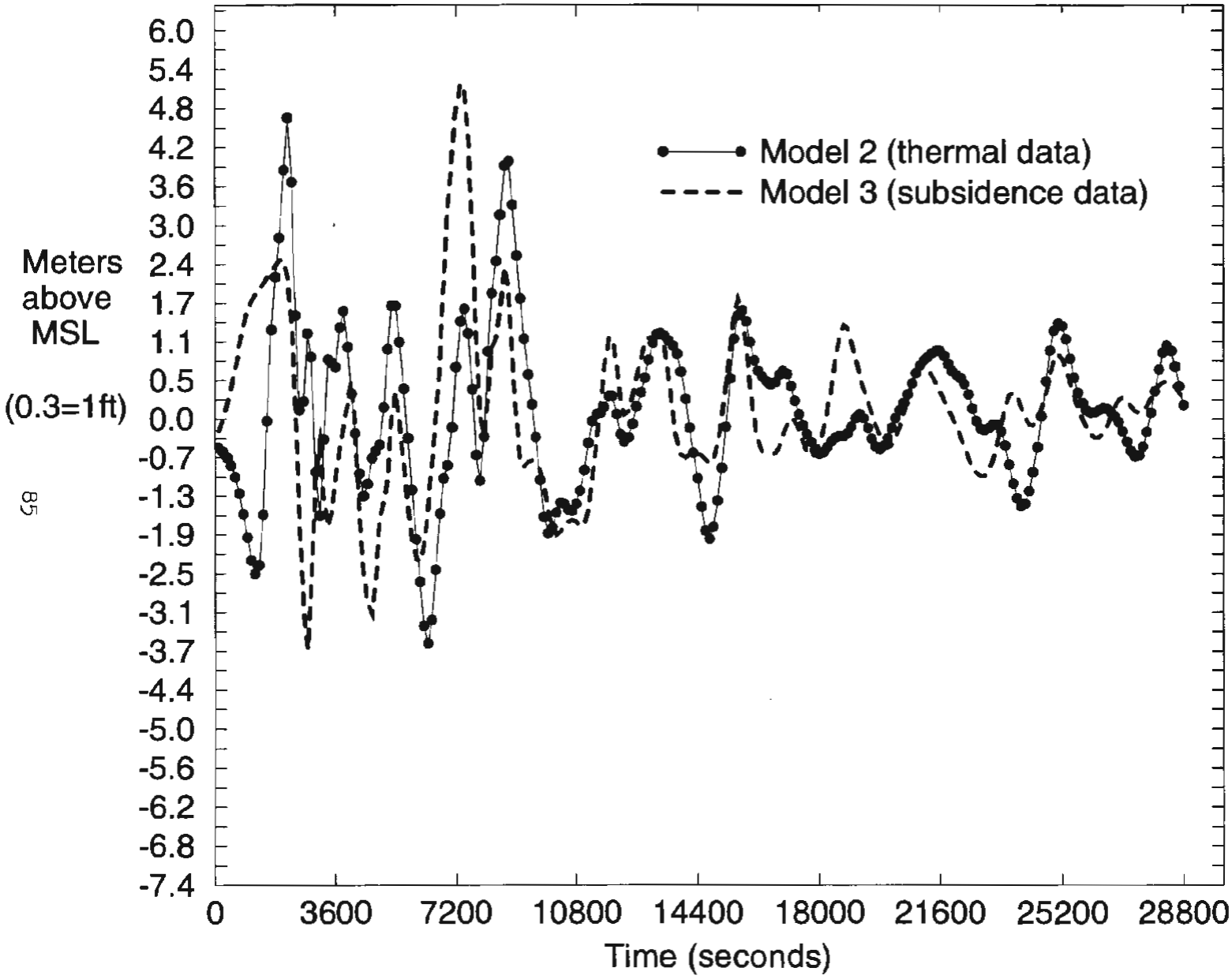


(3600 seconds = 1 hour)
(Plotted points spaced at 2 minute intervals)

# Time History Without Coseismic Subsidence Correction
# OTTER ROCK AREA

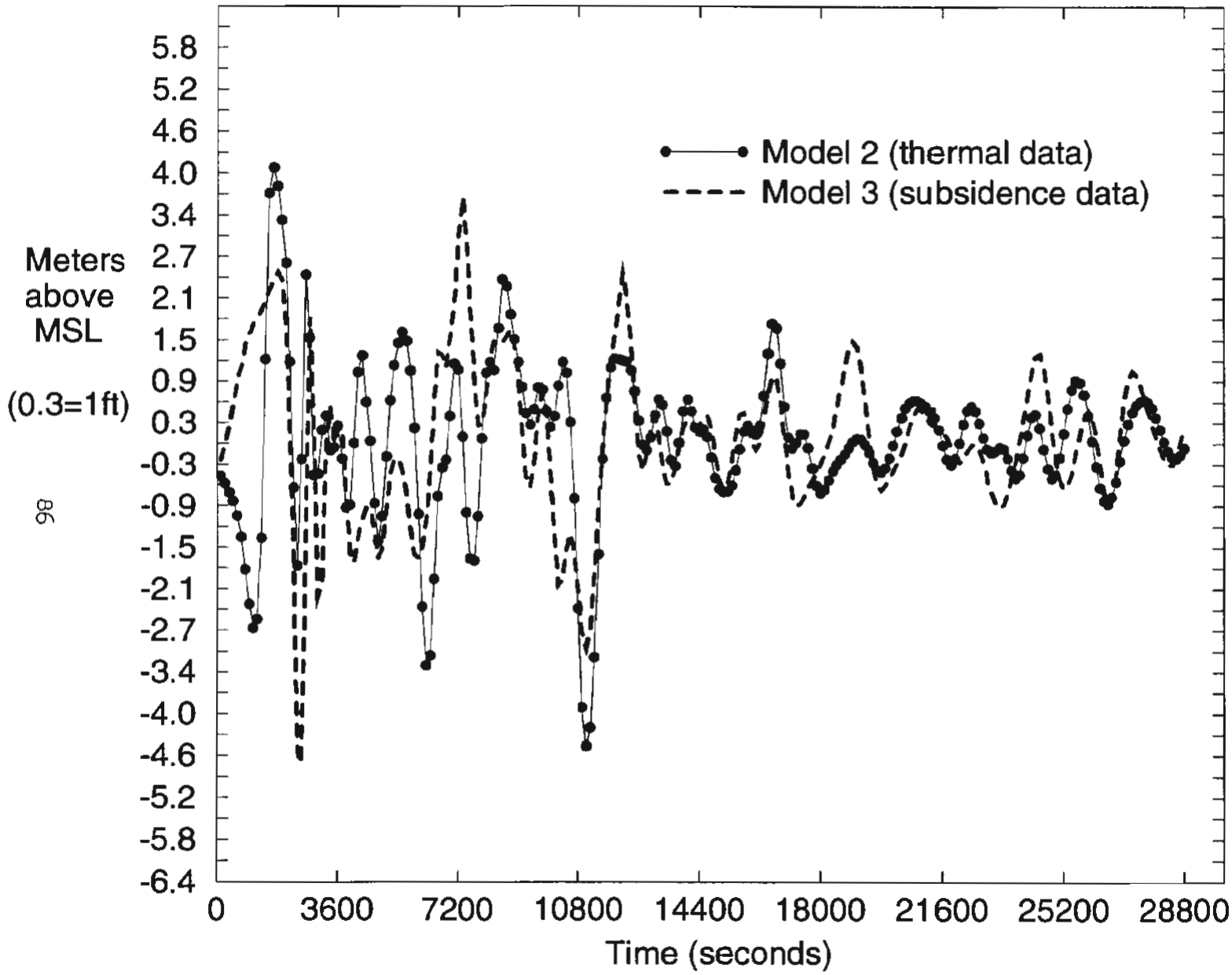


(3600 seconds = 1 hour)
(Plotted points spaced at 2 minute intervals)

# Time History Without Coseismic Subsidence Correction
# PORT ORFORD

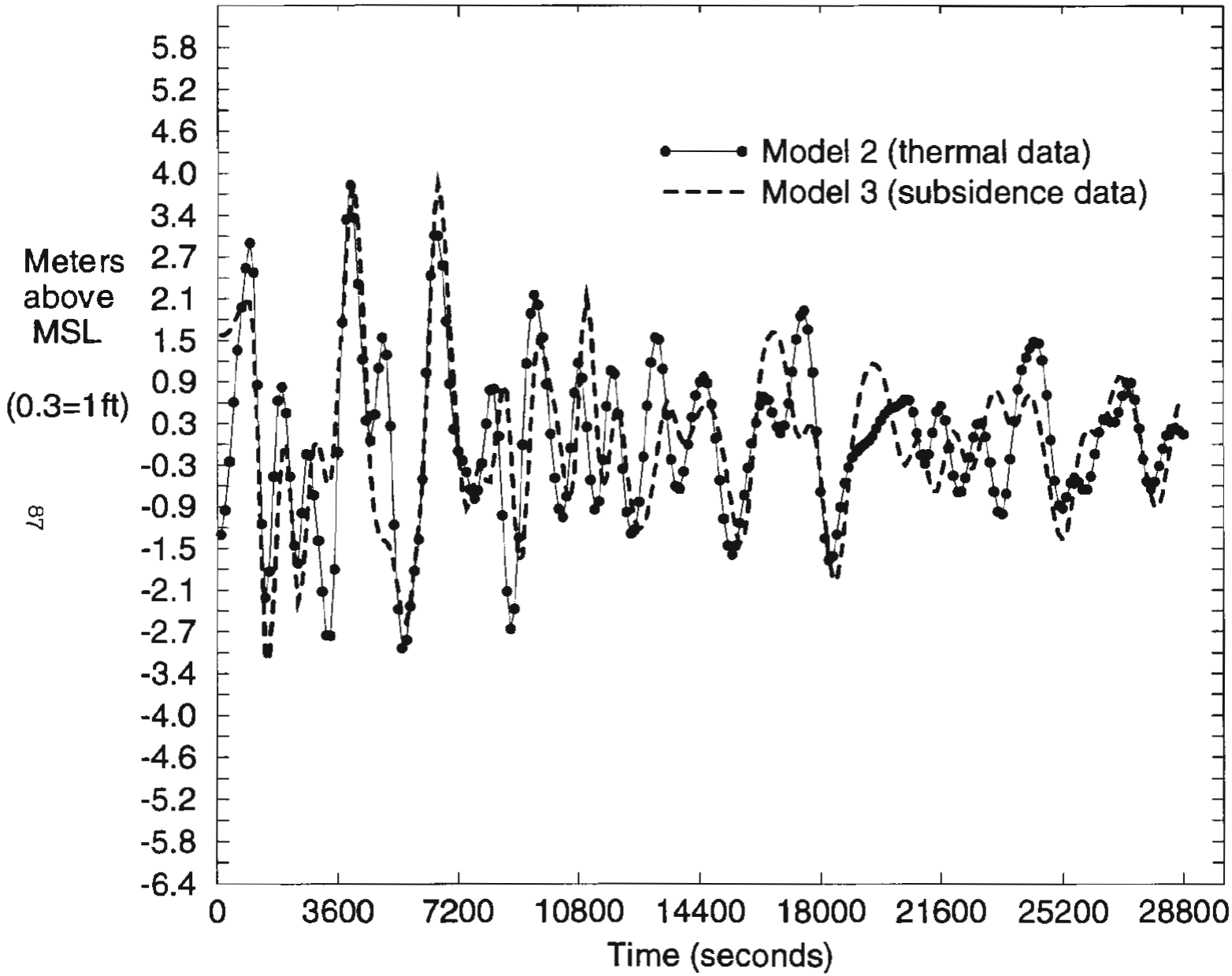


(3600 seconds = 1 hour)
(Plotted points spaced at 2 minute intervals)

# Time History Without Coseismic Subsidence Correction
# ROADS END AREA

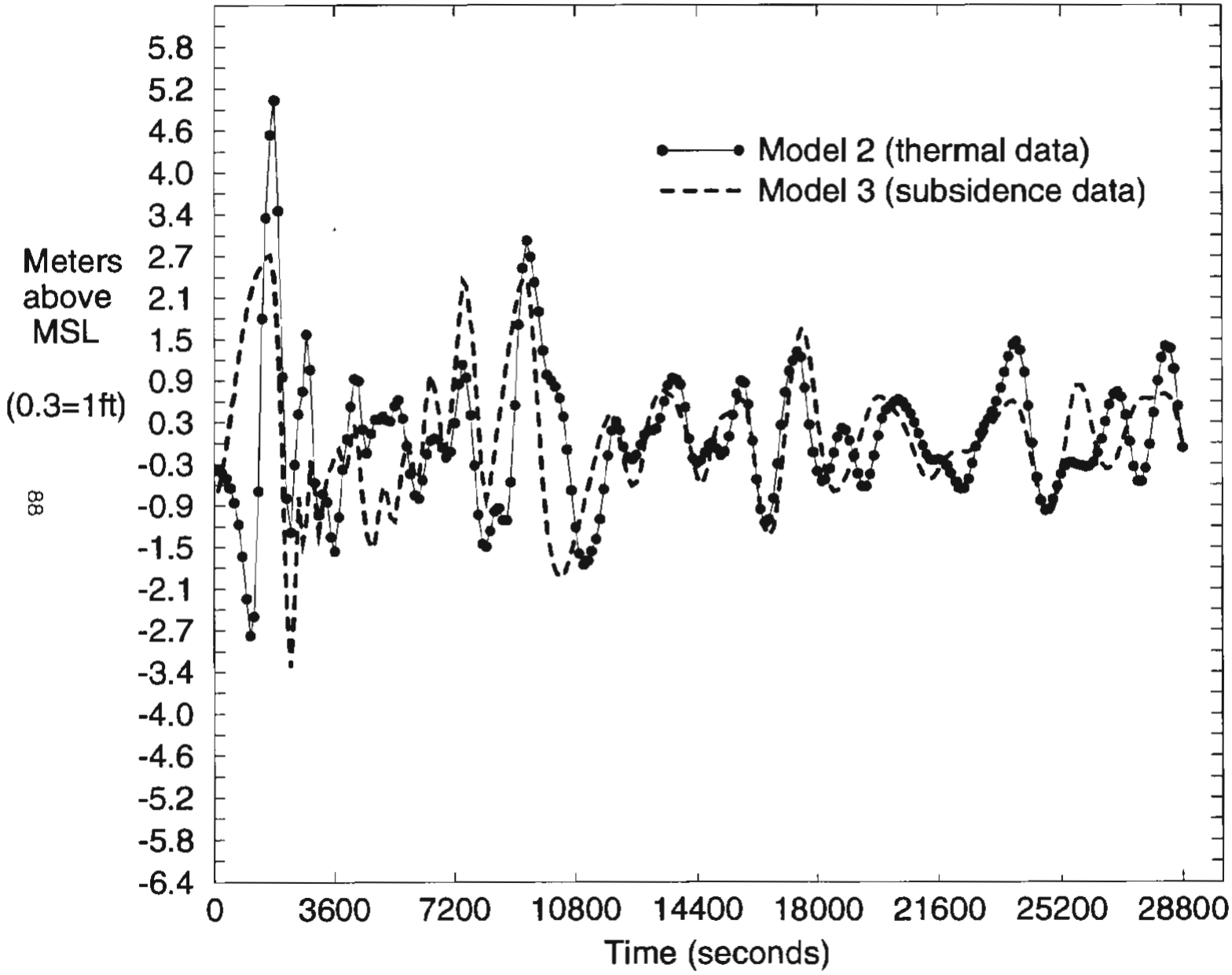


(3600 seconds = 1 hour)
(Plotted points spaced at 2 minute intervals)

# Time History Without Coseismic Subsidence Correction
# SEASIDE AREA

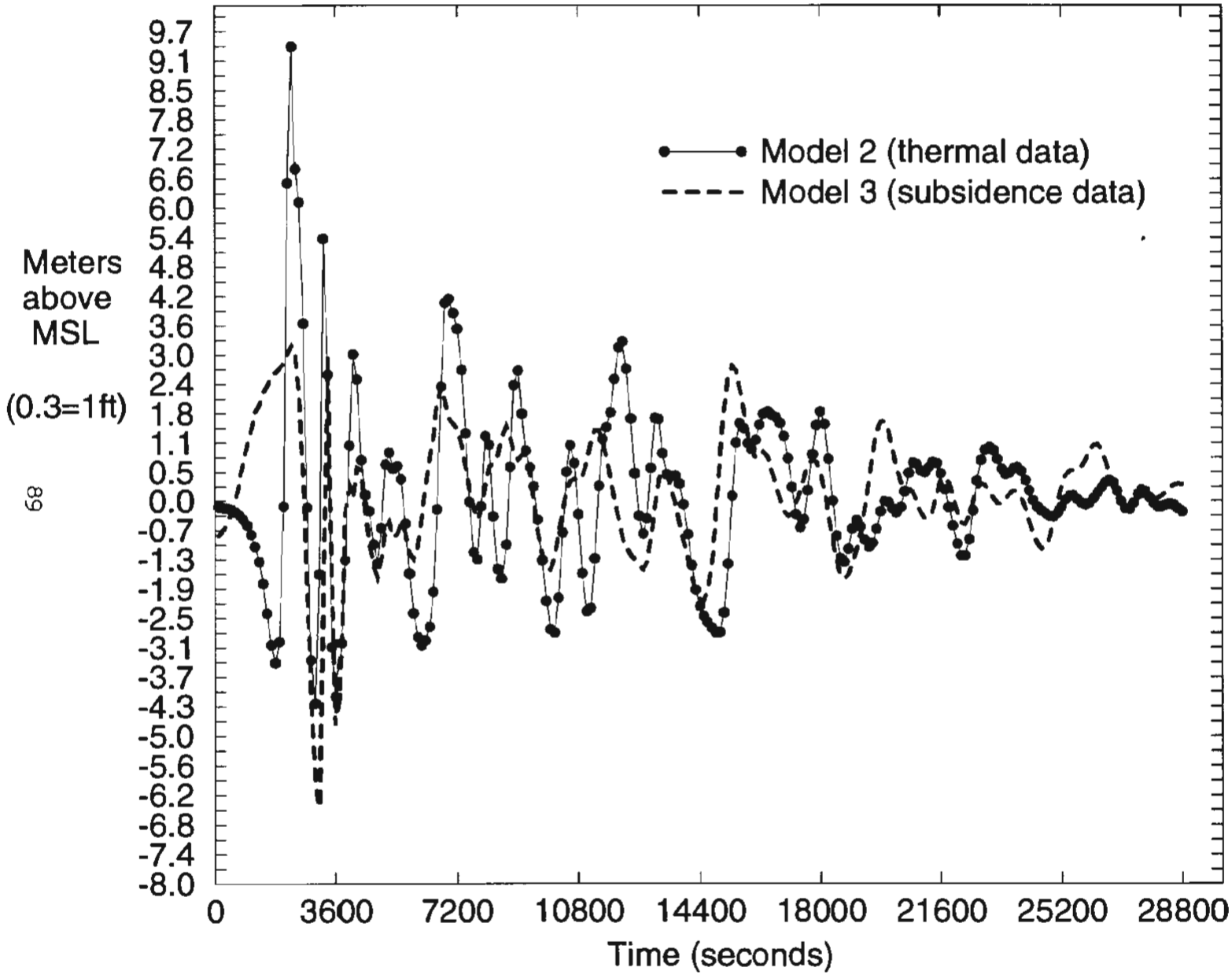


(3600 seconds = 1 hour)
(Plotted points spaced at 2 minute intervals)

# Time History Without Coseismic Subsidence Correction
# SILETZ BAY AREA

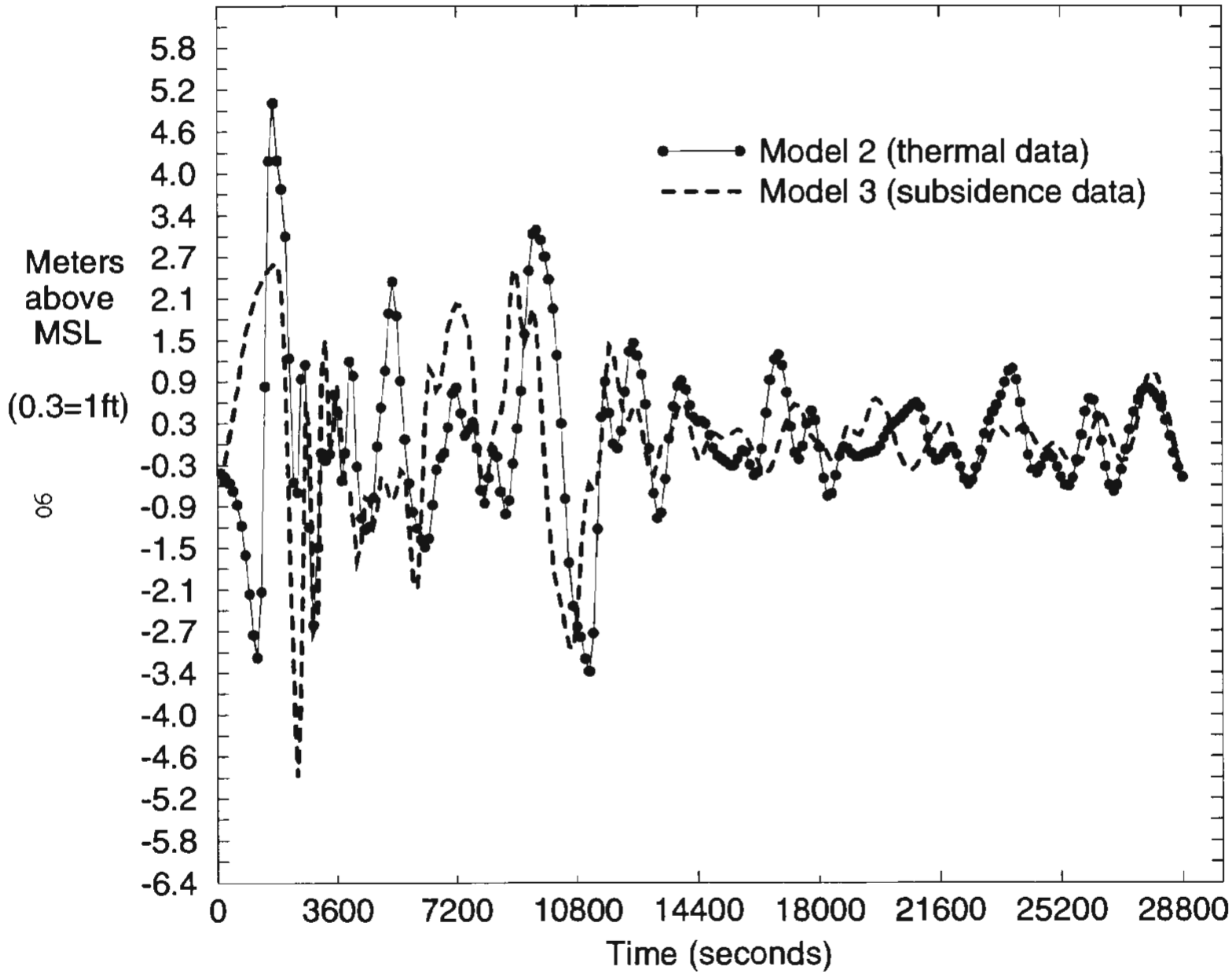


(3600 seconds = 1 hour)
(Plotted points spaced at 2 minute intervals)

# Time History Without Coseismic Subsidence Correction
# SIUSLAW RIVER MOUTH

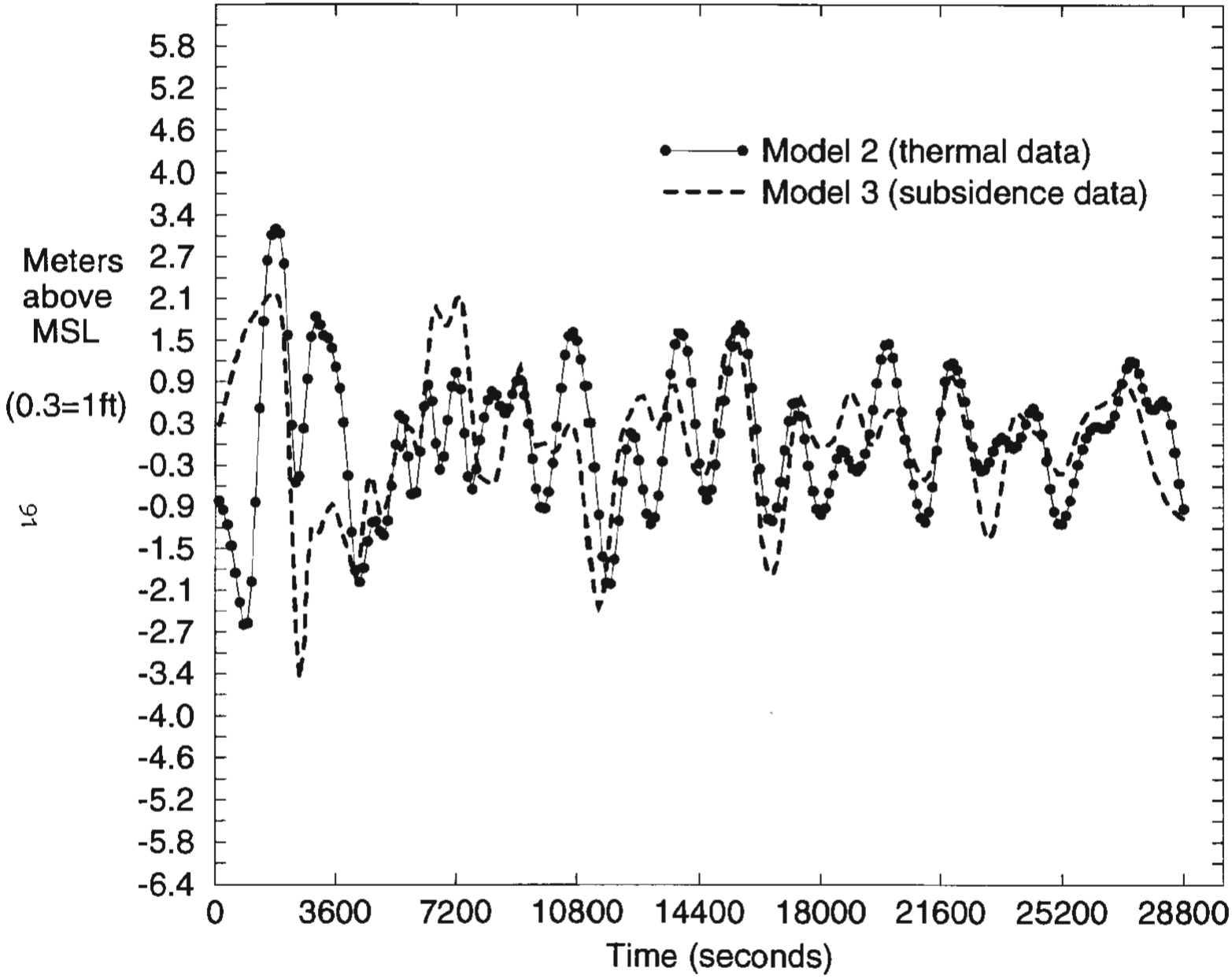


(3600 seconds = 1 hour)
(Plotted points spaced at 2 minute intervals)

# Time History Without Coseismic Subsidence Correction
# TILLAMOOK BAY MOUTH

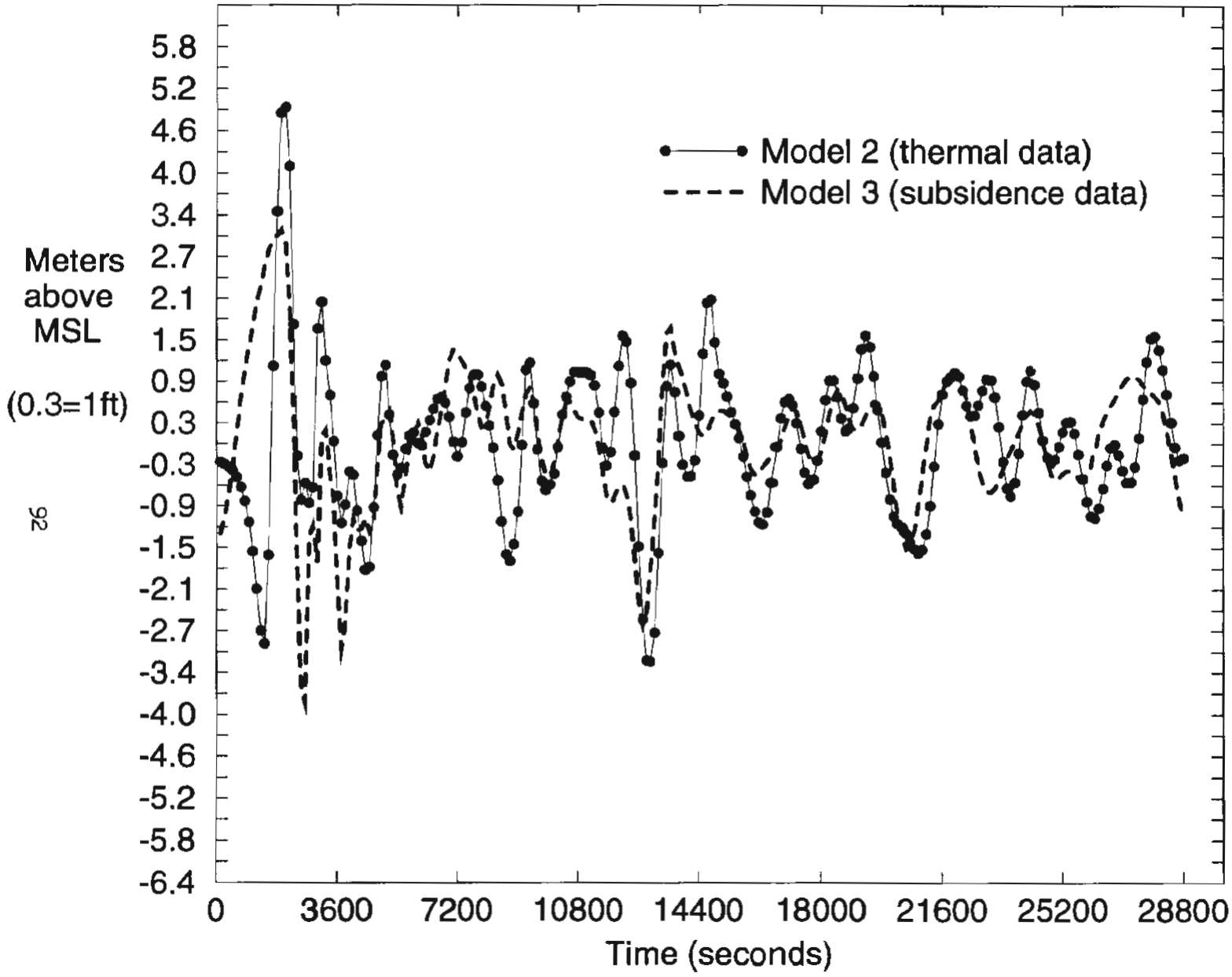


(3600 seconds = 1 hour)
(Plotted points spaced at 2 minute intervals)

# Time History Without Coseismic Subsidence Correction
# UMPQUA BAY MOUTH

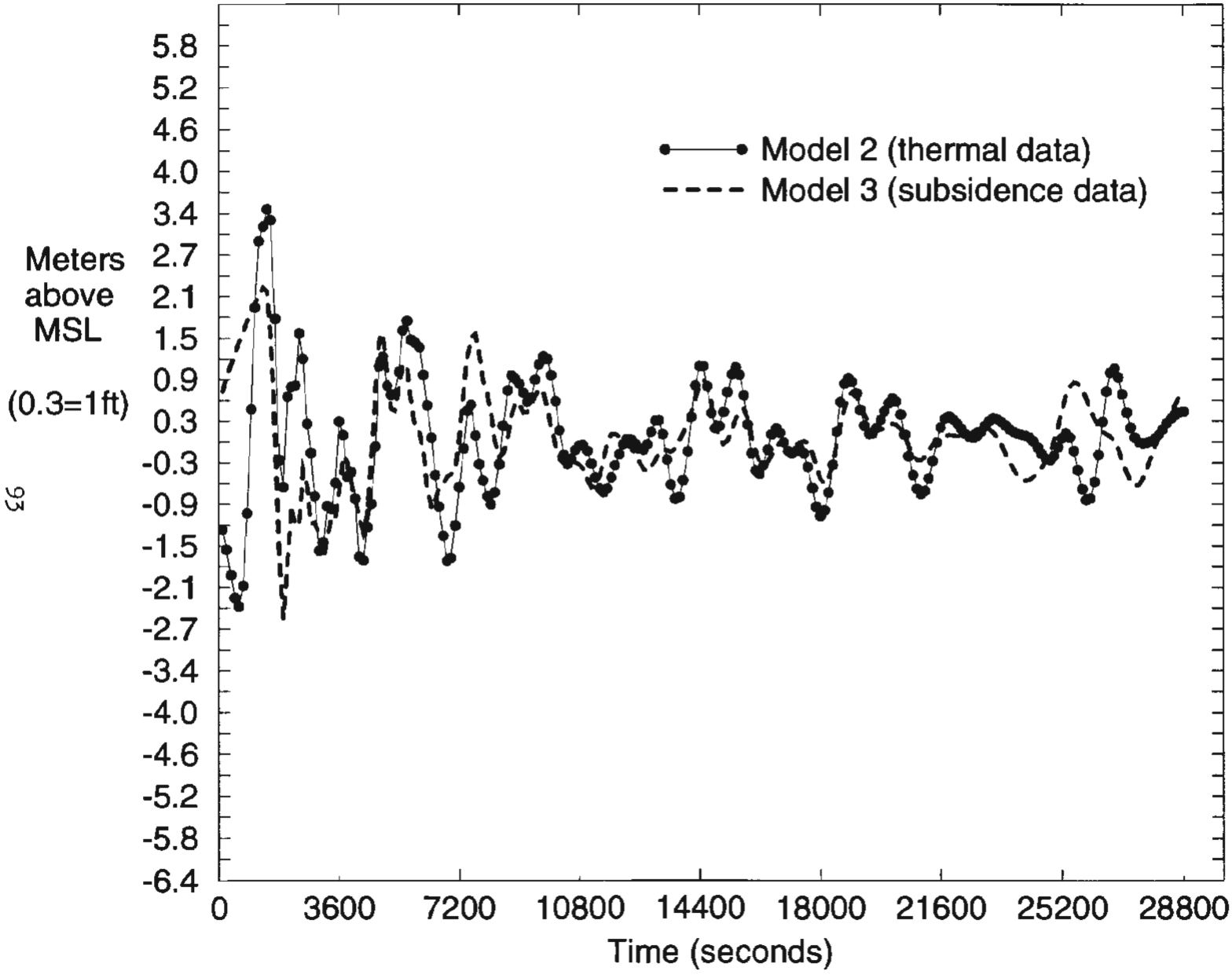


(3600 seconds = 1 hour)
(Plotted points spaced at 2 minute intervals)

# Time History Without Coseismic Subsidence Correction
# WALDPORT

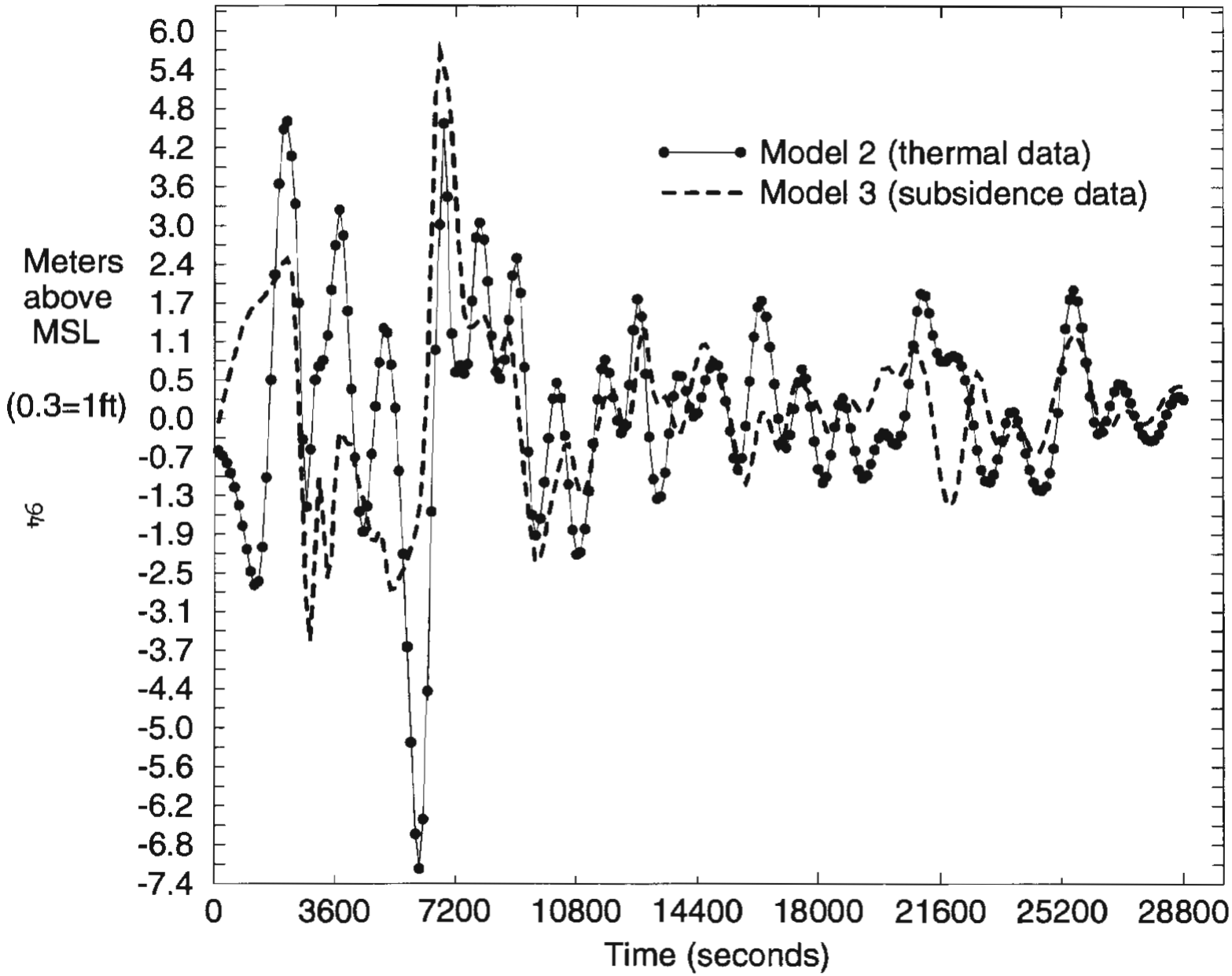


(3600 seconds = 1 hour)
(Plotted points spaced at 2 minute intervals)

# Time History Without Coseismic Subsidence Correction
# WARRENTON AREA

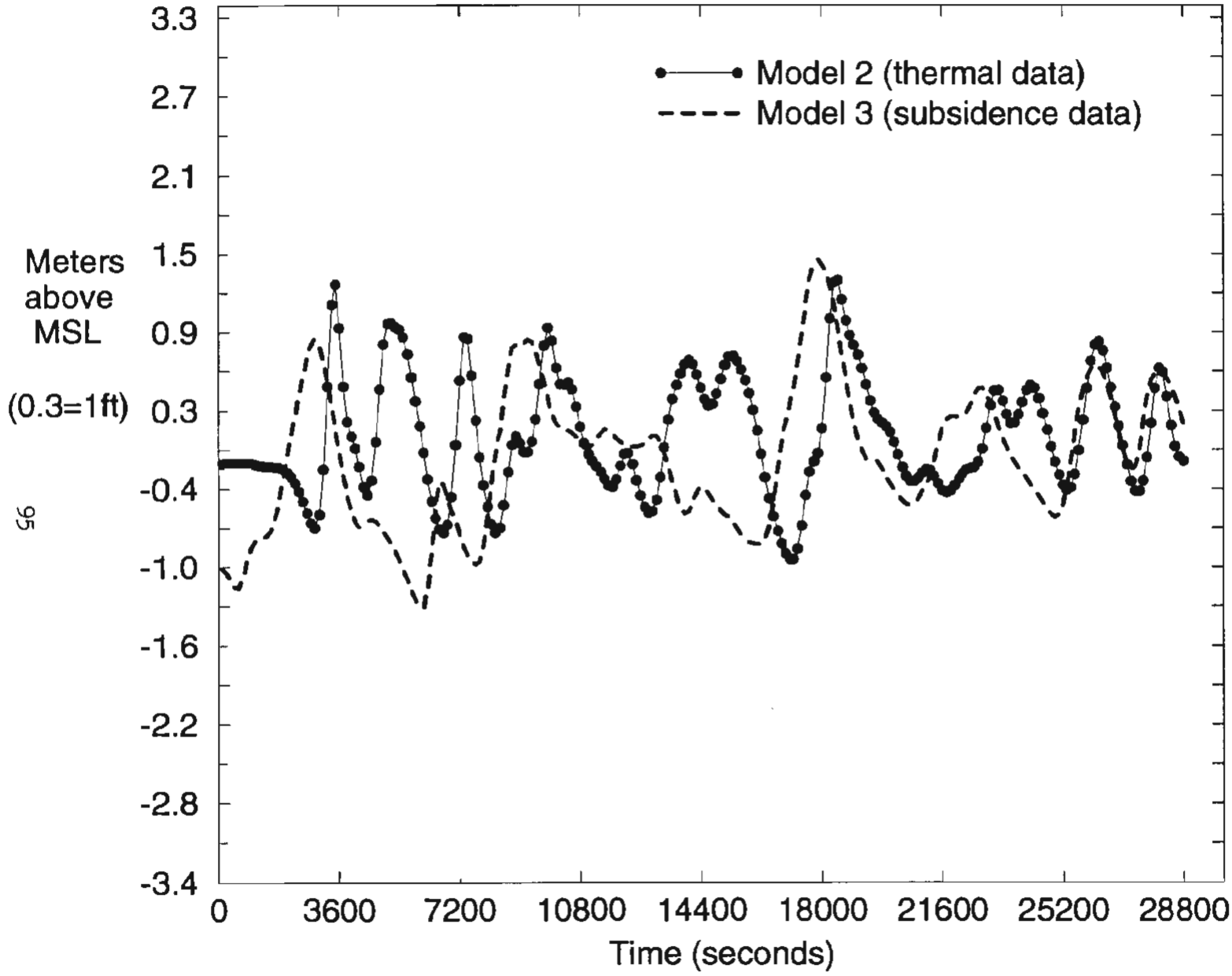


(3600 seconds = 1 hour)
(Plotted points spaced at 2 minute intervals)